Study of trends and variability of atmospheric water vapour with climate models and observations from global GNSS network

Ana Claudia Bernardes Parracho

Université Pierre et Marie Curie

ED 129 Sciences de l'Environnement

LATMOS / LAREG

Etude de la tendance et de la variabilité de la vapeur d'eau atmosphérique à l'aide de modèles de climat et d'observations du réseau GNSS mondial

Study of trends and variability of atmospheric water vapour with climate models and observations from global GNSS network

Par Ana Claudia Bernardes Parracho

Thèse de doctorat de Sciences de l'Environnement

Dirigée par Olivier Bock et Sophie Bastin

Présentée et soutenue publiquement le 12 décembre 2017

Mme GUICHARD Françoise	*Directrice de recherche CNRS*	Rapportrice
M. RIEDI Jérôme	*Professeur, Université Lille 1*	Rapporteur
Mme PICON Laurence	*Professeur, Université Pierre et Marie Curie*	Examinatrice
M. VAN MALDEREN Roeland	*Docteur*, Institut Météorologique Royal de Belgique	Examinateur
Mme BASTIN Sophie	*Chargée de recherche CNRS*	Co-directrice
M. BOCK Olivier	*Directeur de recherche du Développement Durable*	Directeur

Cher (@cher)

Stand & B Counted or Sit & B Nothing. Don't Litter,Chew Gum,Walk Past Homeless PPL w/out Smile.DOESNT MATTER in 5 yrs IT DOESNT MATTER THERE'S ONLY LOVE&FEAR

Résumé

La vapeur d'eau est une composante clé du système climatique. Sa distribution et sa variabilité sont des sources d'incertitude dans les modèles climatiques. L'utilisation d'observations et des réanalyses des Contenus Intégrés en Vapeur d'Eau (CIVE) peut faciliter leur évaluation. Dans ce travail, des données CIVE-GPS retraitées du réseau mondial ont été utilisées pour la période 1995-2010. Afin d'évaluer les incertitudes et les inhomogénéités dans les séries GPS, une comparaison globale avec les données de réanalyse ERA-Interim a été faite. Un bon accord général a été trouvé sur les moyennes, la variabilité et les tendances. Des interruptions et inhomogénéités ont été constatées dans les séries GPS, ainsi que les problèmes de représentativité dans les zones côtières et de topographie complexe. Dans ERA-Interim, des tendances trop fortes ont été constatées dans certaines régions. ERA-Interim a aussi été comparé avec d'autres réanalyses (MERRA-2, ERA-20C, 20CR), et des différences ont été trouvées dans les tendances de les CIVE sur l'Afrique, l'Australie et l'Antarctique. Enfin, les jeux de données CIVE-GPS et CIVE-ERA-Interim ont été utilisés pour évaluer quatre configurations du modèle de circulation générale atmosphérique LMDZ avec deux physiques, libres et guidées avec les vents d'ERA-Interim. Il a été trouvé que la nouvelle physique est plus humide aux latitudes tropicales. Sans guidage, pour les deux physiques, le modèle présente des difficultés à reproduire les tendances et la variabilité obtenues par GPS et par ERA-Interim. Cela confirme l'importance de la dynamique à grande échelle pour les tendances et la variabilité des CIVE.

Abstract

Water vapour is a key component of the Earth's climate system, and its distribution and variability are sources of uncertainty in climate models. The use of long-term integrated water vapour (IWV) observations and reanalyses can help in their assessment. This work pioneered the use of reprocessed GPS IWV data for 1995-2010, converted from estimates of Zenith Total Delay. The conversion was assessed, with the goal of producing a high quality long-term IWV data set. Due to uncertainties in the GPS observations and homogeneity concerns, a global comparison with ERA-Interim reanalysis data was made. Although a general good agreement in means, variability and trends was found, issues in both data sets were highlighted. In GPS, gaps and inhomogeneities in the time series were evidenced, as well as representativeness differences in coastal areas and regions of complex topography. In ERA-Interim, too strong trends in certain regions were found. ERA-Interim was also compared with other reanalyses (MERRA-2, ERA-20C, 20CR), and differences were found in the IWV trends over Africa, Australia, and Antarctica. Finally, GPS and ERA-Interim IWV were used to assess four configurations of the LMDZ atmospheric general circulation model with two different physics and with or without nudging towards ERA-Interim wind fields. Impact of the model physics on the IWV mean was found, with the new physics being moister at tropical latitudes. Overall, the model free runs in both physics have difficulty reproducing the trends and variability observed in ERA-Interim and GPS. This is improved with the nudging, which confirms the importance of large-scale dynamics on IWV trends and variability.

Résumé substantiel

La vapeur d'eau atmosphérique est une composante clé du système climatique de la Terre avec une rétroaction positive sur celui-ci d'environ +1,1 $W.m^{-2}.°C^{-1}$. Elle réside dans l'atmosphère pour une dizaine de jours environ et présente une forte variabilité à de multiples échelles spatio-temporelles. Les modèles climatiques globaux n'ont ainsi pas la résolution suffisante pour représenter précisément la distribution de vapeur d'eau et ses interactions ce qui constitue une source d'incertitude pour l'établissement des scénarios globaux du changement climatique. Il est alors capital d'évaluer cette source d'incertitude en confrontant ces modèles avec des observations à long terme de la vapeur d'eau et des réanalyses météorologiques.

Il existe plusieurs sources d'observations de la vapeur d'eau (p. ex. radiosondes, VLBI, données satellitaires...) et chaque jeu de données présente des avantages et des inconvénients pour l'analyse à long terme. Dans ce manuscrit, le choix a été fait d'utiliser les Contenus Intégrés en Vapeur d'Eau (CIVE) calculés à partir des retards troposphériques humides estimés lors de traitements de données GPS. Dans un premier temps, la conversion des retards troposphériques humides en CIVE a été évaluée afin d'obtenir un ensemble de données CIVE de haute qualité sur le long terme. Pour ce faire, la qualité des données de pression de surface et de température moyenne nécessaires à cette conversion et l'influence de l'interpolation ont été évaluées. Il est ainsi préférable de calculer ces deux variables en utilisant les données de niveau de pression ERA-Interim afin de limiter l'extrapolation des données. Les résultats obtenus à partir de cette étude ont alors été utilisés pour obtenir les CIVE-GPS utilisés dans la suite de ce manuscrit.

En raison des incertitudes associées aux estimations des CIVE (jusqu'à 2 kg.m-2 dans le cas du GPS) et aux problèmes d'inhomogénéité, les réanalyses météorologiques sont également utilisées pour obtenir une description plus cohérente spatialement et temporellement. Afin d'établir une inter-validation entre ces estimations GPS et les sorties d'ERA-Interim, une comparaison globale en termes de moyenne, de variabilité et de tendance a été réalisée pour la période 1995-2010. Bien qu'un accord généralement satisfaisant ait été trouvé, cette étude a mis en évidence des problèmes dans les deux jeux de données. Concernant les CIVE-GPS, il s'agit d'interruptions et d'inhomogénéités dans les séries chronologiques qui affectent la variabilité et l'estimation des tendances. Concernant les sorties d'ERA-Interim, des tendances trop fortes ont été observées dans certaines régions, par exemple : un fort assèchement en Afrique du Nord et en Australie et une forte humidification dans le nord de l'Amérique du Sud. Des différences de représentativité dans les zones côtières et les régions présentant une topographie complexe (chaînes de montagnes, îles) ont aussi été identifiées comme des limites à l'intercomparaison des deux jeux

de données. Les sorties d'ERA-Interim ont donc été comparées à celles d'autres réanalyses (MERRA-2, ERA-20C, 20RC). Des différences ont été observées concernant les tendances obtenues à partir des différentes réanalyses, notamment en Afrique où l'assèchement est moindre et localisé plus au sud dans MERRA-2 et 20-CR par rapport à ERA-Interim et ERA-20C, en Australie où les tendances long terme diffèrent sur la période estivale et en Antarctique avec des tendances contradictoires entre les modèles. Une attention particulière a été portée sur la situation en Afrique du Nord et en Australie occidentale. Cette analyse ciblée a mis en évidence un lien entre les anomalies des CIVE et les anomalies de l'intensité et de la direction du vent (à 925 hPa), ce qui pourrait expliquer les différences de tendances observées pour ces régions dans les deux réanalyses.

Enfin, les jeux de données CIVE-GPS et CIVE-ERA-Interim ont été utilisés pour évaluer quatre configurations du modèle LMDZ de circulation générale atmosphérique du Laboratoire de Météorologie Dynamique de l'Institut Pierre Simon Laplace. Les configurations de modèle utilisées dans cette partie comprenaient deux versions de LMDZ : LMDZ5A (physique « standard »), utilisée pour les simulations IPSL-CM5A; et LMDZ5B (« nouvelle » physique), utilisé pour les simulations IPSL-CM5B du 5ème rapport du GIEC[1]. Deux stratégies ont été suivies pour chaque physique (à une résolution de 1,9 ° x 3,75 °) : une stratégie libre et une autre contrainte par les vents d'ERA-Interim échantillonnés à 6 heures. Les comparaisons en termes de moyennes, de variabilité et de tendances ont été réalisées entre 1995 et 2009. Les problèmes d'inhomogénéité des CIVE-GPS ayant été précédemment rencontrés lors de l'intercomparaison avec ERA-Interim, une homogénéisation sommaire a été effectuée en alignant les moyennes GPS sur ERA-Interim lorsque des changements d'équipement ont été signalés. Un impact de la physique du modèle sur les CIVE moyens a été constaté, la «nouvelle» physique étant plus humide dans les océans tropicaux. Un biais humide dans la « nouvelle » physique a également été trouvé lors de la comparaison du modèle climatique avec les estimations GPS et les sorties d'ERA-Interim aux latitudes tropicales. En ce qui concerne la variabilité et les tendances, la contrainte induite par les vents a un impact relativement plus élevé, les deux physiques montrant des résultats similaires. Sans contrainte, le modèle climatique présente des difficultés à reproduire les tendances et la variabilité obtenues par GPS et par ERA-Interim. Cela confirme l'importance de la dynamique à grande échelle pour les tendances et la variabilité des CIVE.

[1] Groupe d'experts intergouvernemental sur l'évolution du climat (GIEC)

Dans les travaux futurs, nous espérons améliorer l'homogénéisation des données GPS CIVE, étendre la comparaison aux réanalyses plus récentes (e.g. ERA5) et autres modèles climatiques mondiaux (y compris LMDZ6 plus récent) et se concentrer sur l'interaction entre CIVE et d'autres variables par exemple la température et les précipitations. Il serait également intéressant de se concentrer sur une étude plus détaillée des régions où de fortes incertitudes sur les CIVE ont été relevées (par exemple Afrique, Antarctique) Ã l'aide de données complémentaires.

Table of contents

Chapter 1: Introduction

1.1 The role of water vapour in the climate system

1.1.1 Water vapour-temperature feedbacks

Water vapour is the major greenhouse gas in the atmosphere, and accounts for about 75% of the total greenhouse effect of the Earth, contributing to a warming of the climate system by around 24°C (Kondratev, 1972). This is a global average, as the greenhouse effect of water vapour depends on the total amount of water vapour in the column which is spatially heterogeneous, but also to its vertical distribution. Indeed, the greenhouse effect is relatively more sensitive to changes in water vapour in the upper troposphere (Rind, 1998; Spencer and Braswell, 1997). Also, over the humid tropical latitudes, the surface night-time cooling is weak, whereas over the drier subtropical regions the day-night temperature contrasts are larger, as these areas radiate more towards space.

The water-holding capacity of the atmosphere mainly depends on the temperature through the Clausius-Clapeyron (C-C) law (eq. 1.1):

$$\frac{d \ln e_s}{dT} = \frac{L}{RT^2} \equiv \alpha(T) \tag{1.1}$$

Where e_s is the saturation vapour pressure, T is the temperature, L is the latent heat of vaporization and R is the gas constant. For temperatures in the lower troposphere, $\alpha \approx 0.07\ K^{-1}$. So, according to C-C, a temperature increase in the lower troposphere of 1°C leads to an increase in the vertical profile of water vapour of about 7%, which, in turn, as water vapour is a powerful greenhouse gas, increases the temperature further.

"The radiative effect of absorption by water vapour is roughly proportional to the logarithm of its concentration, so it is the fractional change in water vapour concentration, not the absolute change, that governs its strength as a feedback mechanism" (IPCC AR5 WGI Box 8.1). However, the strength of this positive feedback has been debated (Hall and Manabe, 1999; Semenov and Bengtsson, 2002; Held and Soden, 2006; Soden and Held, 2006; Randell et al., 2007). The feedback of water vapour can be estimated from climate models through by-passing the part of the long-wave radiation code that calculates the effect of increasing water vapour (Hall and

Manabe, 1999). The latest IPCC report (Stoker et al., 2014) estimates the water vapour plus lapse-rate feedback to be +1.1 (+0.9 to +1.3, at a 90% uncertainty range) $W.m^{-2}.°C^{-1}$(Fig. 1.1). At regional scale, the effective water vapour content will also depend on the availability of surface water which can explain a deviation from the C-C law. At global scale, observational and modelling studies have suggested that the relative humidity is maintained and that water vapour in the atmosphere closely follows the temperature in agreement with the C-C equation (Held and Soden, 2006; Semenov and Bengtsson, 2002).

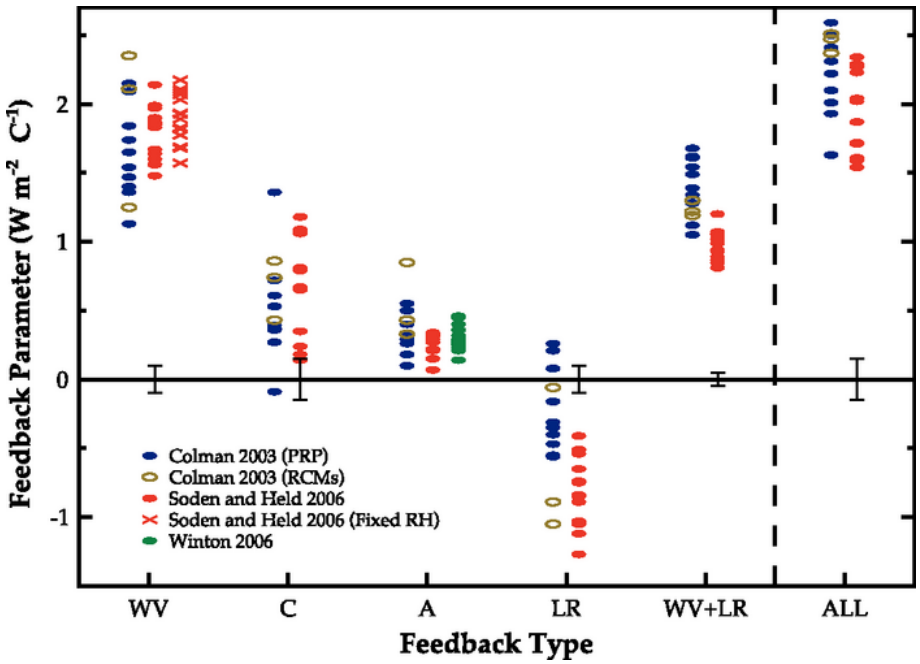

Figure 1.1: Comparison of global climate model feedback parameters for water vapour (WV), cloud (C), surface albedo (A), lapse rate (LR) and the combined water vapour plus lapse rate (WV + LR) in units of W m−2 °C−1. 'ALL' represents the sum of all feedbacks. Results are taken from Colman (2003a; blue, black), Soden and Held (2006; red) and Winton (2006a; green). Closed blue and open black symbols from Colman (2003a) represent calculations determined using the partial radiative perturbation (PRP) and the radiative-convective method (RCM) approaches respectively. Crosses represent the water vapour feedback computed for each model from Soden and Held (2006) assuming no change in relative humidity. Vertical bars depict the estimated uncertainty in the calculation of the feedbacks from Soden and Held (2006). Source: IPCC Fourth Assessment Report.

1.1.2 Relationship between water vapour, temperature and precipitation

Although water-vapour increases at a rate close to $7\%.K^{-1}$, the increase in evaporation and precipitation is constrained to 1-2% (Held and Soden, 2006) by energetics, which limits the slope of the relationship between mean precipitation and temperature (Boer, 1993; Allen and Ingram, 2002; Pierrehumbert, 2002, O'Gorman et al., 2012).

The fact that precipitation increases at a lower rate than water vapour has several consequences. On the one hand, the increase in water vapour residence time in the atmosphere (Roads et al., 1998; Bosilovich et al., 2005) and the slowing down of the large-scale atmospheric circulation are expected with warming temperatures (Held and Soden, 2006; Chadwick et al., 2013). This, in turn, leads to a decrease in the average vertical exchange of mass between the boundary layer and the mid-troposphere (Betts, 1998; Held and Soden, 2006), which, in agreement with climate models, has also been supported by observations (Vecchi et al., 2006; Zhang and Song, 2006). On the other hand, assuming a constant relative humidity in the lower troposphere and that the flow is unchanged, the poleward water vapour transport and the evaporation minus precipitation pattern increase proportionally to the lower tropospheric water vapour. As a consequence, in a warming climate and at a global scale, wet regions get wetter and dry regions get drier (Held and Soden, 2006). However, on a regional basis, Chadwick et al. (2013) and Brown et al. (2016) show that this mechanism is not necessarily verified over the Tropics due to compensation with other contributions. In addition, several studies show that extreme precipitation is projected to increase more than the mean precipitation over some areas (e.g Emori and Brown, 2005). According to the latest Intergovernmental Panel on Climate Change (IPCC) report (Stoker et al., 2014), changes in local extremes on daily and sub-daily time scales are strongly influenced by lower-tropospheric water vapour concentration. They report with medium confidence that these extreme events will increase, on average, by 5 to 10% per degree of warming.

This is important to understand how precipitation might be affected by a warmer climate and how much the water vapour content influences this evolution. It is expected that the total precipitation will increase over the Tropics and mid- to high- latitudes; and decrease over some subtropical to mid-latitude regions, as for instance in the Mediterranean region, California and Texas, southern Africa and southern Australia (Emori and Brown, 2005). Precipitation changes can be separated into the dynamic and the thermodynamic (linked to Clausius-Clapeyron and water vapour content) components (several methods have been proposed; see for instance Emori and Brown, 2005 or Chadwick et al., 2013). While the dynamical component is slightly negative everywhere but over equatorial Pacific, due to the weakening of large scale circulation as explained above, the thermodynamic one is positive in most areas except the aforementioned ones. However, when considering extreme precipitations, the thermodynamical contribution is positive everywhere except Southern Africa.

Another important aspect that links water vapour, temperature and precipitation is convection. Neelin et al. (2009), Holloway and Neelin (2009) and Sahany et al. (2012) conclude that

Integrated Water Vapour is a better proxy than surface humidity, sea surface temperature or saturation for transition to deep convection in the Tropics because at higher temperature, deep convection occurs at lower relative humidity rates. Entrainment processes actually play a substantial role in the onset of deep convection. However, the relationship is a two-way interaction since convection also moistens the free troposphere (the upper-troposphere mainly). This relationship is a key issue for models in a warming climate.

1.1.3 Water vapour in global climate models

It is clear that water vapour has a strong impact on the global climate system and vice-versa and is thus an important part of the response of the climate system to external forcing (Bengtsson, 2010). However, water vapour has a residence time in the atmosphere of the order of 10 days, so that, unlike other greenhouse gases with long residence times (such as CO_2) it is not well-mixed and varies strongly on a small scale, in both space and time. This makes it difficult for global climate models (GCMs) with coarser resolutions to represent its distribution accurately and increases the difficulty in describing the greenhouse effect of water vapour in climate models. It is thus a source of uncertainty in climate change predictions, especially at the regional level. Therefore it is important to assess these models, by using long-term water vapour observations and reanalysis.

On the other hand, a strong positive water vapour feedback is a robust feature of GCMs (Stocker et al., 2001), which is found across models with various schemes for advection, convection and condensation of water vapour. As seen in Fig. 1.2, the scatter plot of temperature and water vapour trends in the tropical oceans for several GCMs has a well-defined slope. The trends in temperature and water vapour themselves show some uncertainty and vary considerably from one model to the other. For instance, note that the temperature (water vapour) trends obtained for IPSL-CM5A-LR are twice (2.5 times) the ones obtained for IPSL-CM5B-LR. These two models will be analysed further in Chapter 4. Still, the relationship between them is close to the 5.7 %.°C^{-1} slope. This is not as clear for the reanalyses and observations, and suggests climate models could also be used to assess observational data sets (Mears et al., 2007). It should be noted also that Fig. 1.2 is representative of the tropical oceans only, for which the median temperature trend is about 0.30°C/decade and the corresponding precipitable water trend is about 1.5%/decade. These are about a factor of 2 larger than the recent global mean trends (IPCC 2014).

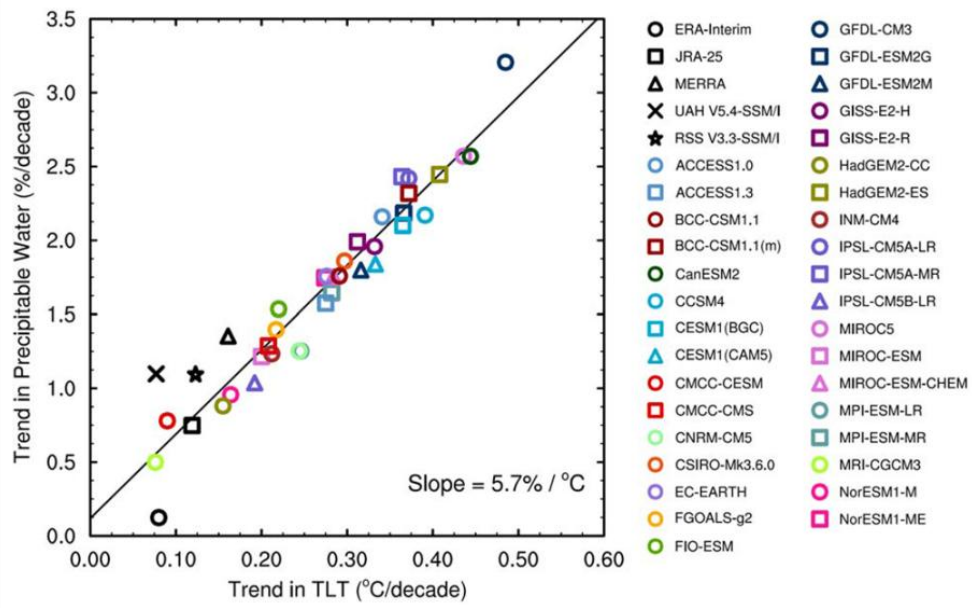

Figure 1.2: Decadal trends in tropical precipitable water and temperature (between 20°S and 20°N, over the ocean) for the 1988-2012 period for different reanalyses, fully coupled ocean-atmosphere climate models, and observations.(Source: Mears et al. (2007); IPCC AR5 WG 1 (Flato et al., 2013))

1.2 Observations of atmospheric water vapour

1.2.1 Measurement techniques

The water vapour content of the atmosphere can be expressed in terms of Integrated Water Vapour (IWV). IWV (expressed in kg.m^{-2}) is defined as:

$$IWV = \int_0^\infty \rho_v(h)dh = \frac{1}{R_w}\int_0^\infty \frac{p_w(h)}{T(h)}dh \tag{1.2}$$

Where ρ_v is the absolute humidity, h is the height of the column, $R_w = 461.522\ \mathrm{J}.kg^{-1}.K^{-1}$) is the specific gas constant for water vapour, p_w is the partial pressure of water vapour and T is the temperature.

The term integrated water vapour is used to state the mass of vapour per unit of area. However, if we refer to the height of a liquid water column, the term Precipitable Water (PW) is used. PW (expressed in mm) is defined as:

$$PW = \frac{IWV}{\rho_w} \tag{1.3}$$

Where $\rho_w = 1000\ kg.m^{-3}$ is the density of liquid water.

Historically, although several methods have been developed to measure the water vapour content of the atmosphere, obtaining consistent and homogeneous observations over a climatological time period is difficult. Table 1 summarizes the main measurement methods that can be used to obtain IWV, as well as their advantages and drawbacks, with regards to long-term analysis and global trend estimations.

Several studies have compared the different sources of IWV observations presented in Table 1.1. Most of these studies have focused on a limited region (or site) and on a limited period (e.g.: Niell et al., 2001; Bock et al., 2004, 2007; Morland et al., 2006 and 2009; Palm et al., 2010; Torres et al., 2010; Buehler et al., 2012; Bock et al., 2013; Liu et al., 2013). The reported differences between techniques vary with each study and do not show an overall consistent pattern.

More recently, Van Malderen et al. (2014) compared the different IWV measurements (from satellites, radiosondes, GPS and sun photometers) at 28 sites in the northern hemisphere, in the context of climate change analysis (i.e. for trend estimation). They considered homogeneously reprocessed GPS-derived IWV (see section 2) as the reference, due to its long-term, all-weather database with global (over land) coverage. They found a bias between techniques of -0.3 to 0.5 $kg.m^{-2}$, with better agreement between ground-based and in situ observations in general, and between GPS and radiosondes in particular. Both are all-weather devices, as opposed to the satellites which require low cloud-fractions. In general, these instruments that suffer from a bias during cloud cover had the lower correlation with the GPS data and higher standard deviations.

Table 1.1: Measurement methods that can be used to obtain IWV, with their advantages and disadvantages, with regards to long-term analysis and global trend estimations.

Measurement method		Advantages	Disadvantages
In situ	**Radiosonde (RS)** – balloon-borne instrument which retrieves profiles of temperature, humidity and pressure. Measurements are transmitted in real-time by radio signal	- Long, continuous observation history (1950s-present) - Near-global coverage: 978 Integrated Global Radiosonde Archive (IGRA) sites, as of 2015 - High vertical resolution	- Lower accuracy under very dry conditions (15% uncertainty, versus about 5% under normal conditions (Miloshevich et al., 2009; Smit et al., 2013; Wang et al., 2013)) - Poor time sampling, with high diurnal time sampling errors, especially when radisondes are released only once a day (10-15 %, as opposed to within 2% for twice-daily radiosonde data) (Wang and Zhang, 2008) - Systematic observational errors, depending on specific sensor limitations or external factors (Wang and Zhang, 2008) - Presence of jumps and other discontinuities due to changes in instrumentation, observing practice, or station location. Although efforts have been made to homogenize humidity records in order to make them suitable for trend analysis (Durre et al., 2009; McCarthy et al., 2009; Dai et al., 2011; Zhao et al., 2012)
Ground-based, upward-looking	**Water Vapour Radiometer (WVR)** – estimates IWV along a line of sight, by measuring the background microwave radiation produced by the atmospheric water vapour molecules.	- High accuracy (uncertainty in IWV of around 1.1 $kg.m^{-2}$; Ning, 2012) and high temporal sampling (~1 min).	- No measurements during rain - Poor quality data under heavy cloud cover - No global network of observations
	Sun photometer – determines the transmittance centred on the 946 nm water vapour absorption line, which is then converted to IWV using a radiative transfer modelling method.	- Global network (AERONET) of around 300 sites with long-term records of IWV (1993-present).	- Only works under clear sky conditions, introducing a negative bias, since cloudy conditions are often associated with higher IWV - Estimated precision of only about 10% (Alexandrov et al. 2009) - Pérez-Ramirez et al. (2014) found a consistent dry bias of 5-6% in IWV from AERONET, with total estimated uncertainty of 12-15%

	Very Long Baseline Interferometry (VLBI) – estimates zenith wet delay based on the time delays obtained from measurements by different antennas and from different astronomical radio sources (e.g. quasars) in different directions when the Earth is rotating.	- Stable instrumentation which leads to high long-term stability in measurements	- Measurements are not continuous (20-30 sessions/year) - Coverage is not global (90% of the total 150 telescopes are located in the northern hemisphere) - Typical formal error of ZWD of 3 mm (around 0.5 $kg.m^{-2}$ in IWV) (Ning et al., 2012)
	Global Positioning System (GPS) – estimates of zenith total delay (ZTD) are obtained from the delay in signal propagation between satellites and ground-based receiver due in part to the water vapour in the atmosphere. The ZTDs are then converted to IWV (more detail in section 2).	- Global network of stable long-term instrumentation (>500 stations, primarily land-based) - Works under all weather conditions - High temporal resolution(5-30 min) - Continuous temporal coverage from 1995-present - Uncertainty in IWV generally under 2 $kg.m^{-2}$ (Deblonde et al., 2005; Wang et al., 2007; Vey et al., 2010; Bock et al., 2013)	- Changes in processing options induce jumps in ZTD time series. Hence, only homogeneously reprocessed data should be used for climate analysis - Equipment changes and measurement conditions changes in the vicinity of the antenna (e.g.vegetation growing) induce breaks and drifts in time series (Vey et al., 2009) - Conversion from ZTD to IWV introduces uncertainties and biases - GPS series are relatively short for climate investigations (available from 1995 only)
Satellite-based – long-term IWV can be retrieved using three types of sensor (more extensive list shown in Fig. 1.3): 1) Thermal infrared sensors, such as HIRS (Shi and Bates, 2011), AIRS and IASI, that measure water vapour by layer, during day and night, over land and ocean. 2) Passive microwave profilers, such as SSM/I (Mears et al., 2007), AMSU-A and AMSR-E, which measure IWV during day and night, but only over the ocean. 3) Near infrared sensors, such as GOME, GOME-II, SCIAMACHY and MODIS, that retrieve IWV during the day, over land and sea (Wagner et al., 2006, Mieruch et al., 2008, Van Malderen et al., 2014).		- Global coverage (although resolution varies with sensor) - High accuracy over oceans - Long term data for HIRS (since 1979), SSM/I (since 1991) and GOME (since 1995, with GOME-II starting in 2006)	- Depending on sensors used, may not provide data under certain weather conditions, times of day, and over land areas

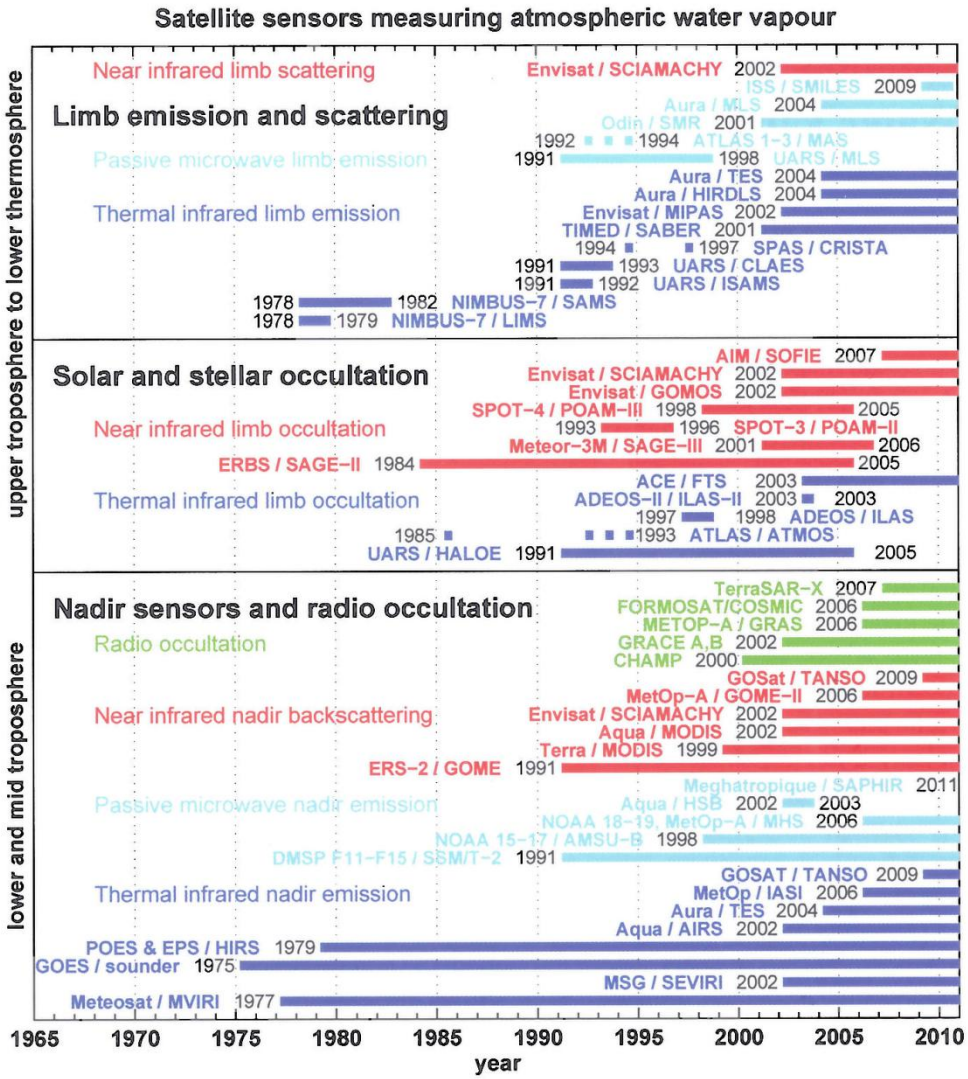

Figure 1.2: List of satellites that perform water vapour measurements in the low and medium troposphere, ordered by measurement type and observation duration (extracted from Kämpfer, 2013). Note: the start of ERS-2/GOME measurements is June 1995, not 1991.

1.2.2 Results from past studies of IWV trends

Several studies have reported on the long-term trends obtained from different IWV datasets. Ross and Elliot (2001) and Durre et al. (2009) have computed IWV trends using radiosonde measurements. Durre at al. (2009) used monthly mean surface-to-500 hPa PW obtained from radiosonde measurements at 300 sites in the Northern Hemisphere between 1973 and 2006. They found an overall positive annual trend, more intense in the Western Tropical Pacific, Japan, Western China, and Western Europe. In winter, they reported negative trends in Eastern Canada and the Mediterranean, which are possibly connected with trends in the North Atlantic Oscillation (NAO). In summer, they reported less intense trends, which are positive, overall.

Trenberth et al. (2005) computed the trends in global IWV datasets from SSM/I (Special Sensor Microwave/Imager, for the 1988-2003 period), ERA-40 reanalysis, NCEP reanalysis (see Table 2 for acronyms description), and the NASA Water Vapor Project (NVAP), which comprises a combination of radiosonde observations, Television and Infrared Operational Satellite (TIROS) Operational Vertical Sounders (TOVS), and SSM/I data sets (for 1988-2001). They found problems with NVAP in general, and with NCEP and ERA-40 over the oceans. The SSM/I data was found to be the only reliable data, but is only available over the ocean. In this case, trends are generally positive (0.4±0.09 mm.decade^{-1} or 1.3±0.3 %.decade^{-1}), which are linked with positive sea surface temperature (SST) trends (both spatially and temporally).

Bock et al. (2014) used IWV from homogenized DORIS (a dual-frequency Doppler system consisting of a receiver flying aboard a satellite and a globally distributed network of ground beacons) data at 81 sites (31 of which had over 10 years of data), and compared it with ERA-Interim reanalysis (ERA-I), GPS, SSM/I and radiosonde measurements. A good agreement was found between DORIS and GPS, ERA-I and SSM/I, with lower correlation and higher standard deviation of difference between DORIS and radiosonde data. The trends were computed for the 31 DORIS sites and were in good agreement with ERA-I. A general increasing trend was found, except in the South of the United States, Central America, Antarctica, and Western Australia. In ERA-I data (but not DORIS), IWV also decreases in eastern Asia.

Wang et al. (2016) used 2-hourly GPS, twice-daily homogenized radiosonde, and monthly mean SSM/I (at a 1°x1° resolution) data to compute a gridded monthly means dataset, for 1995-2011 (with GPS) and 1988-2011 (w/out GPS). They (in agreement with previous studies) found an average increase in PW over land and ocean for all time periods and datasets analyzed: 0.26 mm.decade^{-1} for 1995-2011 in GPS, 0.24 mm.decade^{-1} for 1973-2011 in radiosonde, and 0.34 mm.decade^{-1} for 1988-2011 in SSM/I. Trends were also found to be less intense over land. An

increase in PW was reported for Eurasia, inland Australia, parts of North America and most oceans except parts of the eastern and low-latitude Pacific.

Although there appears to be a general positive trend in the IWV data overall, it is hard to compare the results from different studies, as they relate to (not only different data sources, but also) different time periods, and different sites and spatial coverage.

1.3 Atmospheric reanalyses of atmospheric water vapour

1.3.1 An overview of currently-available global reanalysis datasets

As shown in the previous section, there are uncertainties associated with IWV observations. In order to get a more consistent product in time and space, atmospheric reanalyses are often used. Reanalysis is a scientific method for developing a comprehensive atmospheric record over time that combines observations and a numerical model that simulates one or more aspects of the Earth system in order to generate a synthesized estimate of the state of the system.

Reanalysis data provide a multivariate, spatially complete, and coherent record of the global atmospheric circulation, which means that the estimated parameters must be consistent with the laws of physics and with observations. This is achieved by using a forecast model to assimilate observations of various types and sources. The use of a realistic model also allows for the extrapolation of information from locally observed parameters to unobserved parameters at nearby locations, as well as a propagation of information forward in time. In addition, reanalyses are produced using a single assimilation system and the same version of the numerical model, and are therefore not affected by changes in method or model physics or dynamics, unlike operational analyses produced with Numerical Weather Prediction systems (Dee et al., 2011).

Several institutes produce their own reanalysis (summarized in Table 2). Their reanalyses have improved in quality over successive generations, because of better models and input data, as well as better assimilation methods (Dee et al., 2011). In addition, progress has been made to produce global estimates of the basic dynamical fields which are consistent with observations, given their estimated uncertainties (Dee et al., 2011). The important progresses in data computing have also allowed for assimilation of a growing variety of data products, and for producing reanalyses over longer time periods and at higher resolutions, which have been used extensively in climate research.

Table 1.2: List of currently-available global reanalysis datasets. Source: https://reanalyses.org/atmosphere/comparison-table (Originally submitted by Cathy.Smith@noaa.gov)

Institution	Reanalysis	Period	Approximate Resolution at Equator	Reference
European Centre for Medium-Range Weather Forecasts (ECMWF)	ECMWF 40 year Reanalysis (ERA-40)	1957-2002	125 km	Uppala et al. (2005)
	ECMWF Interim Reanalysis (ERA Interim)	1979-present	80 km	Dee et al. (2011)
	ECMWF 20th Century Reanalysis	1900-2010	125 km	Poli et al. (2016)
Japan Meteolorogical Agency (JMA)	Japanese 25-year Reanalysis (JRA-25)	1979-present	190 km	Onogi et al. (2007)
	Japanese 55-year Reanalysis (JRA-55)	1958-2012 (to be extended to present)	60 km	Ebita et al. (2011)
National Aeronautics and Space Administration (NASA), USA	NASA Modern-Era Retrospective analysis for Research and Applications (MERRA)	1979-2016	75 km	Rienecker et al. (2011)
	NASA MERRA-2	1980-present	5/8° lon x1/2° lat	Gelaro et al. (2017)
National Centers for Environmental Prediction (NCEP), USA	NCEP Climate Forecast System Reanalysis (CFSR)	1979-present	50 km	Saha et al. (2010)
NCEP/ Department of Energy(DOE), USA	NCEP/DOE Reanalysis AMIP (Atmospheric Model Intercomparison Project)-II (R2)	1979-present	320 km	Kanamitsu et al. (2002)
NCEP/ National Center for Atmospheric Research (NCAR), USA	NCEP/NCAR Reanalysis I (R1)	1948-present	320 km	Kistler et al. (2001)
National Oceanic and Atmospheric Administration/ Earth System Research Laboratory (NOAA/ESRL)	NOAA-Cooperative Institute for Research in Environmental Sciences (CIRES)20th Century Reanalysis (20CR)	1871-2012	320 km	Compo et al. (2011)
	NOAA-CIRES 20th Century Reanalysis (20CRV2c)	1851-2014	320 km	Compo et al. (2011)

1.3.2 IWV trends estimated from reanalyses

Nevertheless, to be useful in climate studies and trend estimation, reanalyses must be able to accurately represent variabilities at interannual and decadal scales, and to produce a homogeneous record of a variable, without shifts and spurious signals. These shifts can be introduced by the discontinuities in the assimilated products, which are in general not available throughout the whole period of the reanalysis. This has been analysed by Thorne and Vose (2010), who concluded that in order to produce climate-quality reanalyses, a substantial revamp of the current methodology is necessary. With regards to IWV in particular, this ability, has been called into question by several studies (Bengtsson et al., 2004; Dessler and Davis, 2010; Schröeder et al., 2016).

Bengtsson et al. (2004) assessed the temperature and IWV trends in ERA-40 reanalysis. For the 1979-2001 period, a +0.36 mm.decade^{-1} trend was found in IWV and a 0.11 mm.decade^{-1} in lower tropospheric temperature. This is about twice as high as the expected value according to the Clausius-Clapeyron ratio (assuming constant relative humidity). It is also higher than the trends obtained using free climate model integrations that are driven by the same sea surface temperatures as ERA-40. The authors proposed that the IWV trends computed do not represent genuine trends, but are in fact an artefact caused by changes in the global observing system during the period at study, such as the use of SSM/I and the use of more satellite soundings in the later years. They also show that the recent results are in good agreement with GPS IWV data, which was also concluded by Hagemann et al. (2003) and Bock et al. (2007).

Dessler and Davis (2010) compared five different reanalyses (NCEP/NCAR, ERA-40, JRA, MERRA and ERA-Interim; see Table 1.2) in terms of response of specific humidity to short-term and long-term climate variations. Their study was motivated by the results of Paltridge et al. (2009), who found a decreasing trend in mid- and upper-tropospheric specific humidity from 1973 to 2007 in NCEP data. Dessler and Davis (2010) showed that these negative trends are most likely not realistic. They found that all reanalyses show a generally positive response to short-term variations, but NCEP/NCAR differs from the others with a negative response to decadal warming trends in the tropical mid and upper troposphere. Bock et al. (2007) also showed that over Africa, NCEP/DOE reanalysis performed significantly worse than ERA40 when compared to GPS IWV data.

Finally, Schröeder et al. (2016) compared the IWV from three reanalysis (ERA-Interim, MERRA, CFSR) with three satellite-based IWV data records (HOAPS, REMSS, NVAP-M), for the 1988-2008 period. They analysed anomaly differences relative to HOAPS for averages over the global

ice-free oceans and found break-points, or series of breakpoints, which mostly coincided with changes in the observing system. These breaks were more pronounced in the central Africa, the Sahara, and South America regions. Schröeder et al. (2016) highlight the most important breaks, which are presented in Table 1.3.

Since the representation of climate signals in the reanalyses appears to be affected by changes of the global observing system and the presence of time-varying biases in models and observations, it is important to compare and use reanalysis in tandem with other observation-only datasets.

Table 1.3: Dates of observed break points and coincident changes in the observing system or changes of the input to the assimilation schemes based on the analysis of anomaly differences relative to HOAPS for the global ice-free ocean.(Source: Schröder et al., 2016)

Date	**Break size (kg.m-2)**	**Dataset**	**Event**
Jan 1991	-1.05	NVAP-M	Launch F-10: Dec 1990
Nov 1991	1.92	NVAP-M	Launch F-11: Dec 1991
Dec 1991	-0.62	ERA-Interim	Stop date F-08: Dec 1991
Dec 1994	-0.19	ERA-Interim	Launch of NOAA-14: Dec 1994; approximate stop of assimilation of NOAA-11 data (see Dee et al. 2011)
	0.88	NVAP-M	
Apr 1997	-0.26	ERA-Interim	Approximate change from assimilation of data from NOAA-12 to NOAA-11 (see Dee et al. 2011)
Oct 1998	1.31	CFSR	Begin of assimilation of NOAA-15 data in Oct 1998 (Chelliah et al. 2011); approximate end of assimilation of NOAA-11 and NOAA-14 data; change from assimilation of data from GOES-9 to GOES-10 (Saha et al. 2010)
Nov 1998	0.47	MERRA	Start of assimilation of NOAA-15 data (Rienecker et al. 2011)
May 2000	-0.10	ERA-Interim	Approximate start of assimilation of F-15 data and end of NOAA-11 and NOAA-15 data (see Dee et al. 2011)
Jul 2006	0.24	ERA-Interim	Close to end of assimilation of F-15 data, close to change from GOES-10 to GOES-11, start of Meteosat-5 and Meteosat-8, approximate end of assimilation of NOAA-14 data (see Dee et al. 2011)
	0.18	REMSS	Activation of a radar calibration beacon on F-15; REMSS includes beacon-corrected data from F-15 after July 2006
Sep 2007	0.13	ERA-Interim	Approximate end of assimilation of NOAA-16 data (see Dee et al. 2011)

1.4 Objectives and structure of the thesis

The main goal of this thesis was to characterize the variability and tends in global integrated water vapour in different data sets: GPS observations, weather reanalysis, and global climate models.

In order to do so, at a first stage, the ZTD data was characterized and the conversion of GPS ZTD into IWV was assessed with the goal of improving it. This conversion requires auxiliary data (refractivity constants, surface pressure, and weighted mean temperature) which can be obtained from different sources. Several different sources of surface pressure were compared, as well as different formulas to correct for the height difference between the pressure data and the GPS antenna. Different mean temperature datasets were also compared. The results are presented in Chapter 2, and were used to create a long term GPS IWV dataset.

The aforementioned IWV dataset was then compared with IWV from ERA-Interim, in Chapter 3, with the goal of documenting global and regional means, trends and variability. Both annual and seasonal analyses were performed for the period between 1995 and 2010, and the results from this comparison highlighted problems in both data sets. While in GPS these problems are mostly related with gaps and discontinuities in the time series; for ERA-Interim regions of uncertainty were also identified. These corresponded to areas where there is disagreement between ERA-Interim and GPS (which cannot be explained by errors in GPS), or areas of suspiciously intense trends where there are no long-term GPS stations. This prompted a comparison between ERA-Interim and a different reanalysis: MERRA-2. Two different periods are then assessed, the first one covers 1995-2010 as for the comparison with GPS, and the second one covers 1980-2016 which is the common period of the two reanalyses. Representativeness differences between the GPS observations and gridded fields from the reanalyses are sometimes also a limitation to the intercomparison, especially in coastal and mountainous regions. In a supplement to the core of Chapter 3 which is presented in the form of a paper to be submitted to ACP, a supplement is added in which two other reanalyses are studied: ERA-20C and 20CR. The interest in these reanalyses is that they cover the whole twentieth century and offer thus a comprehensive atmospheric dataset for climate studies over extended periods.

ERA-Interim reanalysis and GPS datasets were then compared with four configurations of the Institut Pierre Simon Laplace (IPSL) Laboratoire de Météorologie Dynamique's atmospheric general circulation model, LMDZ in Chapter 4. For this comparison, the goals were two-sided. On the one hand, GPS and ERA-Interim were used to assess how well the different model

configurations are able to represent the mean, variability and trends in IWV. On the other hand, the differences obtained for the different configurations can be used to interpret the origin of the IWV trends (dynamics vs. moist processes).

Finally, the main conclusions of this thesis are summarized in Chapter 5, and some perspectives for further work are presented.

Chapter 2: Elaboration of a reference long-term IWV dataset from ground-based GNSS measurements

2.1 The ZTD data

In the ground-based Global Navigation Satellite System (GNSS) technique, dual-frequency signals emitted from the satellites are captured by the user's receiver at the surface (Hofmann-Wellenhof et al., 2008). The measurements are expressed as the time of flight of the radio signals that propagate from satellites to receivers, or as the equivalent distance for a signal propagated at the speed of light. From these measurements, parameters such as the zenith tropospheric delays (ZTD) are estimated, using an optimization method (Least Squares or Kalman filter methods). The parametric model includes many physical phenomena that impact the propagation and measurement of the signal, including the propagation delays in the troposphere and ionosphere. The operator has several options for the GPS data processing. These include the session duration, the elevation cut-off angle (elevation angle under which the measurements are not considered), the weighting of observations according to their elevation angle, and the correction models for the different instrumental features (e.g. antenna phase centre variations) and geophysical phenomena that affect the measurements (e.g., tides). The choices depend on the software used and on the optimization method. The tropospheric parameters can be estimated based on a deterministic model (piece-wise linear, such as in Bernese software) or on a stochastic model (Gauss-Markov such as in GAMIT software or random walk in GIPSY software). The results will vary slightly with both the software and the settings used.

The ZTD dataset used in this work was obtained from the International GNSS Service (IGS) *repro1* (first Data Reprocessing Campaign) tropospheric solution produced by NASA's Jet Propulsion Laboratory (JPL) in May 2010, for the period between January 1995 and December 2007. For the period between January 2008 and December 2010, we used the IGS *trop_new* solution, which was reprocessed in a consistent manner by the JPL (Byun and Bar-Server, 2009) but using the operational orbits, clocks and EOP products. The processing characteristics used (in accordance with IGSMAIL-6298) are presented in Table 2.1. The network used is a global network, with 460 stations in total, of which 120 sites have time series spanning 15 or more years (shown in Figure 2.1).

Table 2.4: Processing characteristics of ZTD data used

Software	GIPSY-OASIS[1] II in PPP[2] mode
Fixed orbits and clocks	IGS Final Re-Analyzed Combined (1995-2007), and IGS Final Combined 2008-2011
Earth orientation	IGS Final Re-Analyzed Combined (1995-2007), and IGS Final Combined (2008-2011)
Transmit/Receiver antenna phase center map	IGS Standards (APCO[3]/APCV[4])
Elevation cut-off angle	7 degrees
Mapping function (hydrostatic and wet)	GMF[5]
A priori delay (m)	hydrostatic=1.013×2.27×exp(-0.116×ht); wet=0.1
Data arc	24 hours
Data rate	5 minutes
Temporal resolution of tropospheric estimates	5 minutes
Estimated parameters	station position (daily), station clock (white noise), wet zenith delay (3 mm/h$^{1/2}$ random walk), delay gradients (0.3 mm/h$^{1/2}$ random walk), phase biases (white noise)

[1] GNSS-Inferred Positioning System and Orbit Analysis Simulation Software

[2] Precise Point Positioning

[3] Antenna Phase Center Offset

[4] Antenna Phase Center Variation

[5] Global Mapping Function

The IGS repro1 data was the result of a reanalysis of the full history of GPS data collected by the IGS global network since 1994 in a fully consistent way using the best models and methodology available at the time. This represents a collaborative effort between ten participating Analysis Centers. At the moment, the processing options used in repro1 are out-dated, and a 2nd Data Reprocessing Campaign was launched in late 2013. However, ZTD data from repro1 was the only one available at the beginning of this work. Furthermore, for repro2 (unlike repro1), an official ZTD solution is not available, raising the question of which Analysis Center's solution to use. This is something that will be determined in future work.

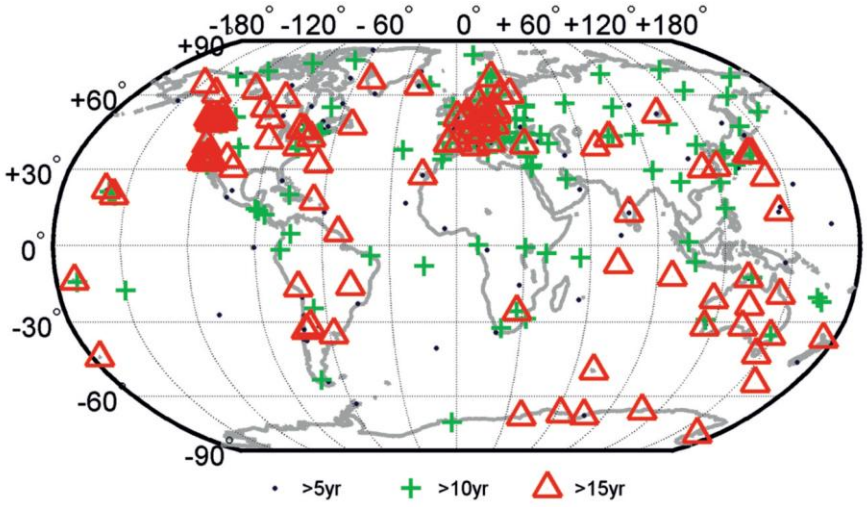

Figure 2.3: Distribution of stations in the IGS global network with the duration of measurements available, between January 1st 1995 and December 31st 2010. Source: O. Bock (2014).

In addition to the IGS, other networks that provide ZTD estimates include the Tide Gauge Benchmark Monitoring Working Group network (TIGA) and the EUREF (European Reference Frame) Permanent GNSS Network (EPN). The TIGA network aims at processing and re-processing GPS data of IGS stations near tide gauges, in order to provide homogeneous, long-term sea level records (Schöne et al., 2009). Ning et al. (2016), used ZTD data from 101 sites that had more than 15 years of data out of 794 sites that had been reprocessed by the German Research Centre for Geosciences (GFZ) in the framework of the TIGA project (their data coverage was from January 1994 to December 2012). The EPN network consists of a network of continuously operating GNSS reference stations, operated by 16 analysis centres that routinely analyse the GNSS data over Europe (http://www.epncb.oma.be/_productsservices/analysiscentres/LAC.php). Two reprocessing campaigns were also conducted by EPN (which relied on the satellite and EOP products issued by the above-mentioned IGS reprocessing efforts). Contrary to the IGS troposphere products (both operational and reprocessed) which are processed by a single analysis centre, the EPN troposphere products are a combination of the solutions processed by all EPN analysis centres (http://www.epncb.oma.be/_productsservices/troposphere/). The EPN repro2 combined solution is claimed as the best GNSS troposphere dataset over Europe (Pacione et al., 2016).

2.2 GPS ZTD data screening

The estimated ZTD parameters often contain outliers, i.e. unrealistic or erroneous values that must be removed before the data can be further used for scientific purposes. This post processing (screening) of the ZTD data is done by applying range checks and outlier checks. The range check defines upper and lower limits to the data which are defined independently of the data itself, while in the outlier check the limits are computed from the data.

2.2.1 Range check

The range check aims at rejecting unrealistic values that do not make physical sense. The upper and lower limits in this check are defined based on physical values, and are constant for all stations and for the entire observation period.

According to Davis et al. (1985), the GPS zenith tropospheric delay (ZTD) can be divided into a priori zenith hydrostatic delay (ZHD) and estimated zenith wet delay (ZWD):

$$ZTD = ZHD + ZWD \qquad (2.1)$$

The limits for ZHD and ZWD were roughly estimated using the rule of thumb formulas given below:

$$ZHD \approx 0.00227\, P_s \qquad (2.1a)$$

$$ZWD \approx IWV/152 \qquad (2.1b)$$

Where P_s is the surface pressure. The units in these equations are: Ps (hPa), IWV (kg m^{-2}), ZHD and ZWD (m). According to ERA-Interim data for August 2012, P_s, is between 521 and 1046 hPa, so that ZHD is between 1.20 to 2.41 m globally, and IWV is between 0.05 to 83 kg.m^{-2}, so that ZWD is between 0.00 and 0.54 m, globally. Therefore, the adopted lower and upper range limits for the ZTD range check were 1 and 3 m, respectively. These values were adopted globally, and might be tightened in the case of a regional analysis where Ps and Tm vary over a smaller range of values.

The formal errors of ZTD (denoted as σ_{ZTD}) are obtained during the processing of the GPS data and can also be used in the range check. They are a measure of precision of the ZTD estimate (but not accuracy), and temporal variations in formal errors indicate variations in the quality of observations. In fact, the larger spikes in formal error coincide with obvious ZTD outliers, and are usually due to a drop in the number of observations. Meanwhile, smaller spikes in formal error help detect potential errors in ZTD which are difficult to pinpoint otherwise.

For the data used in this work, we set the lower and upper limits of the range check for the ZTD formal errors to 0 and 6 mm, respectively. These limits hold for the IGS repro1 dataset used in this work and should be revised for a GPS ZTD dataset determined with different processing options or different software.

2.2.2 Outlier check

The outlier check's goal is to reject inconsistent data, with regard to station climatology (based on yearly means). The outlier check is done through statistical analysis of the ZTD values at each station, and for each year. For the data used in this work, the outlier check for ZTD values was based on a fixed range of ±0.5 m around the station's median yearly values. For formal errors, the lower was set to 0 and the upper limit was set to 2.5 times the median of all yearly values, as illustrated for one station (MATE) in Fig. 2.2.

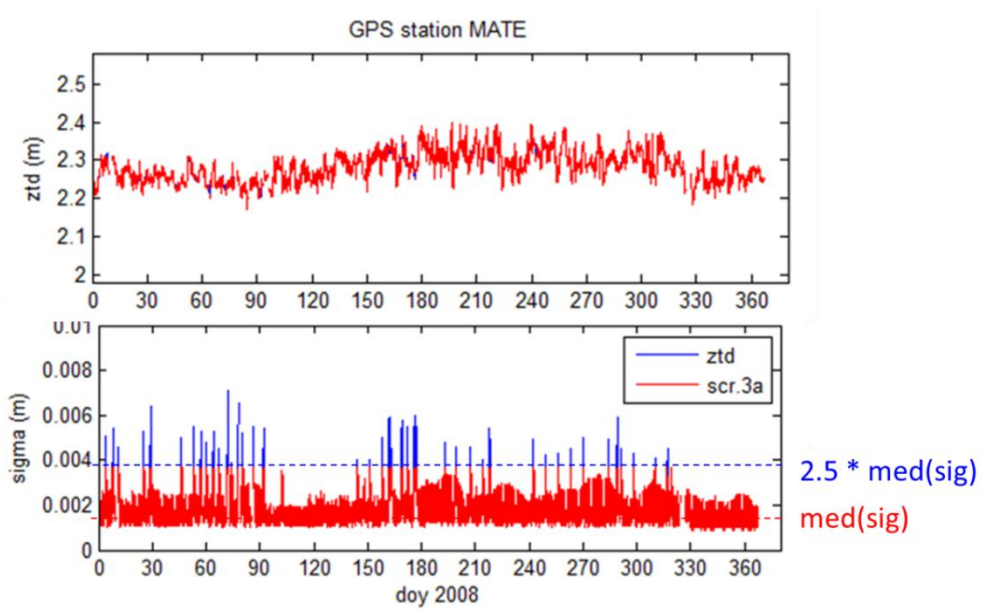

Figure 2.4: Original and screened ZTD and ZTD formal error (sigma) in blue and red, respectively, for the MATE GPS station.

This screening (range and outlier checks combined) leads to a rejection rate of only 0.08% of the values. Figure 2.3 shows the proportion of data rejected due to each of the 4 tests every year. It is seen that around year 2001 there are more data rejected. This peak coincides with a maximum in solar activity (which follows roughly a 11-year cycle) and it is hypothesized that increased ionospheric fluctuations could be the reason for more noise in the GPS measurements. The second maximum of data rejection in 2009 is due to the rejection of ZTDs from the operational IGS trop new solution of 2009 that remained in the IGS archive when the data were reprocessed in 2010. The older ZTD estimates had larger formal errors.

The screening is applied to ZTD data at the nominal 5-minute resolution. After the screening, the ZTD data are averaged into hourly time bins centred on round hours (00, 01 … 23 UTC).

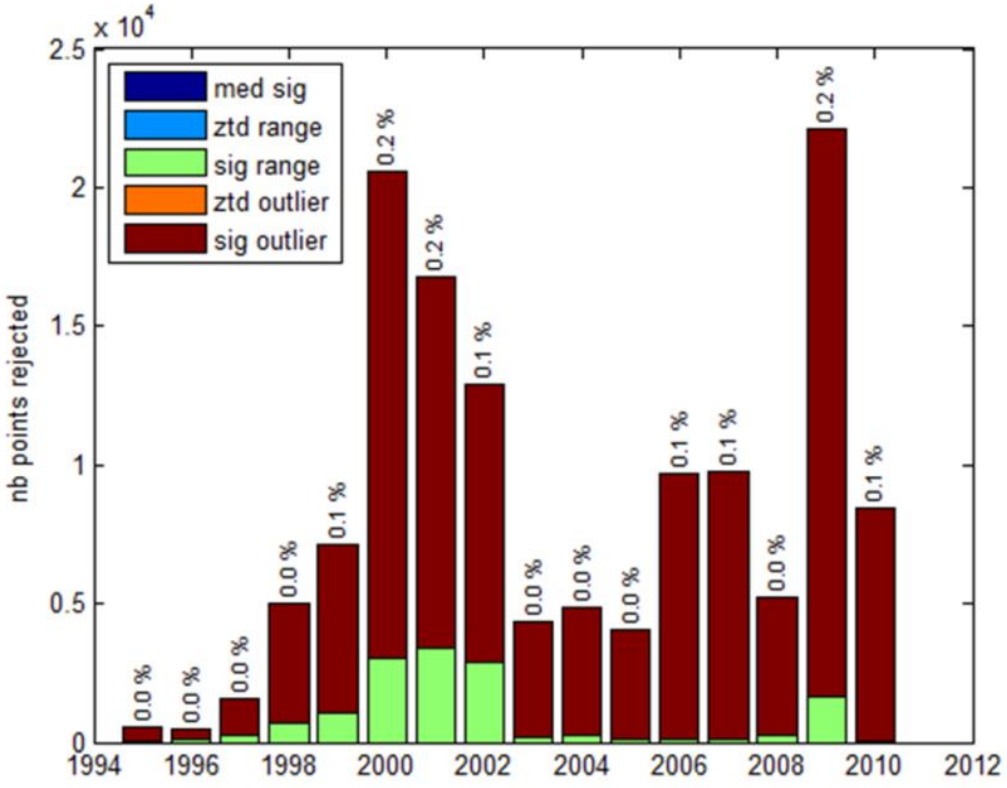

Figure 2.5: Number of points rejected in the ZTD time series divided by year and type of screening. Most rejections occur after formal error range check ("sig range", in green) and formal error outlier check ("sig outlier", in red).

2.3 Conversion of ZTD data to IWV

2.3.1 Basic equations

For our purpose we need a more accurate conversion of ZTD to IWV than computed with the rule of thumb equations (2.1a) and (2.1b). The ZTD and IWV estimates are linked by:

$$IWV = K(Tm) \times ZWD = \kappa(Tm) \times (ZTD - ZHD) \tag{2.2}$$

in which ZHD is computed using (Saastamoinen, 1972; Davis et al., 1985)

$$ZHD = 10^{-6} k_1 \frac{R_d}{g_m} P_s \tag{2.3}$$

And the water vapour mass conversion factor, $\kappa(Tm)$, is computed with (Bevis, 1992)

$$\kappa(T_m) = \frac{10^6}{R_v \left(k'_2 + \frac{k_3}{T_m}\right)} \tag{2.4}$$

where $R_d = 287\, J.K^{-1}.kg^{-1}$ and $R_v = 461.5\, J.K^{-1}.kg^{-1}$are specific gas constants, $k'_2 = k_2 - k_1 \times (R_d/R_v)$; k_1, k_2 and k_3 are refractivity constants, P_s is the surface pressure, and T_m is the weighted mean temperature. The mean gravitational acceleration at the station, g_m, is defined as (Saastamoinen, 1972; Davis et al., 1985):

$$g_m = 9.784(1 - 0.00266 * \cos(2 * \lambda)) - (2.8e - 7) * H$$

where λ is the latitude of the GPS site, and H is the altitude of the GPS site (in meters).

Tm is defined (Bevis, 1992) as:

$$Tm \equiv \frac{\int \frac{Pv}{T} dz}{\int \frac{Pv}{T^2} dz} \tag{2.5}$$

Where Pv is the partial pressure (in hPa) of water vapor, T is the atmospheric temperature (in K), and z the geometric height above the surface (in m). Tm can be estimated using radiosonde profiles and NWP model analysis or forecasts. These account for spatial variations in Tm, although they usually require vertical and temporal interpolations.

The rule of thumb equations (2.1a) and (2.1b) have been determined by replacing the various constants in equations (2.3) and (2.4) by standard values and by refractivity constant from Thayer (1974). A global mean value of $T_m = 268$ K leads to $\kappa = 152$ kg m^{-3} as given in Eq. (2.1b), and g_m =9.784 m.s^{-2} leads to Eq. (2.1a).

2.3.2 Error analysis

An error analysis can be conducted based on equations (2.2), (2.3) and (2.4) to estimate the contribution of the various parameters to the total uncertainty in IWV. Let us first consider the set of independent parameters: ZTD, Ps, and Tm. The total error in IWV resulting from errors in these three parameters can be derived from:

$$\delta IWV = \left(\frac{\partial IWV}{\partial ZTD}\right)\delta ZTD + \left(\frac{\partial IWV}{\partial Ps}\right)\delta Ps + \left(\frac{\partial IWV}{\partial Tm}\right)\delta Tm \tag{2.6}$$

Using Eq. (2.2) to (2.4) the partial derivatives can be expressed as:

$$\left(\frac{\partial IWV}{\partial ZTD}\right) = \kappa \approx 152 \text{ kg m}^{-3} \tag{2.7a}$$

$$\left(\frac{\partial IWV}{\partial Ps}\right) = -\kappa\frac{ZHD}{Ps} \approx -0.35 \text{ kg m}^{-2}\text{.hPa}^{-1} \tag{2.7b}$$

$$\left(\frac{\partial IWV}{\partial Tm}\right) = \frac{10^{-6}.R_v.k_3.\kappa.IWV}{Tm^2} \approx \frac{IWV}{Tm} \approx 0.069 \text{ kg m}^{-2}\text{.K}^{-1} \tag{2.7c}$$

The first approximation in (2.7c) relies on the fact that $k'_2 \ll \frac{k_3}{T_m}$, considering e.g. $k_2 = 64.79$ K.hPa^{-1} and $k_3 = 3.776 \times 10^7$ K^2.hPa^{-1} as determined by Thayer (1974) and $T_m = 268$ K. The final numerical values in all three expressions above are obtained also assuming IWV=18.5 kg m^{-2} (a typical global mean value) and ZHD = 2.3 m (a typical mean sea level value obtained from Ps=1013 hPa).

The set of equations (2.7) quantify the sensitivity of IWV error to errors in the independent parameters. Hence, 1 mm of error in ZTD converts into 0.15 kg.m^{-2} of error in IWV; 1 hPa error in Ps converts into 0.35 kg.m^{-2} error in IWV; 1 K error in Tm converts into 0.069 kg m^{-2} or expressed in a percentage, 1% of error in Tm (ca 2.7 K) converts into 1% of error in IWV (ca 0.18 kg.m^{-2} assuming a global mean IWV of 18.5 kg m^{-2}). If we seek at providing GNSS IWV estimates with an absolute accuracy of say 0.1 kg m^{-2}, then ZTD should be estimated to better than 0.7 mm; Ps should be given to better than 0.3 hPa, and Tm to better than 0.5 K.

When the errors in the individual parameters are known, the total error can be computed from the sum of the individual errors according to Eq. (2.6). When only statistical knowledge is available about the individual errors (e.g. mean and standard deviation of errors) and independence of the errors can be assumed, then Eq. (2.6) can be used to derive the overall mean error (or bias) in IWV as the sum of the individual mean errors and the overall standard deviation as the root sum of squares of the individual standard deviations.

When absolute accuracy of the IWV retrieval is of interest, the uncertainty in the refractivity constants needs also to be taken into account. The total error in IWV resulting from errors in the three refractivity constants can be derived from:

$$\delta IWV = \left(\frac{\partial IWV}{\partial k_1}\right)\delta k_1 + \left(\frac{\partial IWV}{\partial k_2}\right)\delta k_2 + \left(\frac{\partial IWV}{\partial k_3}\right)\delta k_3 \tag{2.8}$$

Using Eq. (2.2) to (2.4) the partial derivatives can be expressed as:

$$\left(\frac{\partial IWV}{\partial k_1}\right) = -\kappa\frac{ZHD}{k_1} + 10^{-6}.R_d.\kappa.IWV \approx -\frac{356}{k_1}\ \text{kg m}^{-2} \approx -4.59\ \text{kg m}^{-2}.(\text{K.hPa}^{-1})^{-1} \tag{2.9a}$$

$$\left(\frac{\partial IWV}{\partial k_2}\right) = -10^{-6}.R_v.\kappa.IWV \approx -0.0715.IWV \approx -0.0132\ \text{kg m}^{-2}.(\text{K.hPa}^{-1})^{-1} \tag{2.9b}$$

$$\left(\frac{\partial IWV}{\partial k_3}\right) = \frac{-10^{-6}.R_v.\kappa.IWV}{Tm} \approx -0.0715\frac{IWV}{Tm} \approx -4.9.10^{-5}\ \text{kg m}^{-2}.(\text{K}^2.\text{hPa}^{-1})^{-1} \tag{2.9c}$$

The sensitivity of IWV error to an error in k_1 is thus: 3.56 kg m^{-2} per 1% of error in k_1 or 4.59 kg m^{-2} per 1 K.hPa^{-1} of error in k_1 (the latter assumes k_1 = 77.6 K.hPa^{-1}, from Thayer, 1974). If we seek at providing GNSS IWV estimates with an absolute accuracy of say 0.1 kg m^{-2} the uncertainty in k_1 should be smaller than 2.8 * 10^{-4} = 0.028% in relative value or 0.022 K.hPa^{-1} in absolute value, the uncertainty in k_2 should be smaller than 7.6 K.hPa^{-1} or 12%, and the uncertainty in k_3 should be smaller than 2.10^4 K^2.hPa^{-1} or 5.4%. From these values, we conclude that the highest sensitivity of IWV errors come from the uncertainties in k1, followed by k3 and k2.

As different authors proposed different values for the refractivity constants and their uncertainties, their impact on IWV uncertainty will be investigated in more detail in the next sub-section.

Last, the uncertainty in ZHD due to g_m using Eq. (2.3) is estimated to be 0.3 mm (Davis et al., 1985). This error source can be neglected for our purpose here. When higher accuracy is required, a more accurate formula derived by Bosser et al. (2007), can be used.

2.3.3 Uncertainty in the refractivity constants

The refractivity constants quantify the interactions between the electromagnetic waves and the atmosphere (molecular polarizability of the air). They have been determined experimentally by direct measurements, using microwave cavities (Boudouris, 1963). However, most measurements were carried out prior to 1960, and efforts to compile and average the experimental results have ensued (e.g. Smith and Weintraub, 1953; Hasegawa and Stokesbury, 1975). Thayer (1974) computed a set of values based on earlier refractivity measurements in the radio and optical portions of the electromagnetic spectrum. Following Davis et al., (1985), we adopted in this work Thayer's (1974) values and uncertainties: $k_1 = (77.604 \pm 0.014)\ K.hPa^{-1}$, $k_2 = (64.79 \pm 0.08)\ K.hPa^{-1}$ and $k_3 = (3.776 \pm 0.004) \times 10^5\ K^2.hPa^{-1}$.

Bevis et al. (1994) computed an average of the constants determined through direct measurements by more than 20 authors, obtaining the following values and uncertainties: $k_1 = (77.60 \pm 0.05)\ K.hPa^{-1}$, $k_2 = (70.4 \pm 2.2)\ K.hPa^{-1}$ and $k_3 = (3.739 \pm 0.012) \times 10^5\ K^2.hPa^{-1}$.

Although these are the most commonly used values in the GPS meteorology community, more recently, Rüeger (2002) has determined a "best average" of the coefficients, based on a thorough reassessment of the existing measurements. Rüeger (2002) has also taken into account the fact that the k_1 constant depends on the relative concentrations of the dry atmospheric gases, so that variations in the carbon dioxide concentration has an impact on k_1. For a CO_2 content of 375 ppm (around year 2004), the following 'best average' coefficients are obtained: $k_1 = (77.689 \pm 0.0094) K.hPa^{-1}$, $k_2 = (71.2952 \pm 1.3)\ K.hPa^{-1}$ and $k_3 = (3.75463 \pm 0.0076) \times 10^5\ K^2.hPa^{-1}$.

Figure 2.4 shows the values and their uncertainties from the three authors mentioned above. For k1 and k2, the largest difference to Thayer (1974) is with Rueger (2002), while for k3 it is with Bevis (1994). The largest uncertainties are those given by Bevis (1994).

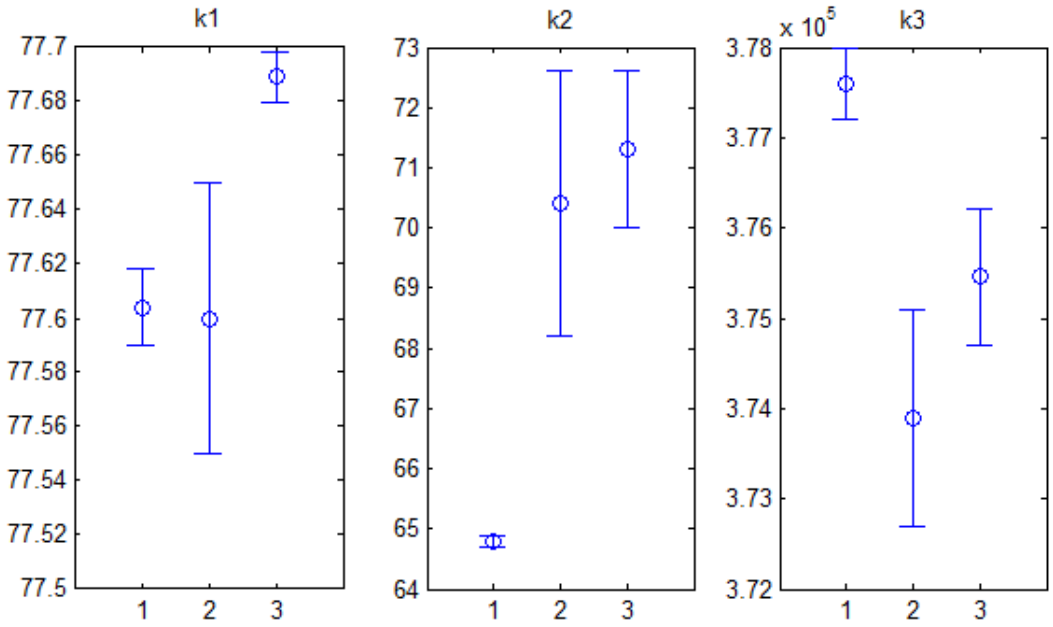

Figure 2.4: refractivity constants (k1, k2, k3) and their uncertainties (error bars) as published by Thayer (1974), Bevis (1994) and Rueger (2002), plotted at position x=1, 2, 3, respectively.

The impact of using the Thayer (1974) refractivity constants on the IWV estimates in place of using those from Bevis et al. (1994) or the Ruëger (2002) is presented in Table 2.2. From these values, we conclude that the maximum uncertainty is due to k1 followed by k3 and then k2. The uncertainty associated with these coefficients calls for a more robust determination of their values. The need for new measurements of these constants was reinforced by Healy (2011), who found that the uncertainty in the k1 refractivity coefficient is larger than expected. Healy (2011) concludes that the k1 coefficient suggested by Rüeger appears to be more robust but should be corrected for nonideal gas effects: $k_1 = 77.643\ K.hPa^{-1}$. In this case, the bias in IWV in relation to Thayer (1974) is -0.18 kg.m^{-2}. The uncertainty estimates used in Table 2 are the most adverse, i.e. those from Bevis (1994).

Table 5: Maximum bias (∆ki) between the constants determined by Thaye,r(1974 (TH74) and those determined by Bevis et al., 1994 (BE94) or Rüeger, 2002 (RU02). For the uncertainty (σki) Bevis (1994) values are used as the most adverse.

		Δk_i	$\Delta k_i/k_i * 100$ (%)	ZHD or ZWD error (mm)	IWV error ($kg.m^{-2}$)
$\Delta k1$	TH74–RU02	-0.039 K/hPa	-0.050%	-2.5	-0.39
$\Delta k2$	TH74–RU02	-6.51 K/hPa	-10%	-0.56	-0.086
$\Delta k3$	TH74–BE94	3700 K^2/hPa	1.0%	1.2	0.18
$\sigma k1$	BE94	0.050 K/hPa	0.064%	1.5	0.23
$\sigma k2$	BE94	2.20 K/hPa	3.4%	0.19	0.029
$\sigma k3$	BE94	1200 K^2/hPa	0.32%	0.38	0.059

2.3.4 Assessment of Ps data

Surface pressure (Ps) data is not often observed at the GPS sites. Only a small number of IGS stations (about 70) are equipped with PTU (Pressure-Temperature-Humidity) sensors, and studies have pointed out inaccuracies in their data (Wang et al., 2007; Heise et al., 2009). The main accuracy issues in PTU data are calibration issues and data gaps. PTU sensors need to be calibrated every 1 to 2 years in order to avoid loss of accuracy due to sensor drifts and aging, and in some remote places there might be long delays after failures and breakdowns in the sensors, before they are replaced.

Nevertheless, Ps can also be obtained from various other sources. It can be retrieved from observations, such as World Meteorological Organization (WMO) surface synoptic observations (SYNOP), or from numerical weather prediction (NWP) model outputs, such as operational analysis/forecasts or reanalysis. Each data source has different availabilities, temporal and spatial resolutions and accuracies. Errors in Ps data include errors in equipment calibration and measurement noise (in the case of observations) and representativeness errors, biases, assimilation increments (in the case of model analysis/ reanalysis), and model drifts (in the case of forecasts or free simulations). Keeping in mind that an error of 1 hPa in Ps leads to an error of 2.3 mm in ZHD and an error of 0.35 $kg.m^{-2}$ in IWV (see Eq. 2.1a and 2.1b), it is important to choose the most accurate pressure data available.

SYNOP stations measure station level pressure at about 8500 sites, with mostly 1- to 6-hourly reports from a synoptic network operated globally by around 200 National Weather Services. The main issues that arise when using SYNOP data for GPS IWV conversion are related to sensor calibration, which has not been performed in a consistent manner across all stations over time, and height correction to the GPS altitude (Ingleby, 1995).

For non-collocated data sources, a correction to the height difference between pressure data and the GPS antenna is required. This correction is commonly made using the following formula by Berg (1948):

$$P_s = P_0(1 - 0.0000226(z_s - z_0))^{5.225} \tag{2.10}$$

in which P_0 is the pressure observation at station height z_0, and $z_s - z_0$ is the height difference.

This is an approximation of (ICAO, 1993):

$$P_s = P_0\left(1 + \frac{\alpha}{T_0}(z_s - z_0)\right)^{-g/\alpha R_d} \tag{2.11}$$

Where two additional parameters are introduced: α the temperature lapse rate and T_0 the temperature at station height z_0. The Berg 1948 formula is obtained assuming the International Standard Atmosphere, with T_0=288 K, α=-6.5 K.km^{-1}, R_d=287 J.K^{-1}.kg^{-1} and g=9.80665 m.s^{-2}.

Although this parametrization of pressure as a function of height might be a good approximation in the troposphere where, according to Yang and Smith (1985) and Wang et al. (2005) α varies between -5 and -6 K.km^{-1} from 70°S to 70°N, it is not a good approximation of the surface temperature lapse rate. In fact, the surface temperature lapse rate has been shown to vary substantially, from -3 to -9 K.km^{-1} for mid-latitude surface conditions (Minder et al., 2009). Furthermore, Rolland et al. (2003), in a systematic comparison of previously published studies, pointed out lapse rates ranging from +2.8 (in the Scrivia River valley, reported by Cortemiglia (1988)) to -12.7 K.km^{-1} (for July, in the occidental Italian Alps (Cortemiglia, 1989)). According to Minder et al. (2009), the surface lapse rates exhibit spatial variability, and depend on the aspect of the slope and relative position to the valleys. In addition, lapse rates also have marked seasonal cycles and diurnal variability, with lower lapse rates applicable in winter and at night (Ingleby, 2014). The impact of the difference in the lapse rate on the pressure height corrections was assessed. The pressure was computed for every α from -2 to -11 K/km, by -0.5 K/km, using

Eq. 2.10, for altitudes from 0 to 2000m. The resulting plots were compared with the case where α is constant and equal to -6.5 K.km^{-1}.

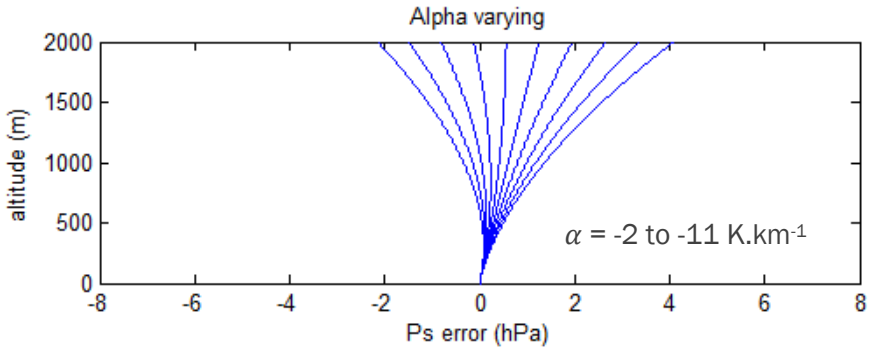

Figure 2.5: Impact of lapse rate variations on the Berg approximation.

As seen in Figure 2.5 the differences in pressure increase as altitude (or difference in altitude) increases, and as the difference between α and the standard -6.5 K.km^{-1}rate (Δα) increases. Even though over the first 500m these differences remain fairly small (up to +/-0.3hPa, for higher Δα), they can reach up to between -2 hPa and 4 hPa just below 2000m (depending on α). The differences also vary with P_0 and T_0 used in the pressure and temperature equations, however the differences are of the same order of magnitude. Therefore, it appears that using the standard value of the temperature lapse rate produces an acceptable uncertainty in Ps (< 0.3 hPa) when extrapolating pressure measurements over altitude differences under 500m.

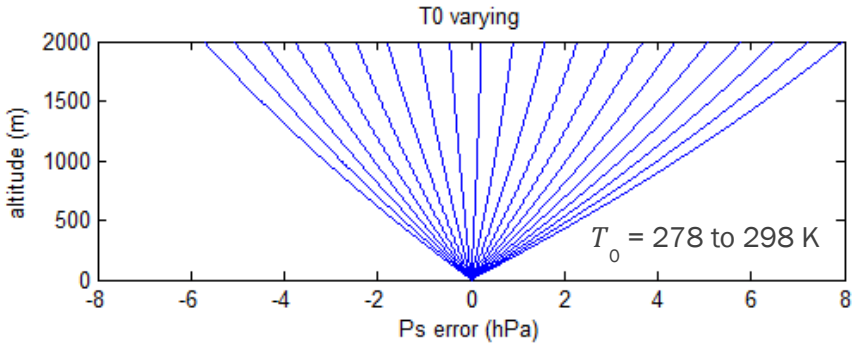

Figure 2.6: Impact of surface temperature variations on the Berg approximation.

The Berg formula (2.5) also considers the T_0 to be constant and equal to 288K. This is of course not true in most of the globe, where surface temperatures vary widely (in time and space). Figure 2.6 shows the error associated when T_0 varies in the range 278 to 298 K. The differences are relatively big, up to ±2 hPa when extrapolating pressure measurements within the first 500m.

We conclude that T_0 is more important in the pressure extrapolation, within 500m, than the temperature lapse rate. This is expected considering Eq. (2.10) and that if $x \ll 1$:

$$(1+x)^a \approx 1 + ax \tag{2.12}$$

This approximation holds for values of vertical distance $(z - z0) < 500$ m where $\frac{\alpha(z-z0)}{T_0} < 10^{-2}$. Hence, Eq. (2.11) can be approximated to:

$$P \approx P_0 \left(1 - \frac{\alpha(z-z0)}{T_0}\frac{g}{R\alpha}\right) = P_0 \left(1 - \frac{(z-z0)}{T_0}\frac{g}{R}\right) \tag{2.13}$$

Equation (2.13) predicts that (for height differences below 500m) the pressure variation does not depend on the lapse rate but only on T_0 and of course the height difference $(z - z0)$.

In addition, the pressure extrapolation can also incur errors if the station heights are not well-known. From Eq. (2.13) we estimate $\frac{\partial P}{\partial z} = -0.12$ hPa.m^{-1}. An error in height of +8 m leads thus to a pressure error of -1 hPa, therefore, the pressure sensor altitude must be known within ±2.5m if pressure is to be known within ±0.3 hPa. While efficient quality control tools have been developed for the assimilation of observations in NWP systems (Ingleby, 2014), inaccurate knowledge of station heights is a major error source with SYNOP stations (Ingleby, 1995). Furthermore, undocumented changes in station height and coordinates (e.g. relocation of a station) can also result in discontinuities. Biases and discontinuities in the Ps data from a subset of European SYNOP observations have been evaluated by comparison with ERA-Interim reanalysis (see below).

Reanalysis data is an alternative surface pressure source with the advantage over operational analyses that the model version and grid resolution are consistent over time. ERA-Interim has been intensively used in recent years. Two “surface pressure” fields are actually archived for ERA-Interim at ECMWF (http://apps.ecmwf.int/datasets/data/interim-full-daily/). One is available as a surface level (SF) field and one as a model level (ML) field. The latter is actually archived as the logarithm of surface pressure (variable name ‘lnsp’) and is used to reconstruct the pressure and geopotential from the spectral model fields.

It was noticed in previous studies that surface pressure from the ML archive available at IPSL Data Centre (climserv) exhibited large biases (up to ±10 hPa) compared to SYNOP observations in some regions. The reason for this difference was not clear (they were not due to biases in observations) and thus mean sea level pressure (MSLP) data from the reanalysis was used instead (O. Bock, personal communication). This problem was reassessed here because using MSLP as P_0 would require extrapolation of pressure over a too large vertical distance for stations in mountains. Figure 2.7 compares both versions of ERA-Interim surface pressure fields (ML and SF) for January 2012. Positive and negative ripples up to ±20 hPa are seen in the differences, mainly in coastal and mountainous areas. Similar ripples can also be seen in the surface geopotential. The reason for these ripples is the Gibbs phenomenon arising when variables represented in spectral space (as is the case for ML fields) are transformed back to grid point space when being extracted to a regular latitude/longitude grid (Uppala et al., 2005). Comparison of both versions to SYNOP observations confirms that the SF version is the one to be used.

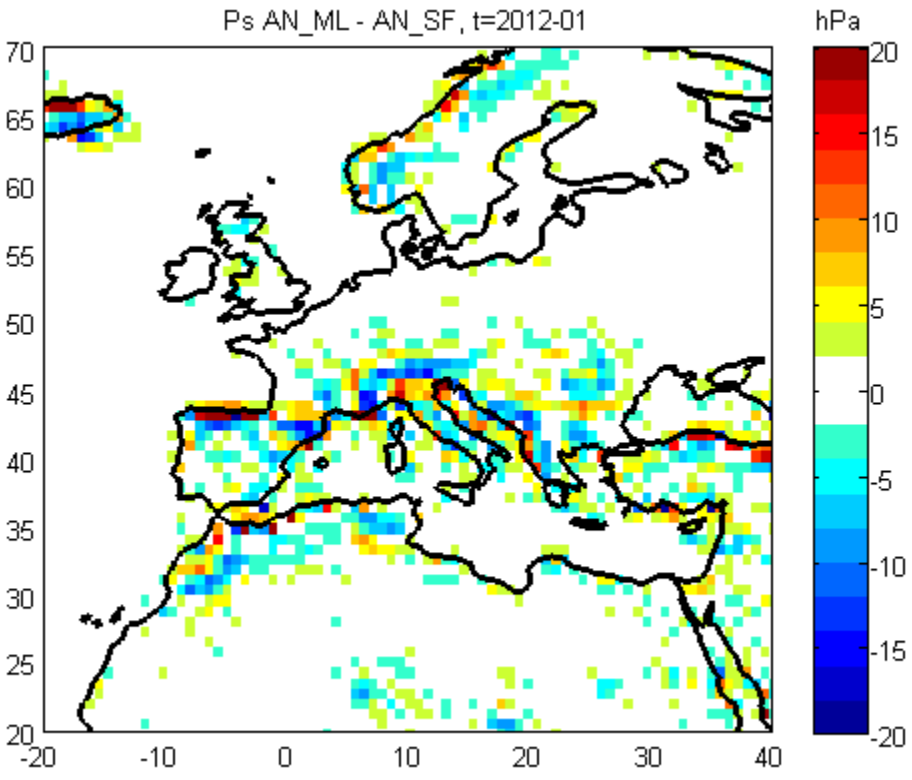

Figure 2.7: Difference fields between surface pressure as a model level field (ML) and surface pressure as a surface level field (SF) in ERA-Interim.

We can now compare the surface pressure extrapolated from MSLP using Eq. (2.11) and surface pressure from SF fields. In Eq. (2.11) we need also the temperature at mean sea level, T_0. This temperature was extrapolated from the temperature field at 1000 hPa using Eq. (2.14) below, where α=-6.5 K.km^{-1}.

$$T_0 = T_{1000} + \alpha(z_0 - z_{1000}) \qquad (2.14)$$

Figure 2.8 shows that the difference is small in regions like Europe, Australia, most of Asia, Africa and Americas, but can become quite large (±15 hPa) in regions at high altitudes (Antarctica, Greenland, Himalaya, Andes). Hence, using MSLP as for the estimation of GPS ZHD at global scale is not recommended.

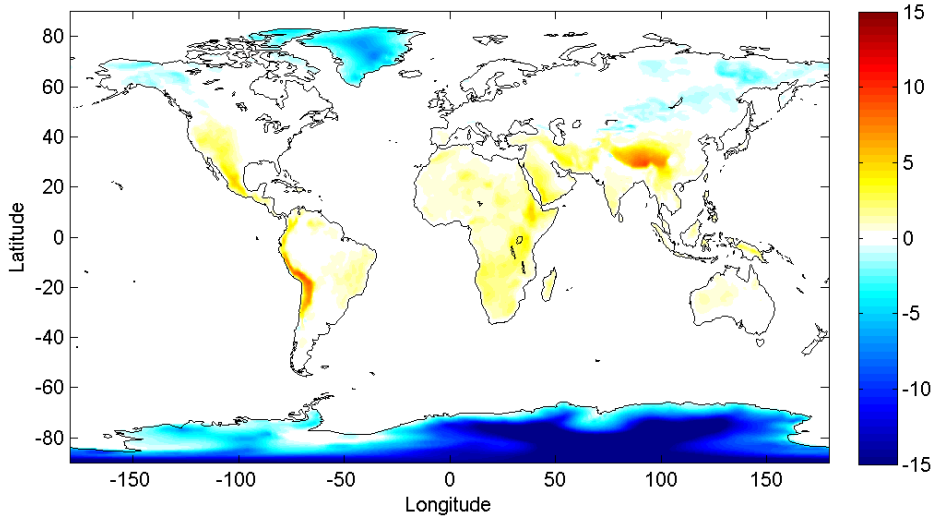

Figure2.8: Mean difference (in hPa) between the surface pressure extrapolated from mean sea level pressure field and the surface pressure archived as SF obtained from the ERA-Interim, for year 2012.

The comparison of GPS altitudes and altitudes of the nearest model grid points for ERA-Interim (Figure 2.81) reveals that differences can range from -1500 m (SANT, Santiago, Chili) to +3200 m (MKEA, Mauna Kea, Hawaii). Even if model surface pressure data is used, a quite large extrapolation can thus be required. In order to minimize pressure extrapolation errors from the usage of Eq. (2.11) and prescribed lapse rate α, we decided to use ERA-Interim pressure level (PL) data which would be more physically consistent. The PL data are archived on 37 levels, from 1000 hPa to 1 hPa.

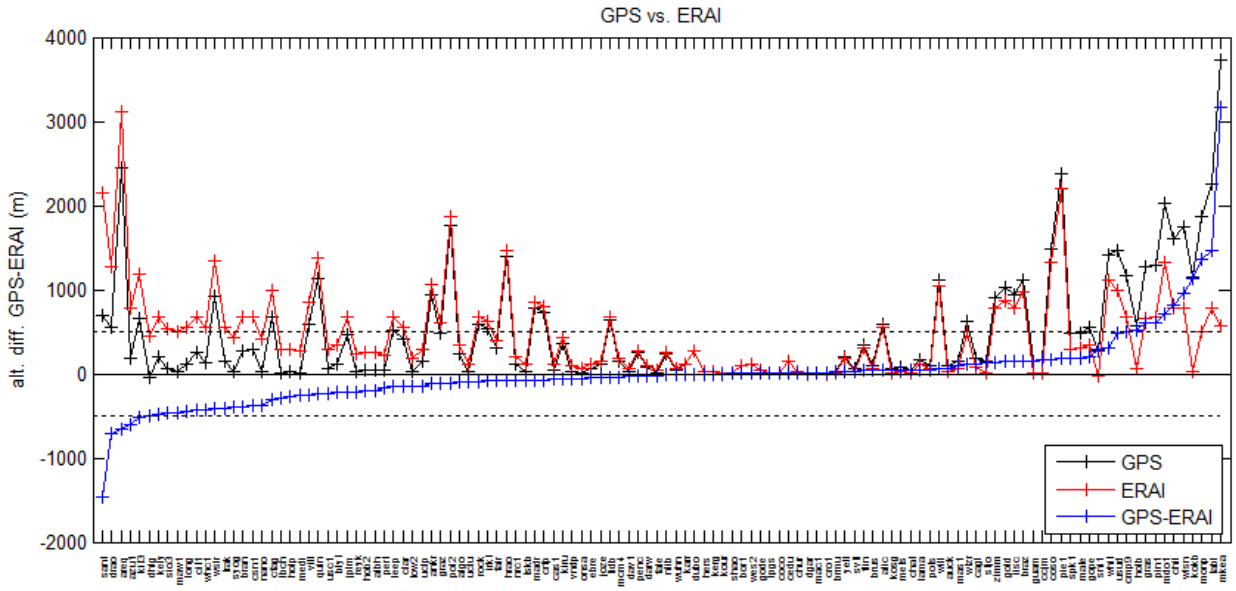

Figure2.81: Altitude of GPS stations (black) and ERA-Interim nearest grid-points (red), and the difference (blue)

Next we compare the ERA-Interim surface pressure (SF fields) and pressure interpolated from the PL data to the model surface. We used a linear interpolation for log(P) as a function of geopotential height between the levels above and below the surface height of each grid point. In the cases where the surface did not have a pressure level below, the pressure was extrapolated downwards from the lowest level (i.e. 1000 hPa) using Eq. (2.11) and (2.14).

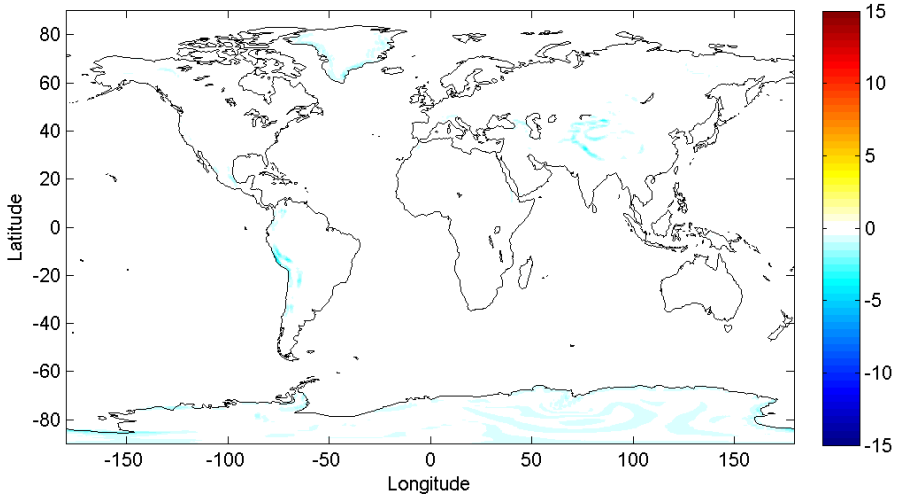

Figure2.82: Mean difference (in hPa) between the surface pressure interpolated from pressure level data (PL) and the surface pressure archived as SF in ERA-Interim, for year 2012.

Figure 2.82 shows that the surface pressure interpolated or extrapolated from PL data is fairly consistent with the model surface pressure data (SF field). So this method is retained for computing the pressure at the GPS stations but also at the SYNOP stations.

Finally, we used ERA-Interim reanalysis to check the SYNOP pressure observations over Europe. The SYNOP data were extracted for 2447 stations from the HyMeX (Hydrological cycle in the Mediterranean eXperiment) database (http://mistrals.sedoo.fr/HyMeX/) in a spatial domain between 20.3 and 70°N and between 13.85°W and 45°E. The mean SYNOP surface pressure observations were compared to the ERA-Interim monthly mean data for September 2012 (Fig. 2.9). The SYNOP pressure was computed using only records at 00, 06, 12, 18 UTC, to match the model's time sampling, for stations that had, at least, 28 (out of 30) days of pressure records. The ERA-Interim pressure was also interpolated to the coordinates of the SYNOP station to compensate for local horizontal gradients. We used a bilinear interpolation from the 4 grid points surrounding the station. The pressure for each grid point was vertically interpolated to the station height beforehand from the PL data as explained above.

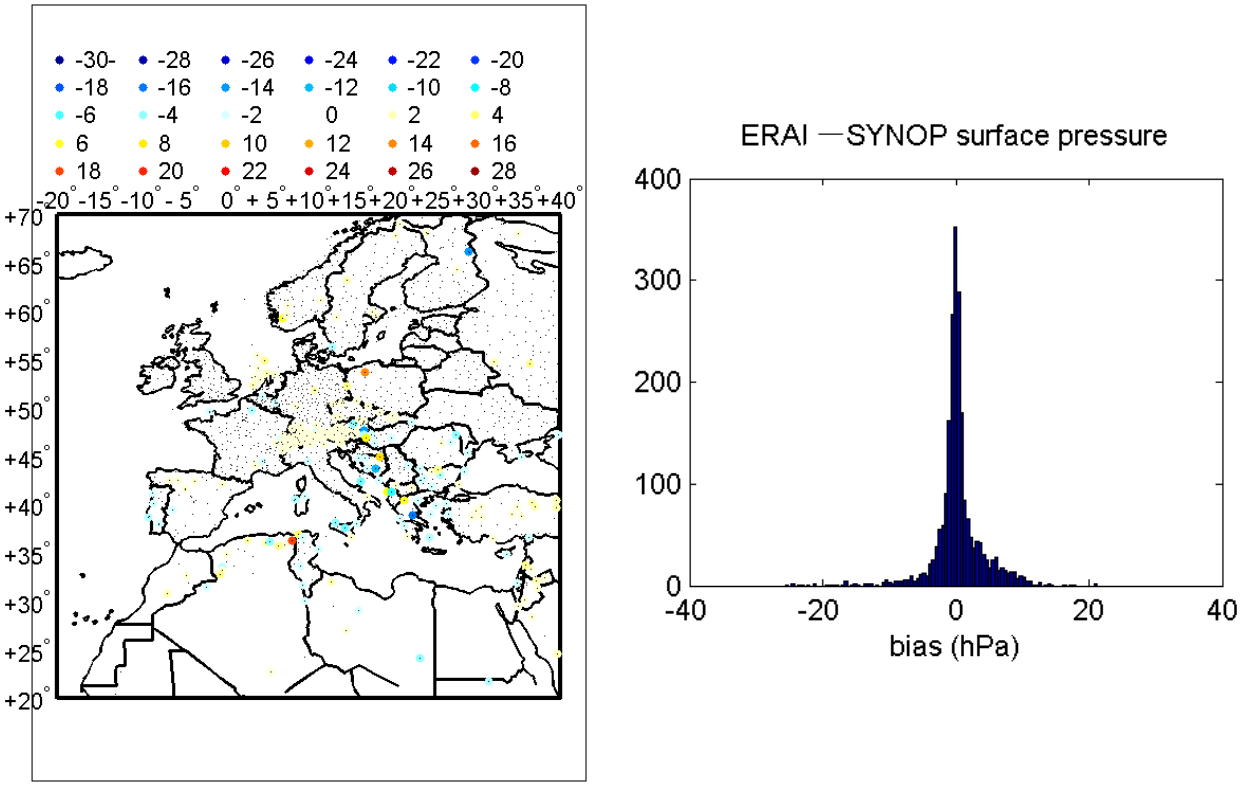

Figure 2.9: (left) Differences between mean extrapolated model pressure and mean SYNOP pressure at 2447 stations, for September 2012. (right) Histogram of the mean differences for all stations.

Figure 2.9 shows that for most stations, the difference between the model pressure and SYNOP is under ±2 hPa (shown as small black dots). However, there are a few stations with relatively high difference in pressure. Inspecting time series for these stations revealed that in some cases the biases were not constant over the time period. An example is shown in Fig. 2.10 for station 10381 which exhibits a break on day 271 when the mean bias shifts from around -1 hPa to -2 hPa. No change in station coordinates was reported by WMO for this station in 2012. The reason of the break might be a change in sensor or a recalibration.

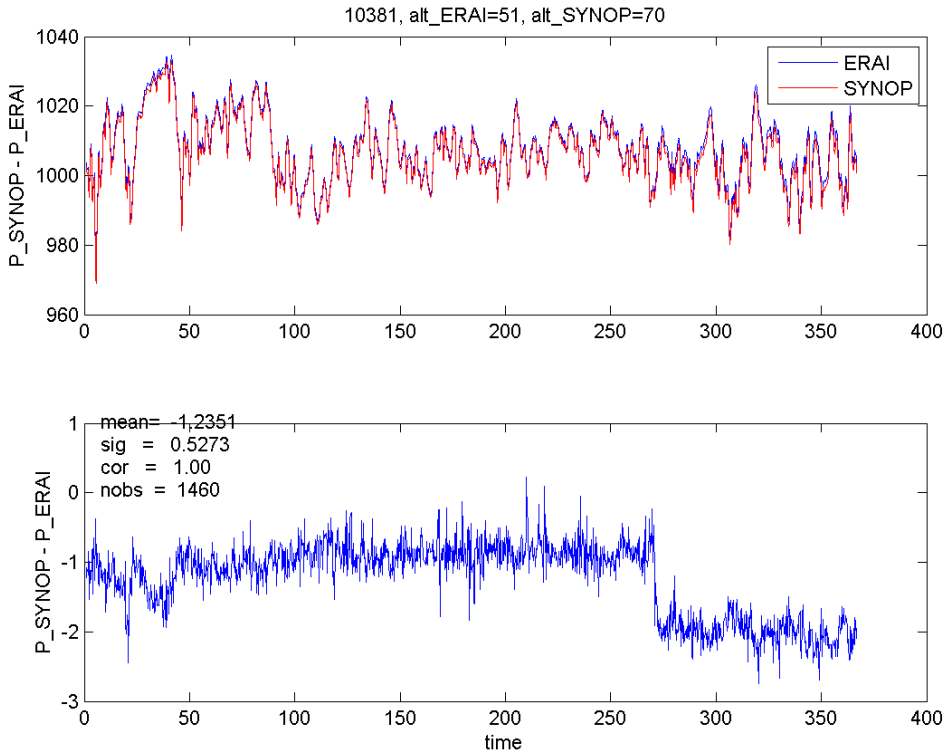

Figure 2.10: Time series of surface pressure measured at SYNOP station 10381 (Berlin, Germany) and ERA-Interim pressure data (interpolated from pressure-level fields), for year 2012. The lower plot shows the difference between both data.

Relocation of SYNOP station with the same ID can lead to big jumps in the pressure time series when station coordinates are not updated. We compared the dates of changes from the SYNOP data files extracted from HYMEX database (daily files) and information available at WMO (WMO Publication No. 9, Volume A). Figure 2.101 shows that altitudes changed by more than ±50 m (i.e. ± 6 hPa) in 2012 (they involved more than 100 stations). It is striking also that changes were not reported at the same date by WMO and in the HYMEX database files which were actually extracted from the Meteo-France climate database.

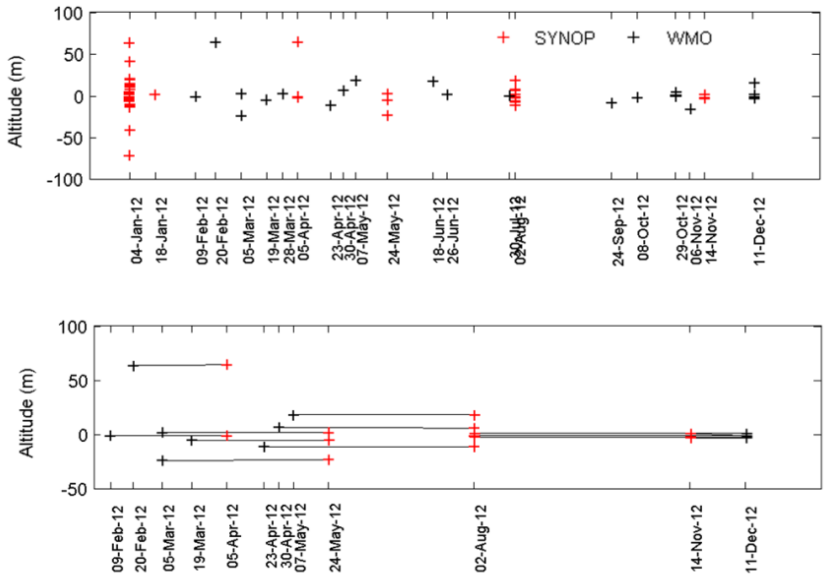

Figure 2.101: Altitude changes in European SYNOP stations reported by WMO and extracted from metadata of the HYMEX (Meteo-France) database, for year 2012.

This study highlights that using surface pressure observations requires careful quality control, screening, bias correction and homogenization. In addition, not all SYNOP sites have 1- or 3-hourly data, and archives for longer periods (e.g. ECA&D) only contain daily or monthly means (van den Besselaar et al., 2011).

For this reason, the pressure data used to produce the GPS IWV data set in this work was computed from 6-hourly ERA-Interim pressure level fields, available on a 0.75° by 0.75° horizontal grid. The geopotential was interpolated to the height of the GPS site when the GPS height is above 1000 hPa. Below 1000 hPa, the pressure at the GPS site is extrapolated using log-linear extrapolation as explained above. The vertical interpolation was performed for the 4 grid points surrounding the GPS station and then a bilinear horizontal interpolation was performed.

2.3.5 Assessment of Tm data

Tm has long been computed from empirical formulas requiring air temperature close to the surface, Ts. Bevis (1992) first proposed sur a linear approximation for Tm:

$$Tm = 70.2 + 0.72Ts \tag{2.15}$$

Although this approach is still commonly used, Wang et al. (2005) reported on its limitations. They found a cold bias in the tropics and subtropics (of up to 6 K), a warm bias in mid- and high latitudes (of up to 5 K). Bock et al. (2007) also evidenced an erroneously large diurnal cycle in Africa due to the strong daily variations of Ts. Finally both authors concluded on its unsuitability in estimating Tm at global scale and high temporal (sub-daily) resolution, and recommended using a NWP model data instead.

Available Tm datasets computed from NWP models include a Tm dataset from the Technical University of Vienna (TUV), computed using the ECMWF operational model (http://ggosatm.hg.tuwien.ac.at/DELAY/), and the Geodetic Observatory Pecný experimental online service, with Tm computed from the ERA-Interim dataset (Douša, http://www.pecny.cz/Joomla25/index.php/gop-tropdb/tropo-model-service).

We made a global intercomparison of the TUV dataset using Tm computed by our own (Eq. 2.5) using ERA-Interim PL data. Data and computation details are given below:

- The TUV dataset is computed from 6-hourly ECMWF's operational analysis, on a 2°x2.5° grid.
- The ERA-Interim data was computed using 6-hourly reanalysis data at 37 pressure levels and 0.75° horizontal resolution, T and Pv are extrapolated/ interpolated for every 50m, from the surface to the top layer. Then, $\frac{Pv}{T}$ and $\frac{Pv}{T^2}$ are computed every 50m and integrated using the built-in Matlab function *trapz*. This Tm was computed at the grid of TUV (through 2-D filtering and interpolation) and using TUV's orography.

Figure 2.11 shows that the mean differences between ERAI Tm and TUV Tm range from approximately -3 to 3 K, with the standard deviations staying mostly below 3 K. There is a positive bias in the TUV data in most of the globe, except for the high latitudes (Greenland and Antarctica), where the bias is negative. The standard deviation of the difference peaks for the regions with highest altitude.

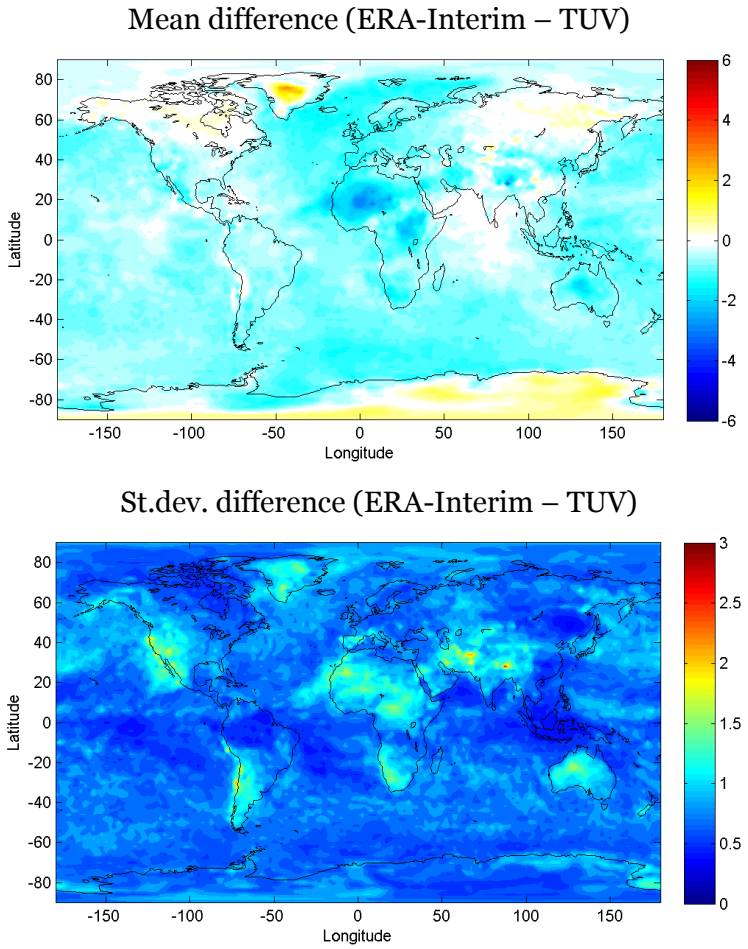

Figure 2.11: Mean and standard deviation of the difference between Tm computed using ERA Interim data and Tm from TUV (in K), for January 2012.

Tm was also computed for a network of 1046 GPS stations for January 2012, using the ERA Interim PL data. In that case, the PL data were interpolated to a 50m vertical grid and the integrals in Eq. (2.5) extended from the GPS height to the top of the atmosphere. This data was then compared with Tm computed by TUV and extracted at the nearest grid point to the GPS station (without horizontal and vertical adjustment).

Fig. 2.12 shows the mean and standard deviation of the difference (ERAI-TUV) against the vertical distance between the station coordinates and the nearest grid point. There is a high, positive correlation (0.98) between the bias and the vertical distance between the station and the nearest TUV grid point. The bias in Tm is roughly 5.4 $K.km^{-1}$, with biases surpassing 10 K for some stations. The standard deviation reaches about 3 K and is also higher for larger height differences.

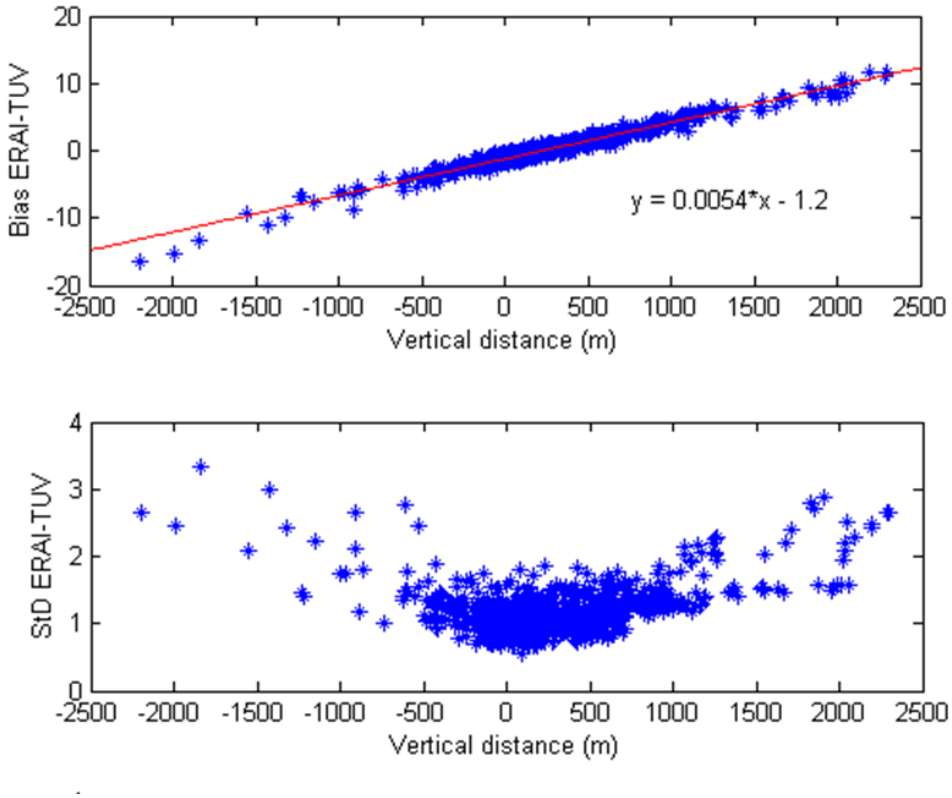

Figure 2.12: Mean and standard deviation of the difference between Tm computed from ERA Interim data at the GPS site and Tm computed by the TUV and extracted to the nearest grid point, as a function of the vertical distance between the nearest grid point and the GPS site.

Using the TUV data for the nearest grid point to the GPS station can thus incur in large biases for stations where the height difference between the station and the nearest grid point is large. Therefore, in this work, the method of computing Tm from the 6-hourly ERA-Interim pressure level data on a 0.75° grid was chosen.

2.4 Homogeneity of the GPS IWV time series

Although in principle GPS measurements should have long-term stability (as they can be traced back to frequency and time measurements), studies have shown that changes in antenna and algorithm details can cause jumps in the data that would affect climate research (Ning et al., 2012; Ning and Elgered, 2012).

Figure 2.13 shows an (extreme) example of discontinuity in the GPS time series, for the CCJM station in Japan. The receiver and antenna changes that occur at the beginning of 2001 prompt a jump in the difference series between ERA-Interim and GPS, which brings the GPS data closer to the reanalysis. This (type of) discontinuity is a problem when computing trends in IWV, and thus should be corrected in the data post-processing. Although several methods to detect temporal shifts have been proposed (e.g. Vey et al., 2009; Ning, 2016), none has been found completely satisfactory. Therefore, in the next section uncorrected GPS data was used. Visual inspection of the time series and use of metadata extracted from IGS site logs revealed that only a few sites might be affected by discontinuities large enough to be detectable in the IWV differences and to impact the trend estimates computed hereafter. Those sites will be pointed out.

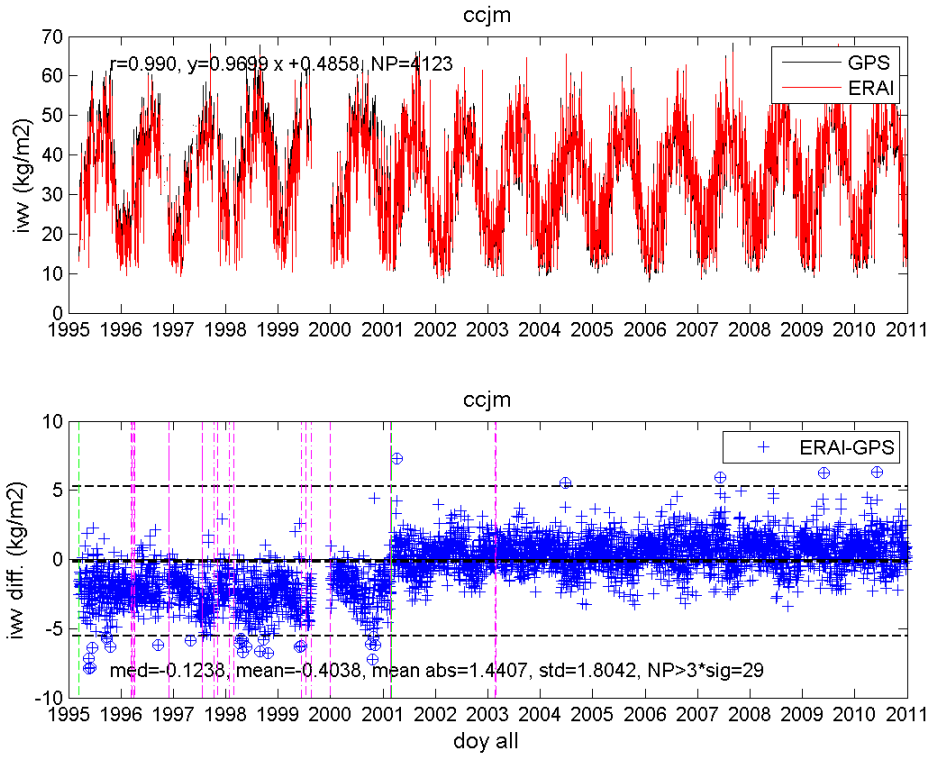

Figure 2.13: Time series at the CCJM GPS station, superposed by the time series for ERA-Interim at the GPS site (top). Time series of the differences between ERA-Interim and GPS (bottom). Vertical lines indicate GPS equipment and processing changes (receiver in magenta, antenna in green).

Chapter 3: Observation of IWV trends and variability from GPS data and reanalyses

3.1 Introduction

In this chapter, GPS IWV and IWV data from reanalyses (ERA-Interim and, later, MERRA-2) were used to analyse global seasonal means and interannual variability, and annual and seasonal trends. This allows for a global characterization of IWV, on the one hand, and an intervalidation of the datasets, on the other.

First, a global comparison between GPS and ERA-Interim was performed in terms of means, interannual variability and linear trends for the 1995-2010 period. Although a general good agreement was found, this analysis highlighted issues in both data sets. In GPS, gaps and inhomogeneities in the time series were evidenced, which affect mainly variability and trend estimation. In ERA-Interim, too strong trends in certain regions (e.g.: strong drying over North Africa and Australia, and strong moistening over Northern South America) were found. Representativeness differences in coastal areas and regions of complex topography (mountain ranges, islands) were also evidenced as limitations to the intercomparison of the datasets.

In order to assess ERA-Interim in regions where no GPS stations are available, MERRA-2 was brought into the discussion. The period of analysis was also extended to 1980-2016. Differences were found in the trends obtained from the two reanalyses, most notably over Africa, Australia and Antarctica. A focus was then put on Northern Africa and Western Australia, which highlighted a connection between the anomalies in IWV and anomalies in the wind intensity and direction (at the 925 hPa level). These results are shown in a paper, which is presented in the following subsection 3.2.

The IWV fields in ERA-Interim and MERRA-2 were then compared in more detail, and used to assess two twentieth century reanalyses, ERA-20C and NOAA-20CR V2. These reanalyses assimilate fewer observations (surface only), but span a longer time period, so that they could be used in climate studies, for instance. The results are presented in a supplement, in section 3.3.

3.2 Paper

Global IWV trends and variability in reanalysis and GPS observations

A.C. Parracho, O. Bock, S. Bastin

Ready for submission to Atmos. Chemistry and Physics

Abstract

Water vapour has a key role in the climate system. However, the short residence time of Integrated Water Vapour (IWV) in the atmosphere and its high variability in space and time make its study a challenge when it comes to trends and variability. There are several sources of IWV data. In this work we use GPS observations, which are compared with and complemented by ERA-Interim reanalyses data. Annual and seasonal means, variability, and trends were analysed and compared for the period between 1995 and 2010. A general good agreement was found, this analysis highlighted issues in both data sets. In GPS, gaps and inhomogeneities in the time series were evidenced, which affect mainly variability and trend estimation. In ERA-Interim, too strong trends in certain regions (e.g.: strong drying over North Africa and Australia, and strong moistening over Northern South America) were found. Representativeness differences in coastal areas and regions of complex topography (mountain ranges, islands) were also evidenced as limitations to the intercomparison of the datasets. A general good agreement was found for the means and variabilities, with the exception of a few stations where representativeness issues are suspected. Annual IWV trends were also found to be in good sign agreement, with the exception of a handful of stations where, in addition to representativeness errors, there might be discontinuities in the GPS time series. Seasonal trends were found to be different and more intense than annual trends, which emphasizes the influence of atmospheric circulation on IWV trends. In order to assess strong trends over regions lacking in GPS stations, a second reanalysis, MERRA-2, was introduced. The period of analysis was extended to 1980-2016 (the longest period the reanalysis have in common) and differences with the shorter period were found. This shows that trends in IWV are dependent on the time period at study and must be interpreted in its context. Temperature trends were also computed for both reanalyses. The Clausius-Clapeyron scaling ratio was found to not be a good humidity proxy at seasonal and regional scales. Regions over North Africa and Australia, where ERA-Interim and MERRA-2 disagree, were investigated further. Dynamics at these regions were assessed by analyzing the wind fields at 925 hPa, and they were found to have an important role in the trends and variability in IWV.

Keywords: Integrated water vapour, trends, GPS meteorology, atmospheric reanalysis

1. Introduction

Water vapour is a key component of the Earth's atmosphere, with a key role in the planet's energy balance. It is the major greenhouse gas in the atmosphere and accounts for about 75% of the total greenhouse effect (Kondratev, 1972). This is a global average, as the greenhouse effect of water vapour depends on the total amount of water vapor in the column which is spatially heterogeneous. At global scale, the total amount of water vapor is mainly controlled by temperature following closely the Clausius-Clapeyron (C-C) equation (Held and Soden, 2006; Semenov and Bengtsson, 2002). According to C-C, a temperature increase in the lower troposphere of 1°C leads to an increase in the vertical profile of water vapour of 6 to 7% (globally). It is thus an important part of the response of the climate system to external forcing, constituting a positive feedback in global warming (IPCC report). However, at regional scale, deviations from C-C law are observed and the strength of the feedback can vary, also because the radiative effect of absorption by water vapour is sensitive to the fractional change in water vapor, not to the absolute change.

Integrated water vapour (IWV) has also been shown to be an important parameter in precipitation onset. Neelin et al. (2009), Holloway and Neelin (2009) and Sahany et al. (2012) concluded that IWV is a better proxy than surface humidity, sea surface temperature or integrated column saturation for transition to deep convection in the Tropics because at higher temperatures, deep convection occurs at lower relative humidity rates. Entrainment processes actually play a substantial role in the onset of deep convection, which is thus sensitive to the lower tropospheric humidity. However, the relationship between IWV and precipitation is a two-way interaction since convection also moistens the free troposphere (the upper-troposphere mainly). This relationship is a key issue for models in a warming climate. Bastin et al. (submitted) used it to evaluate simulations performed in the framework of MED-CORDEX (Ruti et al. 2015) over Mediterranean area and concluded that models with "too light too often" precipitations could be better constrained by IWV-temperature relationship. Therefore, seasonal, interannual and temperature-IWV variability should be studied.

At these (seasonal and interannual) scales, climate variations also result from natural variability. The spatial structure of climate variability at seasonal and longer time scales evidences patterns that result from interactions between the atmospheric circulation and the land and ocean surfaces. These include the El Ninõ Southern Oscillation (ENSO) and the North Atlantic Oscillation (NAO). ENSO is a quasi-periodical oscillation in winds and sea surface temperature

over the tropical eastern Pacific Ocean, which impacts the weather and climate worldwide. The NAO fluctuates at time scales that go from days to decades, and has an impact over the regional climate variability in Europe, particularly in winter.

Although El Niño events are associated with increasing temperatures in the eastern and central Pacific with impact on the global weather and climate, it is not well known if global warming will lead to more frequent or intense El Niño events (Colins et al., 2010). Conversely, although a high positive NAO (when the gradient between the Icelandic Low and the Azores High is enhanced) is associated with warmer winters in the Eurasian landmass, due to the stronger westerly and southwesterly airflow that brings in warmer maritime air, it is not clear how the phase or intensity of NAO has been, or will be, affected by climate change (Visbeck et al., 2001).

All these parameters, and the fact that the time of residence of water vapor in the atmosphere is short, make IWV a highly variable component, making its study in term of variability and trends challenging. Several studies have reported on the long-term trends obtained from different IWV datasets. Although there appears to be a global positive trend in the overall IWV data, which is consistent with a global warming trend, it is difficult to compare results from different studies, as they refer to different data sources, time periods and different sites and spatial coverage.

There are several sources of IWV data, including different types of measurements (using instruments such as radiosondes, Global Positioning System (GPS), and satellites), atmospheric reanalyses, and climate models. For studies at the scale of climate change (seasonal, annual and interannual scales), the data must be available long-term, must be consistent and preferably homogeneous over time so as to not include (or reduce) non-climatic influences such as shifts and spurious signals (Ning et al., 2016). Indeed, differences in trends estimate exist between the existing IWV products, due to a lack of homogenized datasets (Wang et al. 2016).

In this paper, GPS-derived IWV data is used. GPS has the advantage of having a growing global network of mostly land-based stations, which gather data under most weather conditions, at a high temporal resolution, and with a continuous temporal coverage that dates back to 1995. The GPS data has been consistently reprocessed to ensure a homogeneous retrieval of IWV. However, it can still be affected by inhomogeneities, due to (for instance) changes in GPS equipment and algorithm details (Vey et al., 2009).

This data is compared with and complemented by ERA-Interim reanalysis data (a more recent version of the ECMWF reanalysis), which provides a multivariate, spatially complete, and coherent record of the global atmospheric circulation (Dee et al., 2011), thus a priori a good

complement of the more sparse GPS dataset. ERA-interim has been chosen because it is quite recent, is used to drive/force a lot of regional climate simulations, and is often used to assess climate models, which have difficulty in accurately representing the water vapour distribution in the atmosphere, and in describing its greenhouse effect, especially at the regional level.

Nevertheless, with regards to IWV in particular, the homogeneity of the reanalysis data has also been called into question by several studies (Bengtsson et al., 2004; Dessler and Davis, 2010; Schröeder et al., 2016). Schröeder et al. (2016) compared the IWV from three reanalysis (European Centre for Medium-Range Weather Forecasts Interim reanalysis, ERA-Interim; the Modern-Era Retrospective analysis for Research and Applications, MERRA; and the Climate Forecast System Reanalysis, CFSR) with three satellite-based IWV data records (Hamburg Ocean Atmosphere Parameters and Fluxes from Satellite Data, HOAPS; Remote Sensing Systems, REMSS; NASA Water Vapor Project MEaSUREs program, NVAP-M), for the 1988-2008 period. They analysed anomaly differences relative to HOAPS for averages over the global ice-free oceans and found break-points, which mostly coincided with changes in the observing system, and were more pronounced in the central Africa, the Sahara, and South America regions.

The main objective of our paper is thus the assessment of ERA-Interim IWV variability and trends by using the homogenized GPS dataset where available. Trenberth et al. (2005) analysed trends and variability of IWV over the period 1988-2001 and used radiosonde data from Ross and Elliott (1996, 2001) over land to evaluate ERA-40 and NCEP reanalyses. However, radiosondes were shown to be in less agreement with ERA-interim than GPS and DORIS IWV (Bock et al., 2014). In this study, to add new insights in both the evaluation of ERA-interim reanalysis and in the understanding of IWV trends and variability, we separate the analysis into seasons, and consider interannual variability of seasons: it helps to better identify regions with higher uncertainty and to understand the physical processes which can explain seasonal, interannual, spatial variabilities and trends and discrepancies between datasets since dynamical component strongly differ between seasons. Regions with strong trends are singled out, and the MERRA-2 reanalysis is used in complement to ERA-interim when necessary to shed some light on the processes that are instrumental in explaining errors.

This paper is organized as follows: the next section details the datasets and methods used. Section 3 reports on the means and variability found in the GPS and ERA-Interim data, for the 1995-2010 period. Section 4 focuses on the annual and seasonal trends in GPS and ERA-Interim for 1995-2010. In section 5 we introduce a second reanalysis data set, MERRA-2, in order to assess significant ERA-Interim trends in regions where there are no GPS stations, or where GPS

and ERA-Interim are not in agreement. In this section, the comparison between ERA-Interim and MERRA-2 was also extended to the 1980-2016 period and focused on two regions of intense trends: Western Australia and Western and Central Africa. Section 6 concludes the paper.

2. Datasets and methods

Reanalysis data

Reanalysis data from the ECMWF, ERA-Interim (Dee et al., 2011), and NASA, MERRA-2 (Molod et al., 2015), were extracted for the 1980-2016 period, at their highest horizontal resolution (0.75° x 0.75° for ERA-Interim and 5/8° longitude x 1/2° latitude for MERRA-2). As both reanalyses agree generally well, this work presents mostly results from ERA-Interim. However, in some occasions, it was useful to complement the results with MERRA-2, such as in regions where no GPS data was available.

In this work, the two-dimensional (2D) distribution of IWV is investigated with both reanalysis data and GPS observations from 104 stations of the International GNSS Service (IGS) network (Fig. 1). Because GPS heights and model surface heights are not perfectly matched (see the GPS coordinates and ERA-Interim heights in the supplement Table S1), the IWV estimates were adjusted for the height difference using two different methods. In the 2D maps (e.g. Fig. 2), the monthly mean GPS IWV estimates were height corrected to match the nearest ERA-Interim grid point, while for the computation of IWV differences (e.g. Fig. 3), a more elaborate interpolation method was used (described below). For the monthly mean IWV correction, specific humidity from the ERA-Interim pressure level data was integrated over the layer of atmosphere bounded by the model's surface height and the height of the GPS station. The ERA-Interim pressure level data contains a total of 37 levels between 1000 and 1 hPa, and 27 levels between 1000 and 100 hPa. This ensures a good vertical sampling of the troposphere where most of the water vapour is located.

The height differences between GPS stations and nearest model grid points range from -1457 m (at the SANT (Santiago, Chile) station) to +3167 m (at the MKEA (Mauna Kea, Hawaii) station), where a negative difference means GPS height is below the model surface. The mean IWV corrections for these two stations amount to -3.4 $kg.m^{-2}$ and 21.7 $kg.m^{-2}$, respectively. Globally, 102 out of the 104 stations have a correction smaller than 7.7 $kg.m^{-2}$ in absolute value and the inter-quartile range is [-1.40 , 0.39] $kg.m^{-2}$.

A more rigorous approach is adopted for the quantitative evaluation of the reanalysis IWV data with respect to GPS IWV data, in order to minimize temporal and spatial sampling issues. In this case, we time-match the 6-hourly data and perform a spatial interpolation of the reanalysis IWV estimates to the latitude and longitude of the GPS site. A bilinear spatial interpolation is computed from the model IWV estimates at the 4 grid points surrounding each GPS station. The IWV model estimates are then recomputed from the pressure level data by vertically integrating the specific humidity between the height of the GPS station and the top of the atmosphere. Most GPS station heights fall between two pressure levels and the specific humidity data can be interpolated. However, for stations located below the 1000 hPa level, the reanalysis data must be extrapolated. Interpolation and extrapolation are done linearly for specific humidity and temperature, and exponentially for pressure. This procedure minimizes differences between the reanalysis IWV data and the GPS estimates with better results than previous correction methods (e.g. Bock et al., 2014). However, a perfect match between observations and model data (Lorenc, 1986) is hindered by representativeness errors, especially in mountainous and coastal regions.

GPS data

The reprocessed GPS data set used in this work was produced by the NASA Jet Propulsion Laboratory (JPL) in 2010-2011. Basic details on the operational GPS data processing procedure are described by Byun and Bar-Server (2009). Compared to the operational version, the reprocessed data set is produced with more recent observation models (e.g. mapping functions, absolute antenna models) and consistently reprocessed satellite orbits and clocks (IGSMAIL-6298). Inspection of file headers revealed that the processing options were not updated for a small number of stations for a period of nearly one year between March 2008 and March 2009. The comparison of solutions with old and new processing options showed that this inconsistency only slightly impacts stations at high southern latitudes (mainly stations in Antarctica). The data set covers the period from January 1995 to December 2010 for 456 stations. Among these, 120 stations have nearly continuous time series over the 15-year period. However, the geographical distribution is quite unequal between hemispheres and even within a given hemisphere. Moreover, a cluster of 20 stations in the western USA is associated with the same 4 ERA-Interim grid points. In order to avoid over-representation of this region, 16 of these stations have been discarded (the selection retained those with the longer time series). The final GPS IWV dataset used in this study is thus limited to the selected 104 stations.

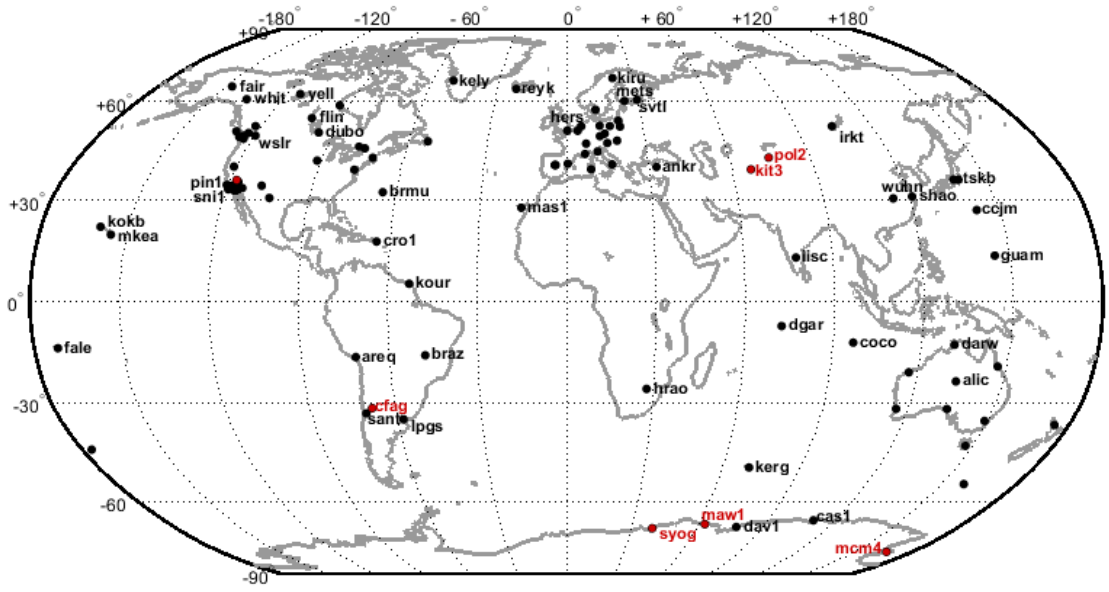

Figure 1: Map with the 104 GPS stations used in this study, with the stations mentioned in the text named.

The basic observables in this study are the Zenith Tropospheric Delay (ZTD) estimates available at a 5 minute rate. The ZTD data were screened using an adaptation of the methods described by Bock et al. (2014) and Bock et al. (2016). First, we applied a range check on the ZTD and formal error values using fixed thresholds representing the spatial and temporal range of expected values: 1 – 3 m for ZTD and 0 – 6 mm for formal errors. Second, we applied an outlier check which consists in rejecting data based on the comparison of ZTD and formal error values with respect to site-specific thresholds: median ± 0.5 m for ZTD and formal error < 2.5 × median. The median values are updated yearly. Using these thresholds, we detected no ZTD values outside the limits. This is because the limits were sufficiently large to accommodate for the natural variability of ZTD values (Bock et al., 2014). On the other hand, the formal error check rejected 8.8×10^{-4} (i.e. less than 0.1%) of the data overall. After screening, the 5-minute GPS ZTD data were averaged in 1-hourly bins.

The conversion of GPS ZTD to IWV was done using the following formula: $IWV = ZWD \times \kappa(Tm)$. Where κ (Tm) is a function of a weighted mean temperature, and ZWD is the zenith wet delay, obtained from: $ZWD = ZTD - ZHD$, where ZHD is the hydrostatic zenith delay computed from surface pressure (see Wang et al. (2005) or Bock et al. (2007) for further details). In this work, the surface pressure used to compute ZHD and the temperature and humidity profiles necessary to obtain Tm were computed using ERA-Interim pressure level data, using a procedure similar and consistent with the IWV integration explained above. The profile variables are first

interpolated or extrapolated to the height of the GPS stations at the 4 surrounding grid points and then interpolated bi-linearly to the latitude and longitude of the GPS stations. At this stage, the GPS and ERA-Interim data were time-matched (within ±1 hour) for both the ZTD to IWV conversion and IWV intercomparison. Based on our experience, this methodology of ZTD data screening and conversion into IWV is the most elaborate and accurate to date.

Afterwards, monthly means of the 6-hourly IWV estimates are computed and those months which have less than 60 values (i.e. at least half of expected monthly values) are rejected. Seasonal means are computed from the monthly values when at least 2 out of 3 months are available. These selection criteria ensure that the computed values are representative of the monthly and seasonal means.

Regarding the homogeneity of our GPS IWV time series, we have to mention that it is only guaranteed at the processing level. Jumps in ZTD and thus IWV series due to equipment changes or changes in the observational conditions were not corrected. Visual inspection of time series and use of metadata extracted from IGS sitelogs revealed that only a few sites might be affected by discontinuities large enough to be detectable in the IWV differences and to impact the trend estimates computed hereafter. Those sites will be pointed out and discarded when overall statistics are computed and discussed.

Computation of trends

The linear trends were computed using the Theil-Sen method (Theil, 1950 & Sen, 1968), a non-parametric statistic that computes the median slope of all pairwise combinations of points. This method was found to be more robust than the least square fitting (Rousseeuw and Leroy, 2003), as it is less sensitive to outliers in the time series and does not require a normal distribution of the data. In addition, Wang et al. (2016) found this method to be less sensitive to the start and ending of time series with sparse data (a concern when using the GPS data, with gaps).

The Theil-Sen method was applied to the anomalies obtained by removing the monthly climatology from the monthly data. In the case of seasonal trends, the mean anomalies for the months of December, January and February (DJF); and June, July and August (JJA) were used (when there are at least two months of data available per season). The statistical significance of the annual and seasonal trends was assessed using a modified Mann-Kendall trend test (Hamed and Rao, 1998), which is suitable for autocorrelated data, at a 10% significance level.

3. Means and variability in GPS and ERA-Interim IWV (1995-2010)

The ERA-Interim and GPS data have been used to investigate the mean seasonal IWV distribution and its interannual variability for December-January-February (DJF) and June-July-August (JJA).

Globally, the mean IWV (Figs. 2 a) and b)) is strongest in the tropics where strong evaporation occurs from the warm oceans and land surface and where trade winds transport moisture to the Intertropical Convergence Zone (ITCZ). Lower evaporation occurs at mid and high latitudes due to the cooler oceans and land surface. Lower IWV observed at these latitudes is also explained by the limited moisture-holding capacity of the relatively cooler tropospheric air (Trenberth et al., 2007; Lorentz and DeWeaver, 2007). The rapid decrease of water vapour saturation pressure with altitude as predicted by Clausius–Clapeyron equation also explains the lower IWV contents over elevated land surfaces. Minimal IWV values are found over major mountain ranges (e.g. the Himalayas and the Andes cordillera). The lack of surface water is another strong limitation for evaporation and thus atmospheric humidity as observed in arid regions (e.g. Sahara, Arabic peninsula, south-eastern Africa, Australia). Strong seasonal variation is driven by the movement of the incoming solar radiation from one hemisphere to the other and back along the course of the year. The resulting global swinging of the trade winds and ITCZ across the Equator is a cause for the regional wet monsoon seasons usually associated with rainfall (e.g. India and southern Asia, West Africa, and southern North America in JJA; northern Australia, central and southern Africa, and the central Amazon River basin in South America in DJF). The high rainfall patterns (not shown) coincide well with the high IWV patterns shown in Fig. 2.

For the analysis of the interannual variability we computed the relative standard deviation of the seasonal IWV time series (i.e. standard deviation of seasonal time series divided by its mean value). The relative variability emphasizes both regions where the variability is high compared to the mean IWV and regions where the mean IWV contents are small (e.g. cold dry polar and/or mountainous regions and warm dry desert areas). In DJF (Fig. 2 c)), strong interannual variability (> 15%) is found for northern high-latitude regions (north-eastern Canada and eastern Greenland, polar Artic area, and a large part of Russia and north-eastern Asia) and for the tropical arid regions (Sahara, Arabic peninsula, central Australia). Large linear correlation coefficients between the seasonal IWV anomalies and the North Atlantic Oscillation (NAO) index (Barnston and Livezey, 1987) are found (not shown) over Siberia (r = 0.5) and Greenland (r = -0.5). Noticeable variability is also seen in the central tropical Pacific in DJF but this is due to the extremely large variability in absolute IWV contents (up to 6 $kg.m^{-2}$) associated with the El Nino

Southern Oscillation (ENSO). Linear correlation coefficients between the seasonal IWV anomalies and the Multivariate ENSO Index (MEI; Wolter and Timlin, 1993, 1998) in this region reach r = 0.80 (not shown). In JJA, large interannual variability is observed mainly over Antarctica and Australia (Fig. 2 d)). Locally enhanced variability is also seen over the Andes cordillera, but this is mainly due to the very low IWV values at high altitudes.

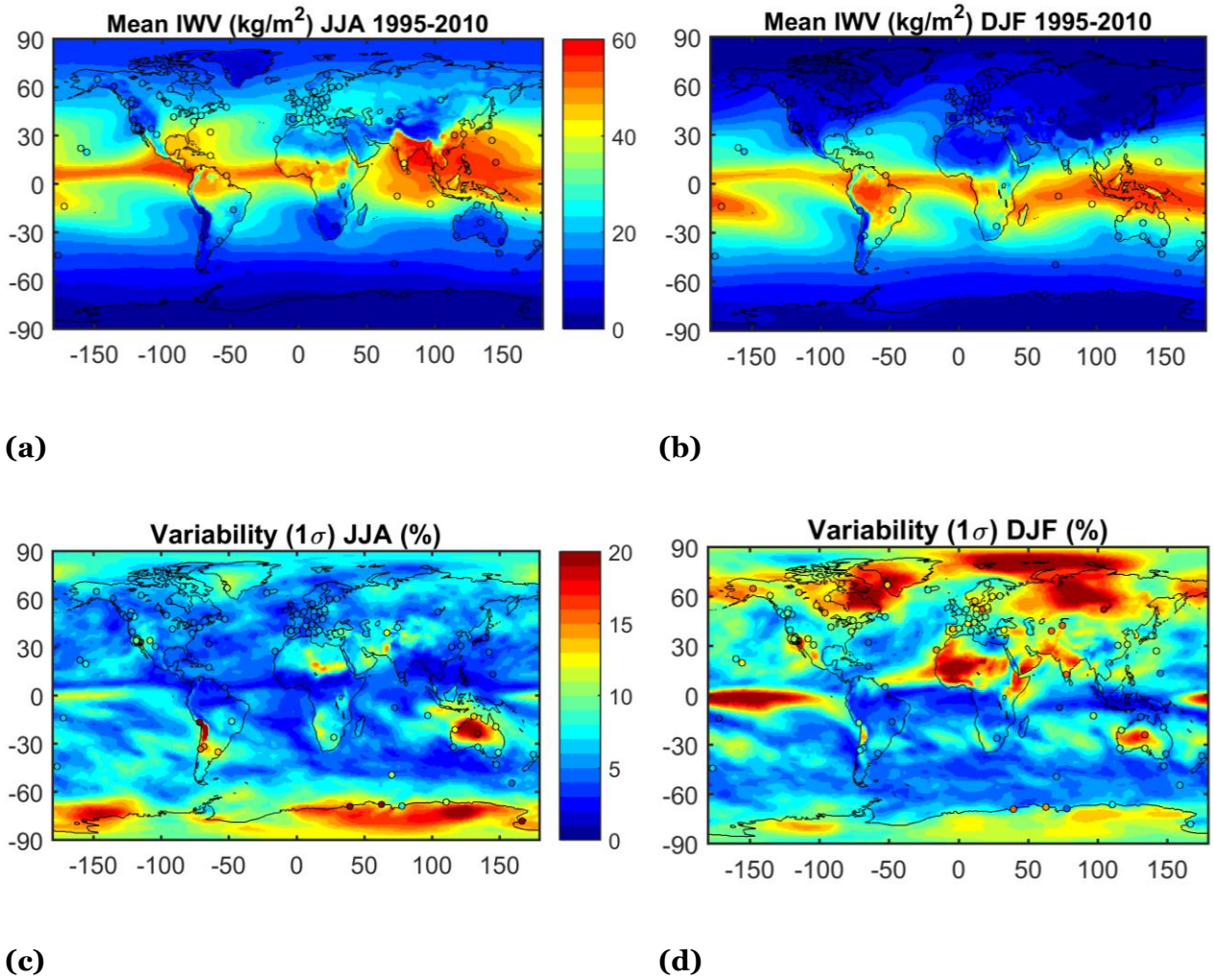

Figure 2: a) Mean value of IWV from ERA-Interim between 1995 and 2010 for JJA. Filled circles correspond to IWV retrieved by GPS. b) same as a) for DJF. c) relaive variability (standard deviation of the IWV series divided by its mean) for JJA, between 1995 and 2010. d) Same as c) for DJF.

In general, there is good agreement between ERA-Interim and GPS. In the maps of the means (Figs. 2 a) and b)), we can see that ERA-Interim reproduces the spatial variability well, including the sharper gradients in IWV, for instance, on the northern and southern flanks of the ITCZ in

both seasons, and in the regions of steep orography (for example, along the Andes region, in South America).

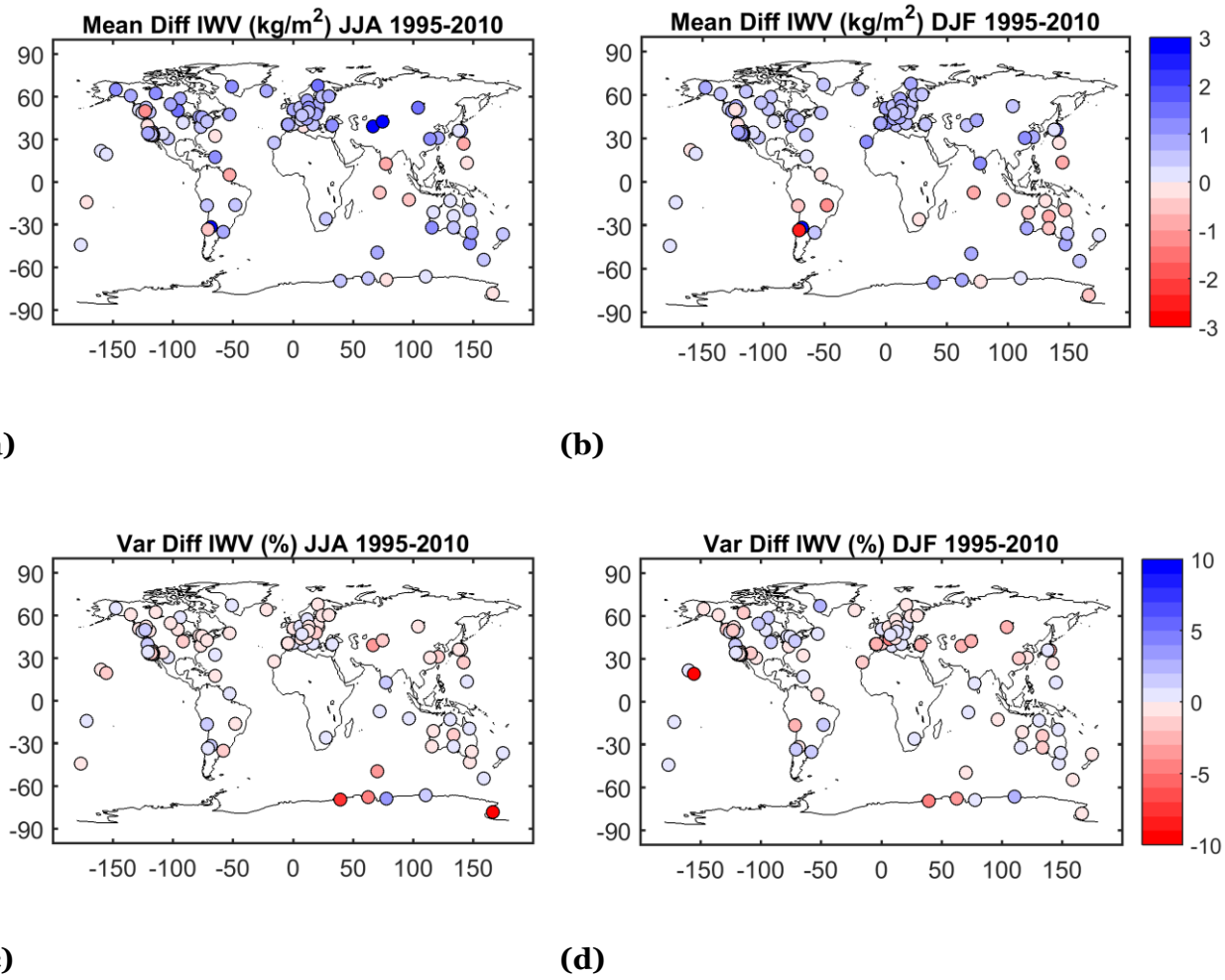

Figure 3: a) Difference of IWV means between ERA-Interim and GPS between 1995 and 2010 for JJA. b) Same as a) for DJF. c) Difference of relative standard deviations of IWV between ERA-Interim and GPS between 1995 and 2010 for JJA. d) same as c) for DJF.

The mean IWV differences are shown in Figs. 3 a) and b) for all 104 GPS sites. It can be noticed that in negative differences (ERA-Interim drier than GPS) are all located approximately within the ITCZ, except a few stations in North-West America in JJA and station MCM4 in Antarctica in DJF. A paired two-sample t-test detected 20 stations with significant differences in the mean IWV values at 0.01 confidence level in DJF and 17 in JJA. The sites with most notable differences, either absolute (in $kg.m^{-2}$) or relative (in %) are: CFAG in the Andes cordillera with a bias of 6.5 $kg.m^{-2}$ (43%) in DJF and 3.9 $kg.m^{-2}$ (26%) in JJA and, SANT in Chile with -2.4 $kg.m^{-}$

^{2} (-15%) in DJF, and TSKB (in Japan) with 1.9 kg.m^{-2} (24%) in DJF. In JJA, three other sites have large biases: KIT3 in Uzbekistan with a value of 6.2 kg.m^{-2} (35%), POL2 in Kirghizstan with 3.1 kg.m^{-2} (20%), SYOG in Antarctica with 0.6 kg.m^{-2} (32%), and MAW1 in Antarctica with 0.4 kg.m^{-2} (31%). The inspection of the time series shows that at some of these stations the biases are not constant in time but contain large variations, such as e.g. at CFAG (Fig. 4 a)) or KIT3 (Fig. 4 b)).

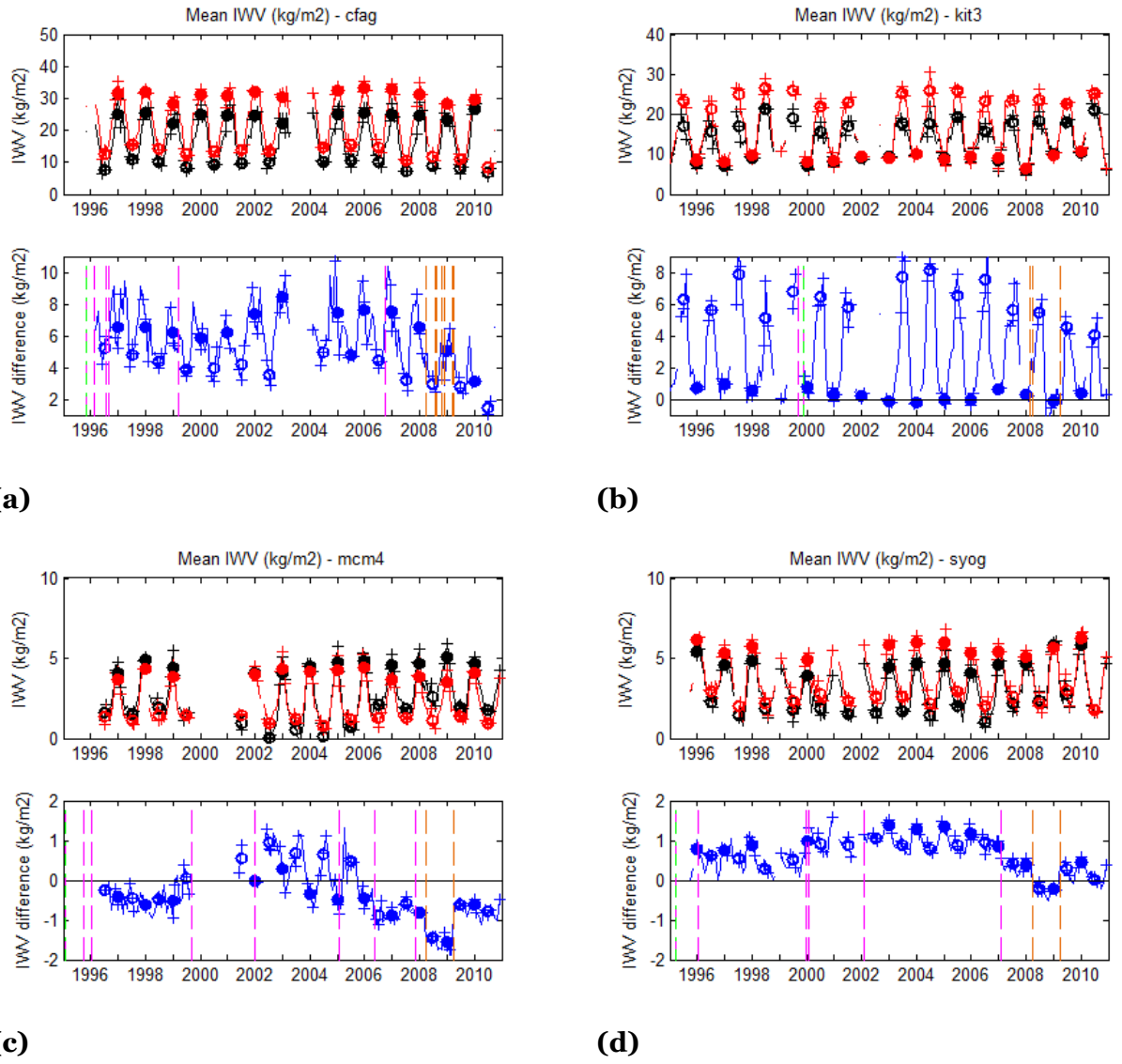

Figure 4: Time series of IWV from GPS (black) and ERAI (red) and IWV difference (blue) at stations (a) CFAG, (b) KIT3, (c) MCM4 and (d) SYOG. Filled circles show the DJF values and opern cicles the JJA values. Crosses show the individual months inboth seasons. Vertical dashed lines indicate GPS equipement changes (receiver in magenta, antenna in green) and processing (in orange). Note the change invertical scales between figures.

These sites are located in coastal regions and/or regions with complex topography. Although we used an elaborate spatial and temporal matching of reanalysis and GPS data, representativeness errors are suspected to be the cause of these biases. To investigate this point, we compared the (vertically adjusted) IWV values from the 4 grid points surrounding the GPS station to the interpolated value and found that for CFAG, KIT3, POL2, SYOG, and MAW1, the interpolated value does not minimize the IWV bias compared to GPS. This is explained by large variations in the altitude of the grid points (between 500m and 1000m) and the difficulty for the vertical interpolation method to properly predict the IWV variations over such large altitude ranges. In the case of SANT, although the interpolated value matches the GPS value better than any of the four surrounding grid point values, there is still a large bias explained by a variation in the altitude of the grid points of over 1500m. Results for all the stations can be found in Table S2 of the Supplement. Overall statistics given in Table 1 indicate that ERA-Interim is slightly moister on average than GPS. The median bias is 0.51 kg m^{-2} (5.1%) in DJF and 0.51 kg.m^{-2} (2.6%) in JJA, and the standard deviation of the bias across the network amounts to 0.84 kg.m^{-2} (6.2%) in DJF and 0.95 kg.m^{-2} (6.3%) in JJA. As noticed above, there is some spatial consistency in the mean difference, namely a negative mean difference in the tropics (ERA-Interim < GPS) which is compensated in the global mean by the larger number of stations in the extra-tropics which have a positive difference (ERA-Interim > GPS).

Table 1: Statistics (median ± one standard deviation over 104 stations) for the difference of mean IWV contents and the difference of relative standard deviations.

	Diff. of mean IWV (ERAI – GPS)	**Diff. of rel. std. (ERAI – GPS)**
DJF	+0.51 kg.m^{-2} ± 0.84 kg.m^{-2} +5.8% ± 6.2%	-0.07% ± 1.69%
JJA	+0.51 kg.m^{-2} ± 0.95 kg.m^{-2} +2.6% ± 6.3%	-0.14% ± 4.05%

Most of the marked regional features of interannual variability are also confirmed by GPS observations (Figs. 2 c) and d)). One can especially notice the good representation of the relative variability over Australia or South America, both in DJF and JJA, and in the northern high latitudes, where the gradients are strong and well captured. Figures 3 c) and d) show the difference in relative standard deviation between GPS and ERA-Interim. Overall the differences are small except at a few stations. The overall statistics for the comparison of variability given in Table 1 indicate a median difference close to zero for both DJF and JJA with a standard deviation across the stations of 1.7% in DJF and 4.1% in JJA. See Table S2 in the supplement

with the results for all stations. We used a two-sample F-test to detect the stations where the variances differ significantly. However, this test detected only one result with a p-value < 0.01 (station MCM4 in JJA) and two with a p-value < 0.10 (MCM4 and CFAG in JJA). This statistical test is probably not very efficient in the case of our short time series (14 to 16 points). In JJA, the four stations with the largest differences (ERAI – GPS) are located in Antarctica: MCM4, SYOG, MAW1, and DAV1 with differences of -39% (p=0), -7.7% (p=0.63), -4.8% (p=0.81), and +3.9% (p=0.27), respectively. In DJF, the largest differences are found for MKEA (Hawai) and SYOG, where they amount to -11.4% (p=0.52) and -4.8% (p=0.30), respectively. In the case of SYOG, MAW1, and DAV1, representativeness errors are suspected again because of the large variability in the IWV values of the surrounding grid points connected with large variations in the altitudes (> 500m) of these grid points. In the case of MKEA, the variation in the altitude of the surrounding grid points is quite small because of the limited imprint of Mauna Kea Island on the 75-km resolution grid of ERA-Interim. However, the difference in altitude between the GPS station and all four grid points is larger than 3000 m which is far beyond the prediction capability of the interpolation method described in Section 2. In the case of MCM4 and SYOG, the inspection of the time series of monthly mean IWV and IWV differences (shown in Figs. 4 c) and d)) reveals variations in the means which coincide with GPS equipment changes and processing changes and unexplained variations in the amplitude of the seasonal cycle resulting in a marked oscillation in the monthly mean differences (ERAI – GPS). Variations in the means introduce a spurious component of variability in the GPS IWV series (e.g. at MCM4 the standard deviation of GPS IWV is 0.78 kg m^{-2} compared to 0.21 kg m^{-2} for ERAI).

Three possible causes for the differences in the IWV means and variability between GPS and ERAI exist. As already discussed above, representativeness differences are expected in regions of complex terrain where the environmental conditions can differ. Strong horizontal gradients in IWV are a limitation for the bi-linear horizontal interpolation that we used. This kind of situation is generally encountered when the altitudes of the grid points surrounding the stations are very different (e.g. AREQ, SANT, KIT3, MAW1, SYOG, POL2). This problem is enhanced when the altitude of the GPS station is below the model surface (e.g. SANT, AREQ, KIT3, MAW1, SYOG), because the model profile data are extrapolated below the ground, and/or the model and GPS surface altitudes are very different (e.g. MKEA). According to IWV and altitude variations, representativeness errors are expected at 20 stations among which are those cited just above. However, they don't explain all the significant biases and differences in variability actually observed. The second aspect is connected with errors in the GPS data, e.g. due to instrumental malfunctioning or measurement interferences, or changes in equipment resulting in variations

in the mean IWV estimates. Such problems can be detected by comparison with IWV measurements from nearby GPS receivers or from other collocated instruments such as DORIS or VLBI (Bock et al., 2014; Ning et al., 2016). The third cause stems from errors in the reanalysis IWV data which are expected in data-sparse regions and regions where the performance of model physics and dynamics are poor. These can be diagnosed by comparing several reanalysis based on different models and different observational data or hypothesized by eliminating the other causes.

4. Trends in GPS and ERA-Interim IWV (1995-2010)

Next, the ERA-Interim and GPS data were used to study the trends in IWV over the period 1995-2010. Results obtained with ERA-Interim based on the full monthly time series are discussed first (Figs. 5 a) and b)). Generally significant positive trends (moistening) are observed over most of the tropical oceans and over the Arctic. Significant negative (drying) trends are observed in south-tropical eastern Pacific region, west of the United States and generally south of 60°S. The dipole structure in the south-eastern tropical Pacific area is consistent with the findings of Mieruch et al (2014) and is due to the different ENSO phases for this time period, as reported by Trenberth et al (2005). Over land, significant positive trends are observed in equatorial region along the ITCZ, especially in northern South America, Central Africa, and Indonesia, and in the northern hemisphere, especially over northern North America, Greenland, most of Europe and Siberia. Significant negative trends over land are observed over North Africa, Australia, Antarctica, central Asia, and most of the USA. In general, there is continuity between oceanic and continental trends (e.g. North and South America, Central Africa). However, the magnitudes of the larger trends (e.g. -3.5 kg m^{-2} per decade or -17% per decade over North Africa) are questionable. To be physically explained such trends would imply a significant change in the regional and global water cycle. Alternatively, they might be due to inhomogenities in the observations assimilated in the reanalysis system. Comparison to GPS observations, when they are available, helps to address this question.

In general, the monthly trends computed at the GPS stations are in good agreement with ERA-Interim (Figs. 5 a) and b); see also Table S3 in the supplement). Many stations are operated in Europe and North America. Most of them show fairly consistent trends with ERA-Interim even in regions of marked gradients (e.g. between western Canada and the USA, or from central to Western Europe). Australia is also well documented with several stations, in the center and along the coasts, and good agreement is found both in the sign and spatial variations of trends. The

eastern Australia's moistening trend, although not significant in ERA-Interim, is also observed by GPS. Many isolated stations in other regions confirm the ERA-Interim trends. Moistening trends are observed by stations KOUR and BRAZ (northern part of South America), HRAO (South Africa), IISC (India), KELY (Greenland), DGAR (in the center of the Indian ocean), FALE (in the Pacific ocean), CRO1 (Puerto Rico), MAS1 (Canary Islands) and REYK (Iceland). In terms of drying trends, ERA-Interim and GPS trends are largely in agreement over the west coast of the United States, the southern half of South America (including the Andes region, which has steep IWV gradients) and the western half of Australia. It is also noteworthy that BRMU (in Bermuda) has a drying trend that is also captured in the ERA-Interim data. Overall, GPS absolute trends are greater (in arithmetic sense) than ERA-Interim trends at 62 sites out of 104, while relative trends in GPS are greater than in ERA-Interim at 65 sites out of 104 (Table S3). The reason for this asymmetry is not yet explained.

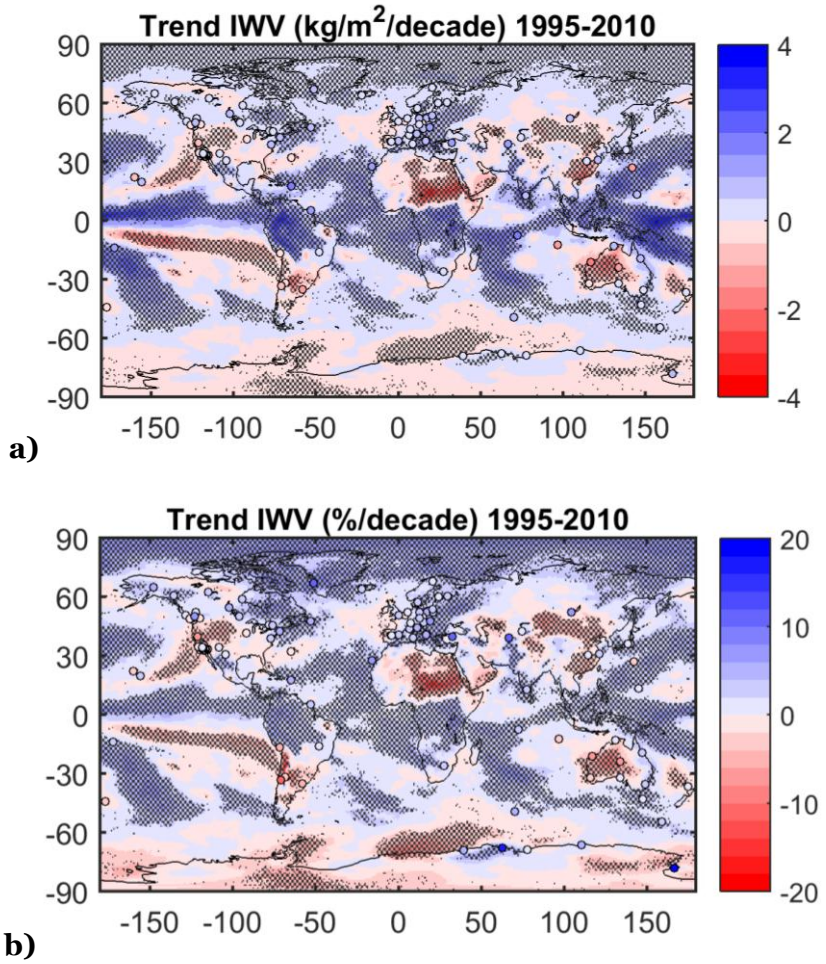

Figure 5: Absolute (a) and relative (b) IWV trends for the 1995-2010 period from ERA-Interim and GPS (stations marked as circles). The statistically significant trends from ERA-Interim are highlighted by stippling. Absolute trends are in kg.m^{-2} per decade and relative trends in % per decade.

Inspection of Fig. 5 a) shows that there are a number of GPS stations where the trend estimates in kg m^{-2} per decade are large and of opposite sign compared to ERA-Interim: CCJM (south of the Japanese home islands), DARW (northern Australia), WUHN (eastern China), IRKT (central Russia), ANKR (Turkey), KOKB and MKEA (Hawaii), and MCM4 (Antarctica). Some of them (DARW, ANKR, KOKB, MKEA) are located in areas where the ERA-Interim trends change sign and a perfect spatial coincidence between the reanalysis and observations might not be expected. On the other hand, stations CCJM, WUHN, IRKT, and MCM4 are located within regions where the ERA-Interim trends are strong and significant, and extend over large areas. For these stations, the most plausible reason for the discrepancy is that the GPS time series have gaps and/or inhomogeneities which corrupt the trend estimates. Inspection of time series confirms the presence of inhomogeneities at MCM4 (already discussed in the previous section, see Fig. 4 c)) and at CCJM (Fig. 6 a)). At CCJM, the GPS minus ERA-Interim IWV difference time series has a large offset in 2001 which coincides with a GPS equipment change (receiver and antenna). This offset is responsible for a large negative trend estimate in the GPS series (-1.40 kg m^{-2} per decade) whereas the time-matched ERA-Interim series gives a positive trend (+0.98 kg m^{-2} per decade) consistent with the large-scale trend in the reanalysis seen in Fig. 5 a). For WUHN (Fig. 6 b)), the IWV difference time series shows a negative offset at the end of 2006 while no equipment change is reported at that time. As a result the GPS trend estimate is positive (0.34 kg m^{-2} per decade) while the ERA-Interim estimate is negative (-1.45 kg m^{-2} per decade). Here, it is suspected that a GPS equipment change occurred but was not reported. An unreported GPS equipment change is also suspected at IRKT (not shown). Figure 5 b) shows that a few other sites have also large differences in terms of relative trends, such as SANT (Chile), MCM4 and MAW1 (Antarctica), and ANKR (Turkey). At these four sites, the GPS trends and ERA-Interim trends from the nearest grid point differ by more than 10 % per decade, though the GPS IWV time series are corrected for the height difference but differences may arise from gaps in the GPS time series. When time-matched series are compared (Figs. 7 a) and b)), the agreement is improved, especially at sites SNI1, DARW, MKEA, FALE, ANKR, and WUHN. However, absolute differences larger than 1 kg m^{-2} per decade and relative differences larger than 10% per decade are still found at some stations, presented in Table 2. At some of these sites (CCJM, WUHN, MCM4, SHAO, WSLR, KERG, PIN1), inspection of the time series suggests inhomogeneities in the GPS series. Representativeness differences are suspected at mountainous and coastal sites (e.g. CFAG, CRO1, and other sites discussed in previous section). Some sites show also more gradual drifts in the times series which don't seem connected with GPS equipment changes (e.g. MAW1). At such sites, drifts in the reanalysis are plausible. Comparison to other datasets and studies might confirm this assumption.

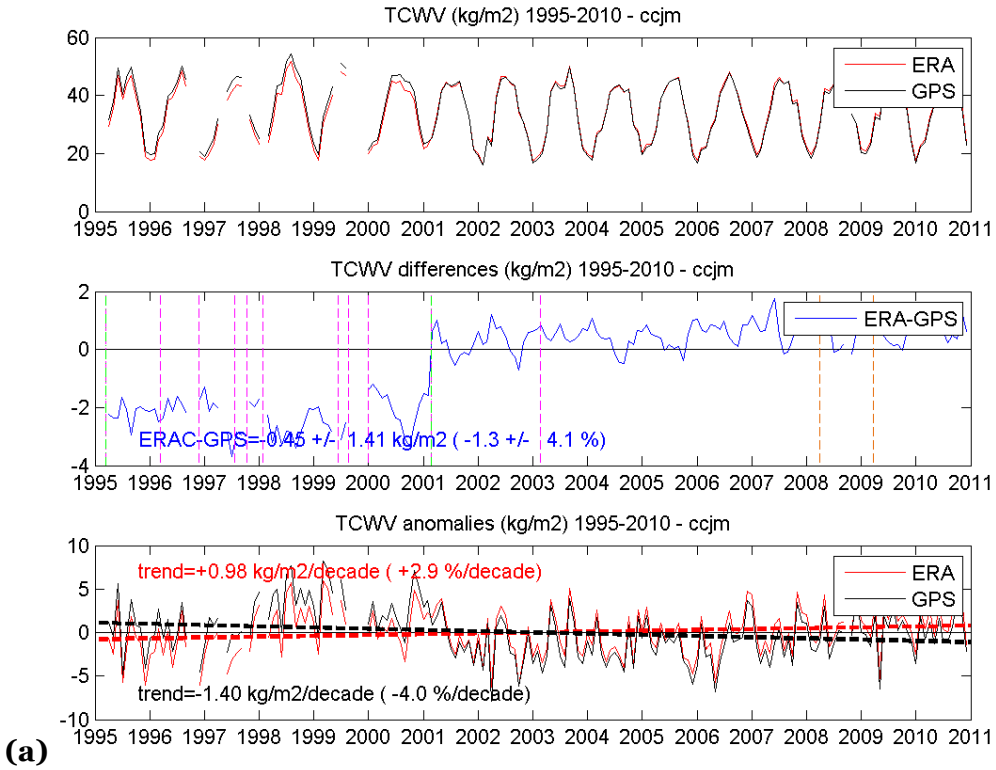

(a)

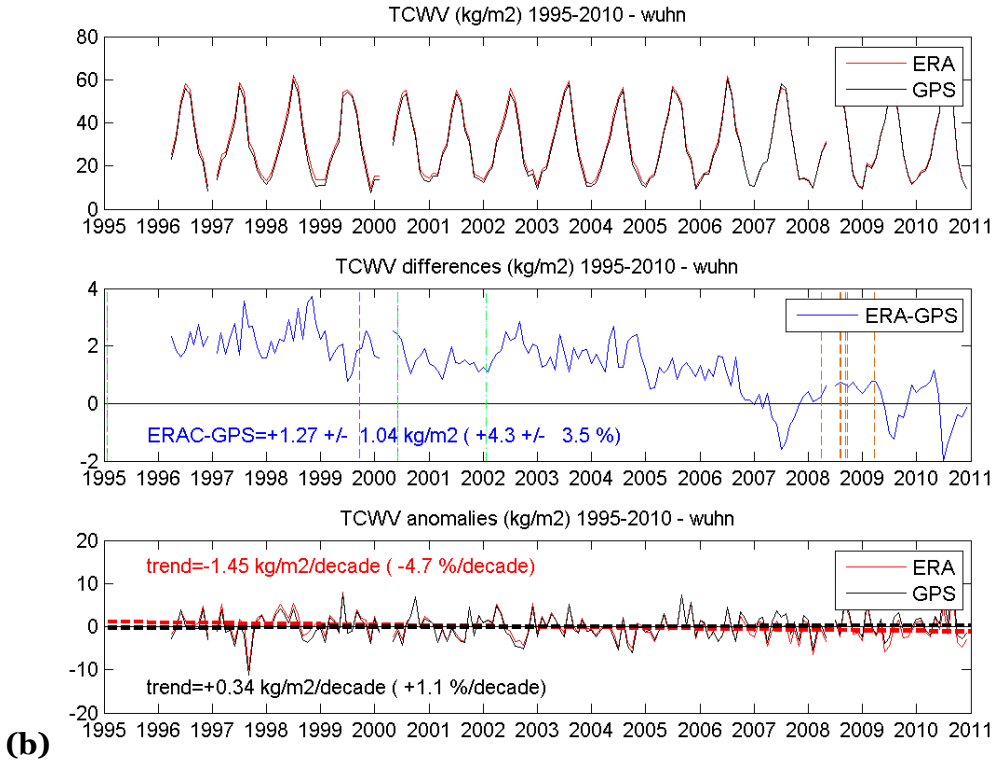

(b)

Figure 6: GPS (black) and ERA-Interim (red) IWV time series (top) and difference (bottom).

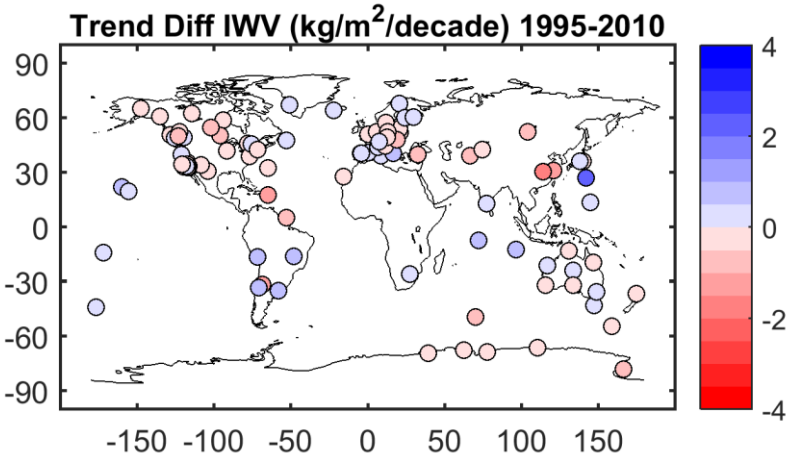

(a)

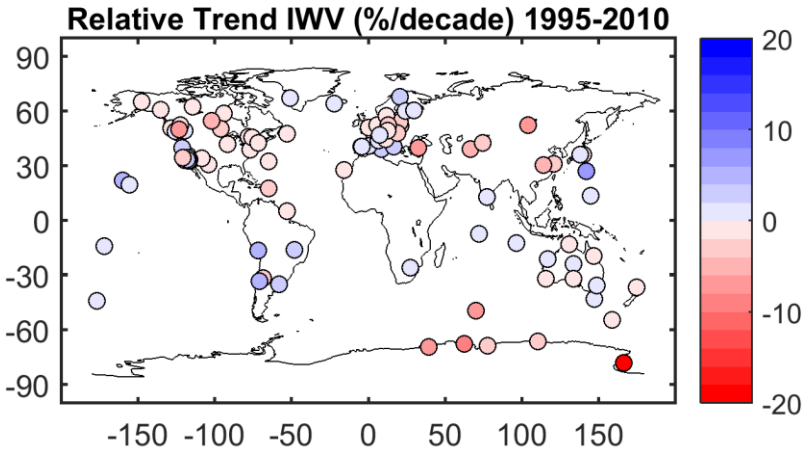

(b)

Figure 7: Difference of IWV trends between ERA-Interim (corrected to the GPS station height) and GPS between 1995 and 2010 for time-matched series: (a) trends in kg.m^{-2} per decade and (b) relative trends in % per decade.

Table 2: Stations with most intense trend difference (ERA – GPS) computed from time-matched GPS and ERA-Interim IWV series.

	Annual	DJF	JJA
Trend diff > 1 kg.m^{-2}.decade^{-1} < -1 kg.m^{-2}.decade^{-1}	CCJM, CFAG, CRO1, SHAO, WUHN	CCJM, COCO, DARW, GUAM, LPGS, PIN1, SANT, WUHN	CCJM, CFAG, CRO1, KOUR, POL2, SHAO, WSLR, WUHN
Trend diff > 10%.decade^{-1} < -10%.decade^{-1}	MCM4	CCJM, IRKT, KIRU, PIN1, POL2, WSLR, WUHN, YELL	AREQ MAW1 MCM4; SYOG
Significantly diff. (p < 0.01)	CCJM, KERG, MCM4, WSLR, WUHN		

Wang et al. (2016) studied nearly the same period (1995-2011) by using radiosonde and GPS stations over land and microwave (MWR) satellite data over oceans. Over the oceans, results that are significant in ERA-Interim are in good agreement with those obtained by Wang et al. (2016), despite the fact that they are not always significant in the latter study. Over land, none of the values computed by Wang et al (2016) are significant but the drying over Western Australia is also observed. No results are obtained over most of Africa and the north-western part of South America due to a lack of data. The drying for north-eastern Africa and moistening over Central Africa and north-western South America are therefore not confirmed by the Wang et al. (2016) study. For the other continental areas with weaker trends, results are not always in agreement, for instance over Central Asia, where a moistening trend is generally observed in Wang et al. (2016). The western part of USA presents a strong spatial variability in both studies but results are generally not consistent locally. Greenland trends also present opposite signs, even though very low values are obtained in both cases. When comparing with the GPS results obtained by Wang et al. (2016), there is a general good agreement, with some differences in Central Australia (ALIC station) and Iceland (REYK). These differences may be due to the extra year in their analysis (as differences in the beginning and ending of time series have an impact on the trend estimation, especially when trends are of low intensity and not significant, and the period at study is relatively short (16 years in our study)).

Although the study does not concern the same period, Trenberth et al (2005) reported similar trend signs to ERA-interim over Africa and South America in the NVAP data (1988-2001) and positive trends over western Pacific, the Indian and Atlantic oceans with SSM /I data (1988-2003). As discussed above, differences are observed over Eastern Pacific where El Niño events strongly affect the trend estimates. Note also a difference in the sign of the trend over Australia (an area which will be discussed later). Wagner et al (2006) studied the IWV trends in satellite observations from the Global Ozone Monitoring Experiment for the 1996-2002 period. Although their study period is short, they also found positive IWV trends over the western tropical Pacific Ocean and large parts of the southern oceans, and negative trends over North Africa. Over northern Australia, they found a negative trend, which is in agreement with what we obtain but not with Trenberth et al. (2005). This area is thus likely sensitive to the period at stake. The western part of the USA is also an area where differences between the studies are present, but it seems that spatial variability is strong and thus results strongly depend on the resolution of the datasets, and not only on the period. Thus, despite the different periods and the use of different observing systems, some areas show consistent trend signs with ERA-Interim which indicates that the results are likely robust. However, the trends obtained in our study can differ from those

presented by other authors for other periods, as the trend estimation is highly dependent on the time period at study.

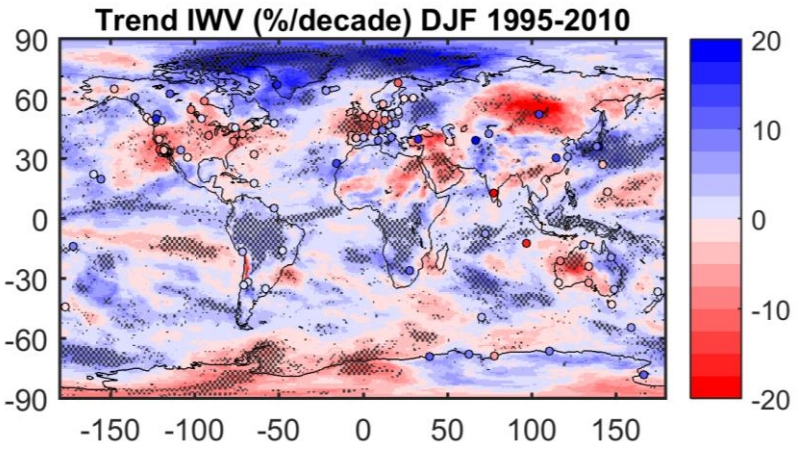

a)

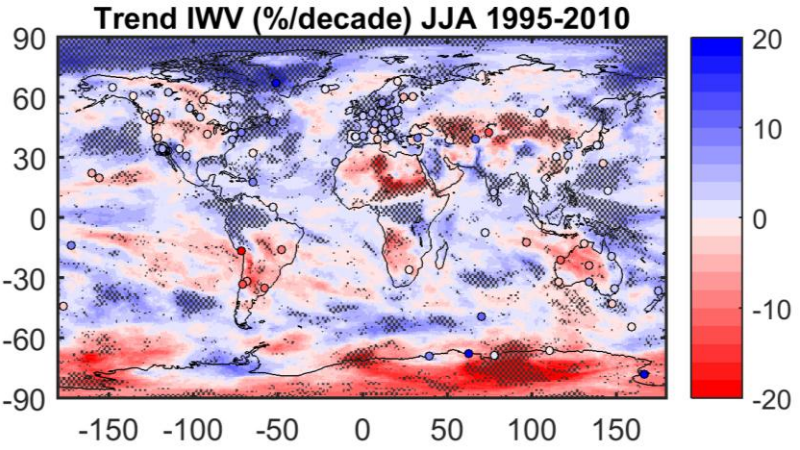

b)

Figure 8: Seasonal IWV trends for the 1995-2010 period from ERA-Interim and GPS (stations marked as circles) for DJF (a) and JJA (b). The statistically significant trends from ERA-Interim are highlighted by stippling.

To better understand the trends, we separated them by seasons (DJF or JJA), which are presented in Figs. 8 a) and b), respectively. These trends emphasize that atmospheric circulation (which is largely changing between seasons) plays an important role in IWV trends. Trends can be of opposite signs between winter and summer. Figures 8 a) and b) show that a strong drying occurs over Antarctica in JJA and over central Asia during JJA and DJF (though not exactly at the same location), while moistening occurs over the Artic in both seasons but in different

sectors (100°W to 50°E in DJF and 150°E-50W in JJA). A drying is also observed over Western Europe in winter (DJF), while a moistening occurs in summer, which explains the weak trend when considering the whole year. Over Australia, according to ERA-Interim, the drying is stronger in DJF, i.e. when associated with a decrease of the intensity of the moist flow during the monsoon period. The differences between our study and the one of Trenberth et al. (2005) are consistent with the theory that precipitation over Western and northern Australia (the part of Australia mostly influenced by the monsoon flow in DJF) are strongly sensitive to the SST over the western central Pacific Ocean (10°S-10°N; 150°-200°E) (Brown et al., 2016). In ERA-Interim and Wang et al. (2016), during 1995-2010, the SST over this part of ocean has increased (indicated by a moistening, according to C-C law), and is associated with a drying over Australia, while during 1988-2001, a strong drying is observed over central western pacific ocean, associated with a moistening over Australia. Another area likely sensitive to the intensity of the monsoon flow is North Africa, where the drying is occurring in JJA over a band covering Chad, Sudan and Eritrea, eastern of Sahel. More details will be given in the discussion section.

The comparison of ERA-Interim and GPS seasonal trends leads to consistent conclusions with the annual trends. However, the differences are generally of larger magnitudes (e.g. IRKT, ANKR, and MAS1, in DJF and MCM4, MAW1, KERG, in JJA). A few more sites also show trends of opposite signs in DJF, e.g. KIRU (Sweden), HERS (U.K.), FAIR and WHIT (Alaska). This is mainly due to the enhanced impact of time gaps for the short seasonal time series (based on 16 years at best).

5. Trends in ERA-Interim and MERRA-2

Global analysis

To complete the study and try to determine if these differences are due to errors in ERA-Interim or in the GPS data, a second reanalysis was also analyzed, and the IWV trends were computed for MERRA-2 and presented in Figure 9. The results for MERRA-2 appear to be different from ERA-Interim over several parts of the globe, in particular over Indonesia and Indian Ocean, central Africa, Western (coastal) and Northern Africa, Central Asia and Antarctica. We first discuss the areas where GPS are available and are not in agreement with ERA-Interim. Other areas are discussed in the next section.

Over Sweden, the trends obtained for DJF in MERRA-2 are consistent with ERA-Interim, with a positive (yet not statistically significant) trend that is opposite to the trend in the GPS data. The same is observed for the two stations over Finland (METS and SVTL) and for the ANKR station

in Turkey, where the ERA-Interim trends are supported by MERRA-2. The trends in MERRA-2 are also consistent with ERA-Interim in DJF over North America (although less intense, in better agreement with the GPS trends in DUBO and FLIN) and Russia, suggesting there might be a homogeneity issue in the IRKT GPS station.

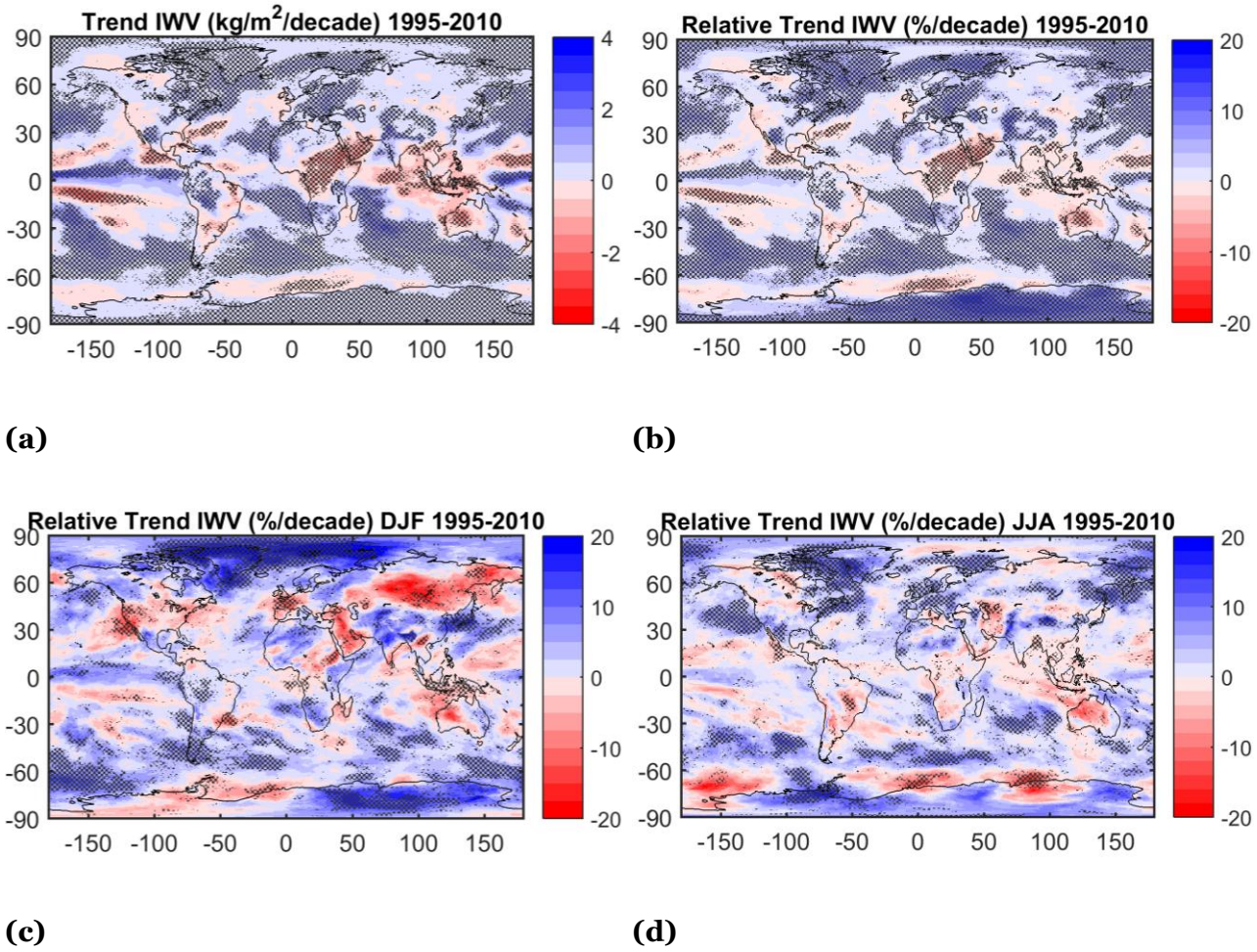

Figure 9: Absolute (a) and relative (b) trends in IWV in the MERRA-2 reanalysis for the 1995-2010 period. Relative trends in IWV in the MERRA-2 reanalysis for the 1995-2010 period for DJF (c) and JJA (d). The statistically significant trends are highlighted by stippling.

Over Antarctica, the annual trends in MERRA-2 are significantly positive over land, in agreement with the GPS stations, and in opposition to ERA-Interim. In JJA, the trends in MERRA-2 are positive over most of Antarctica, including in the region surrounding the SYOG, MAW1 and MCM4 stations; and negative at around DAV1 and CAS1. This is in better agreement with GPS (in terms of sign of trends) than ERA-Interim. In DJF, the trends around the GPS stations in Antarctica are mostly positive in both MERRA-2 and ERA-Interim, although they are

more intense in MERRA-2, which is also more consistent with the GPS trends. Overall, there appears to be some uncertainty with IWV trends in this region.

Trenberth et al. (2005) argued that the dominance of the 1997-98 El Niño event suggests that a longer time series may be required to obtain fully stable patterns of trends. The number of years needed to obtain a statistically significant trend in IWV in some regions, given its high variability, may never be achieved. However, in order to assess how consistent the trends we obtained for the 1995-2010 period (when GPS data is available) are with longer-term trends in ERA-Interim, trends were computed for the full length of the ERA-Interim/ MERRA-2 data (1980-2016). The results are presented in Figure 10.

ERA-Interim

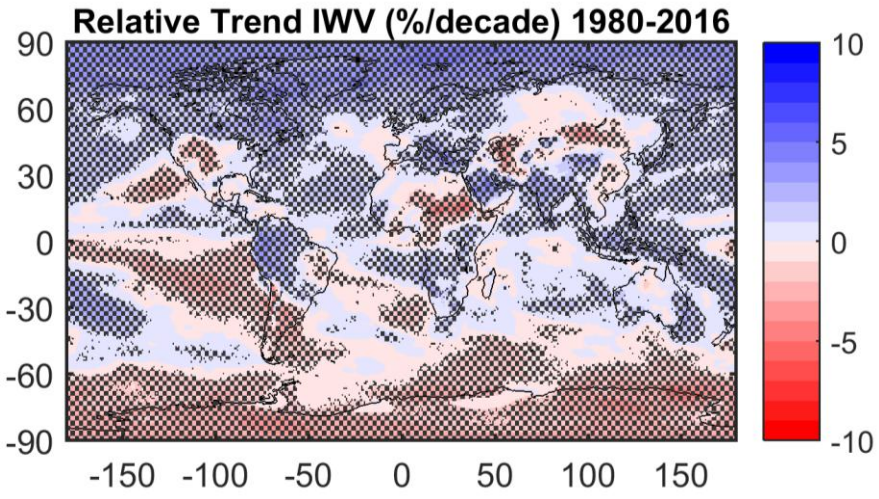

MERRA-2

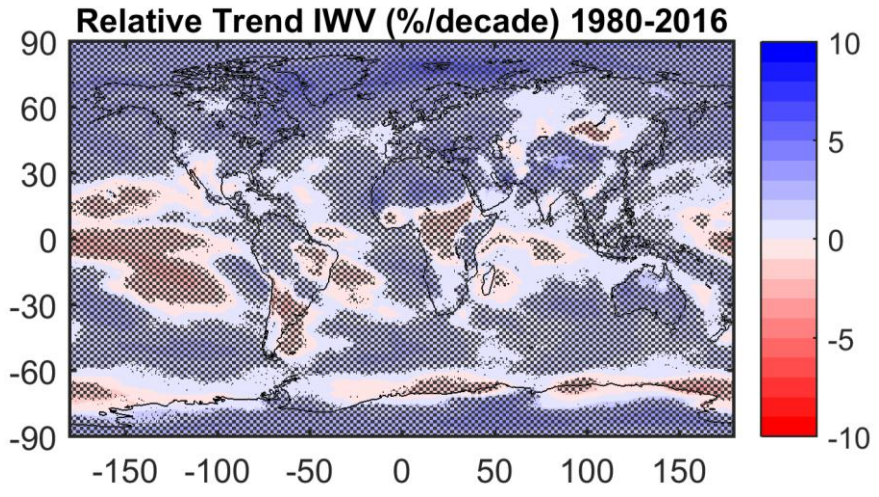

Figure 10: Annual trends in IWV for ERA-Interim's full time period (top), and MERRA-2's full time period (bottom).

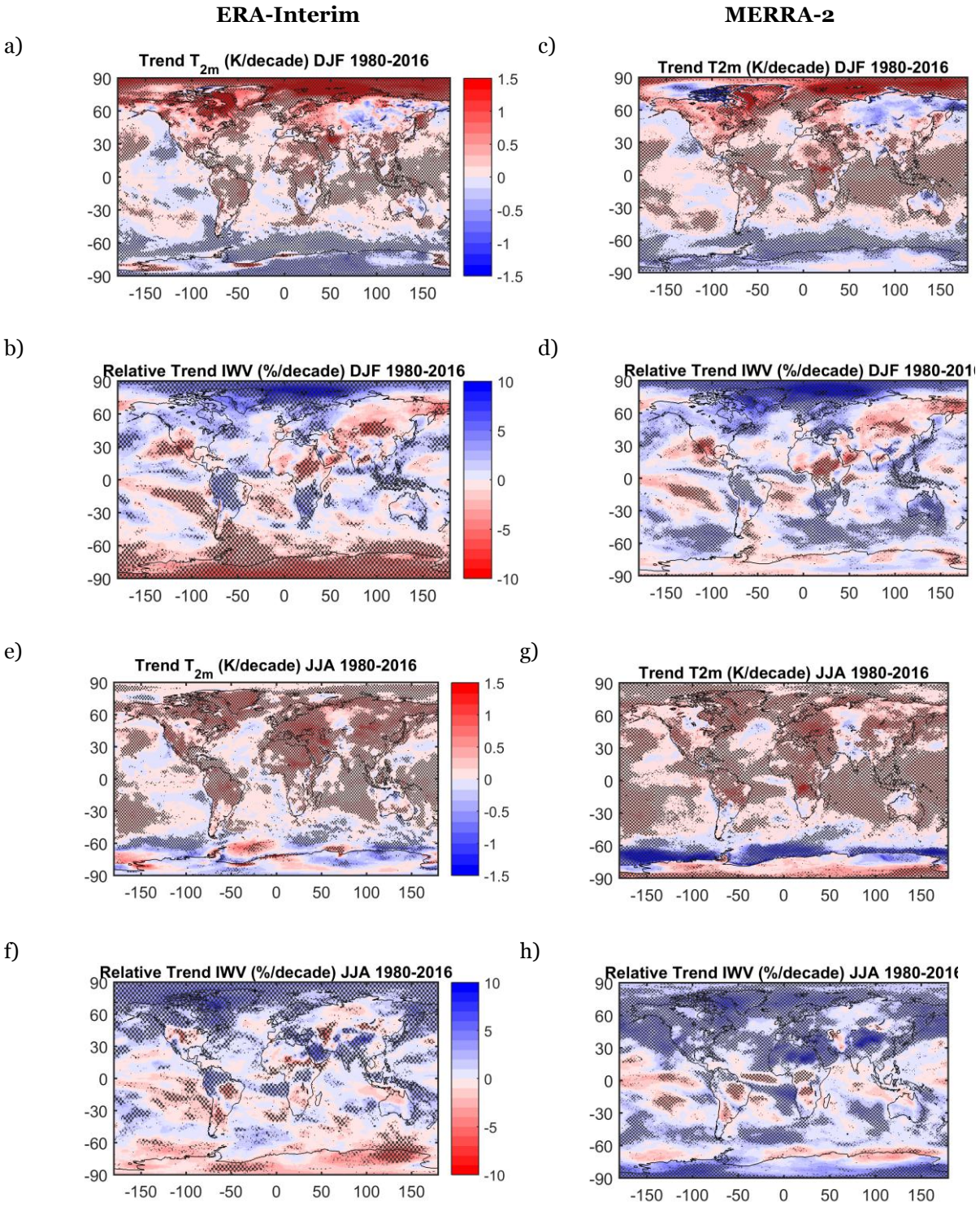

Figure 11: Seasonal trends in T2m and IWV for ERA-Interim's full time period (left), and MERRA-2's full time period (right).

On the annual trends, most structures are similar for both periods of ERA-Interim, although the intensities are weaker for the longer period (note that the colorbars are different for Figs. 5 and 10), but mostly significant. Over land, the drying and moistening trends over Africa and South America show similar patterns, as well as the moistening trends over eastern and northern regions of Europe and drying trends over Antarctica. The main differences appear over the Arabic Peninsula, Western Australia, Mexico, and a small part of Antarctica. The drying trend over Australia observed for the shorter period is not observed in the long term. For this longer period, trends are mostly not statistically significant, which suggests that there might have been a moistening trend before the drying trend. Over the oceans, an overall moistening trend (except strong drying off the coast of Antarctica) is observed, especially in the northern hemisphere, but several areas show different patterns for both periods. For the Atlantic Ocean, a different sign is observed along the eastern coast of North America, with a significant moistening for the longer period, while a drying is confirmed by GPS around Bermuda for the shorter period. In the south, the drying trend is spatially more extended and statistically more significant for the longer period. Over the Indian ocean, for the short period, the western part moistens and the eastern part dries, and opposite trends are obtained over the longer period. Over the Pacific Ocean, even though the patterns look similar, the spatial variability is stronger for the shorter period, with a more intense moistening along the equator, and west of Patagonia and a weaker moistening around Alaska.

Concerning the seasonal trends, the JJA patterns are mostly consistent over land and ocean between the two periods. Slight differences appear over India (where the moistening trend is more spatially extended in the longer period), Australia (where the trend is no longer significant), and Antarctica, where the drying trend is shifted eastward. For DJF, stronger differences exist. While the moistening trend of the short period over northern South America, southern part of Africa, Central and northern Europe, western Canada and Alaska and Artic are consistent with the longer period, the ones over Patagonia, part of China and Afghanistan, part of Antarctica and western Africa are no longer visible. The drying trends over Antarctica are extended to the entire continent for the longer period. The eastern USA that dries between 1995 and 2010 presents a moistening trend when considering the longer period. The strong drying obtained over Australia in DJF is mostly cancelled over the long period. Over the oceans, differences exist over the Indian Ocean, western Atlantic (along the east coast of USA), part of the south Atlantic and Pacific and mostly around Antarctica.

According to the Clausius-Clapeyron (C-C) equation, it is expected that an increasing temperature trend corresponds to an increasing IWV trend, especially over the oceans where the source of humidity is infinite. In order to assess the link between temperature and IWV trends, the trends in the 2-meter temperature were computed (even if the use of 2-m temperature may not be the best proxy of temperature in C-C equation). Annually and globally (not shown), over the oceans, the temperature and water vapour trends have the same sign, despite some small-scale differences. Over land, all areas show an increase in T2m, except the high latitudes of the southern hemisphere. This means that, except over Antarctica, the drying observed in the afore-mentioned areas cannot be explained by temperature. When we consider each season separately (shown in Figs. 11 a) and e)), some areas indicate a cooling, which can thus partly explain the drying. This is observed over Antarctica and to a lesser extent over Central Asia in DJF. Over eastern Australia, and South Africa, a weak cooling is observed while a significant moistening has been computed. For JJA, all continental areas show a significant warming, with the exception of parts of Antarctica, and a small area over northern Australia, where a drying is also displayed, albeit not significant. Thus the C-C scaling ratio is not a good proxy for humidity when considering seasonal and regional variabilities and trends due to the important role of dynamics which allow the advection of dry or wet air masses (e.g. over USA, South America, eastern Sahel, and South Africa in JJA).

As already discussed over the short period, MERRA-2 presents different trends from ERA-Interim over some areas over the long period (Fig. 10), which result from both the uncertainties that exist when computing trends, and from the differences in the physics and dynamics of the two products.

It is evident that MERRA-2 presents a more general moistening trend than ERA-Interim, especially in the southern hemisphere in DJF, and in both hemispheres in JJA (Fig. 11). The main differences in the trends over oceans appear all around Antarctica, and those over continental areas are observed over Africa (where trends are positive in the North and negative in Central Africa in MERRA-2 and the opposite in ERA-Interim) and USA in JJA, over Australia in DJF and over Antarctica in both JJA and DJF. Over Africa and Antarctica, the important differences which exist between ERA-Interim and MERRA2 for both long and short term periods suggest that the physical processes are not well represented. These areas correspond to areas with very few observations available for data assimilation, reducing the constraint on the models. A more detailed investigation of the dynamics over Africa and Australia is presented in the following subsection.

Other regions, such as the Indo-Pacific region have different trends over the shorter period, but are in better agreement over the longer period. This is more obvious during JJA (although there are also differences in DJF) and can be explained by the strong variability that requires longer time series in order to obtain meaningful trends. The good agreement between reanalyses over this area is an important result regarding the fact that CMIP5 models have large biases over this region in present day Sea Surface Temperature, which has direct consequences on the future projection of precipitation over Australia (Brown et al., 2016; Grose et al., 2014). However, the link between IWV trends over these oceans and Australia is not that strong here, since over Australia, while reanalyses were in good agreement over the shorter period, the western part presents a significant moistening in MERRA-2 over the long period in DJF, and a weak and not statistically significant drying in ERA-Interim. This area is thus investigated in more details in the next subsection. This may suggest discontinuities in the reanalysis data or an uncertainty in the computation of long-term trends (due to the presence of different sign shorter term trends during the longer period).

Analysis over Western Australia

Figure 12 displays the time series of IWV and temperature anomalies for a box over Western Australia for both the short and long term, and the differences are computed, for both the full time series and the DJF period. For the 1995-2010 period, the drying trends are present in both reanalyses and the annual trends are statistically significant. For the longer time period, on the contrary, the annual trends are positive (moistening) for both reanalyses on average over the box, but not significant for ERA-Interim.

One reason that explains the difference in the trend estimates comes from the fact that ERA-Interim IWV starts with higher anomalies than MERRA-2 until 1990, but ends with lower anomalies after the late 2000s, so that the resulting trend is close to zero and not significant in ERA-Interim. But what is striking when looking at the time series is the existence of extreme humid periods in both reanalyses, with a strong occurrence around the 2000s, which impact the trend estimate over the short period more strongly than over the long period. These periods correspond to DJF 1997, 1999, 2000, 2001, 2006, 2011. Power et al. (1998) and Hendon et al. (2007) have shown that during DJF the correlation between wetter years and colder years is strong at interannual time scales. Here, more humid years (in terms of IWV) do not seem to be strongly correlated with colder periods, suggesting a more complex interaction between

temperature, IWV and precipitation. However, most studies over Australia conclude that dynamics mostly explain the variability and trend of temperature and precipitation.

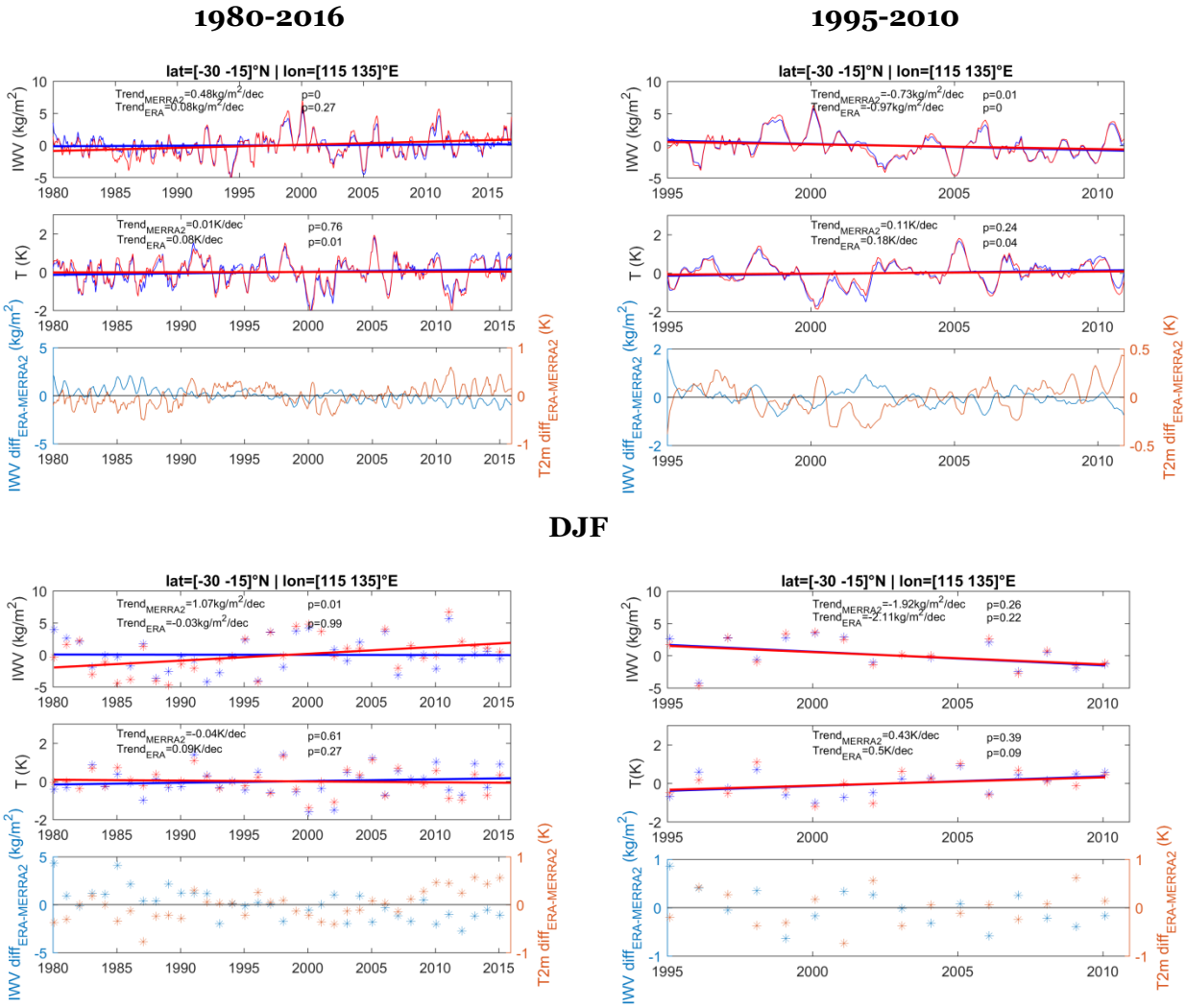

Figure 12: Temperature and IWV anomalies time series for a box over Western Australia, using ERA-Interim (blue) and MERRA-2 (red) data, for both the 1995-2010 and the 1980-2016 time periods (both annual and DJF analysis).

Here, we consider the wind at 925 hPa to assess the role of dynamics in these trend and variability. Figure 13 displays the time series of wind vectors and wind anomaly over the same box as Fig. 12 for the two periods and it is clear that the anomalously moister winters are associated with a dynamical anomaly, with a weaker wind, and a direction switching from south-easterly to easterly. The amplitude of wind direction difference is stronger in MERRA than in ERA-Interim but both reanalyses are consistent. Figure 14 presents the mean zonal and meridional components of the wind, superposed by the trends of each component in contours.

The mean states in u925 and v925 are similar in both reanalyses showing mainly an easterly wind, but with a convergence within the box in DJF, from north-easterly in the northern part of the box and from south-easterly in the southern part. The trends show a reinforcement of the easterly component and a very weak trend of the meridional component in DJF, confirming that the wind had a more south/south-easterly direction at the beginning of the period than at the end when it becomes more easterly, which is consistent with a moister air mass at the beginning when it is advected from the Pacific ocean.

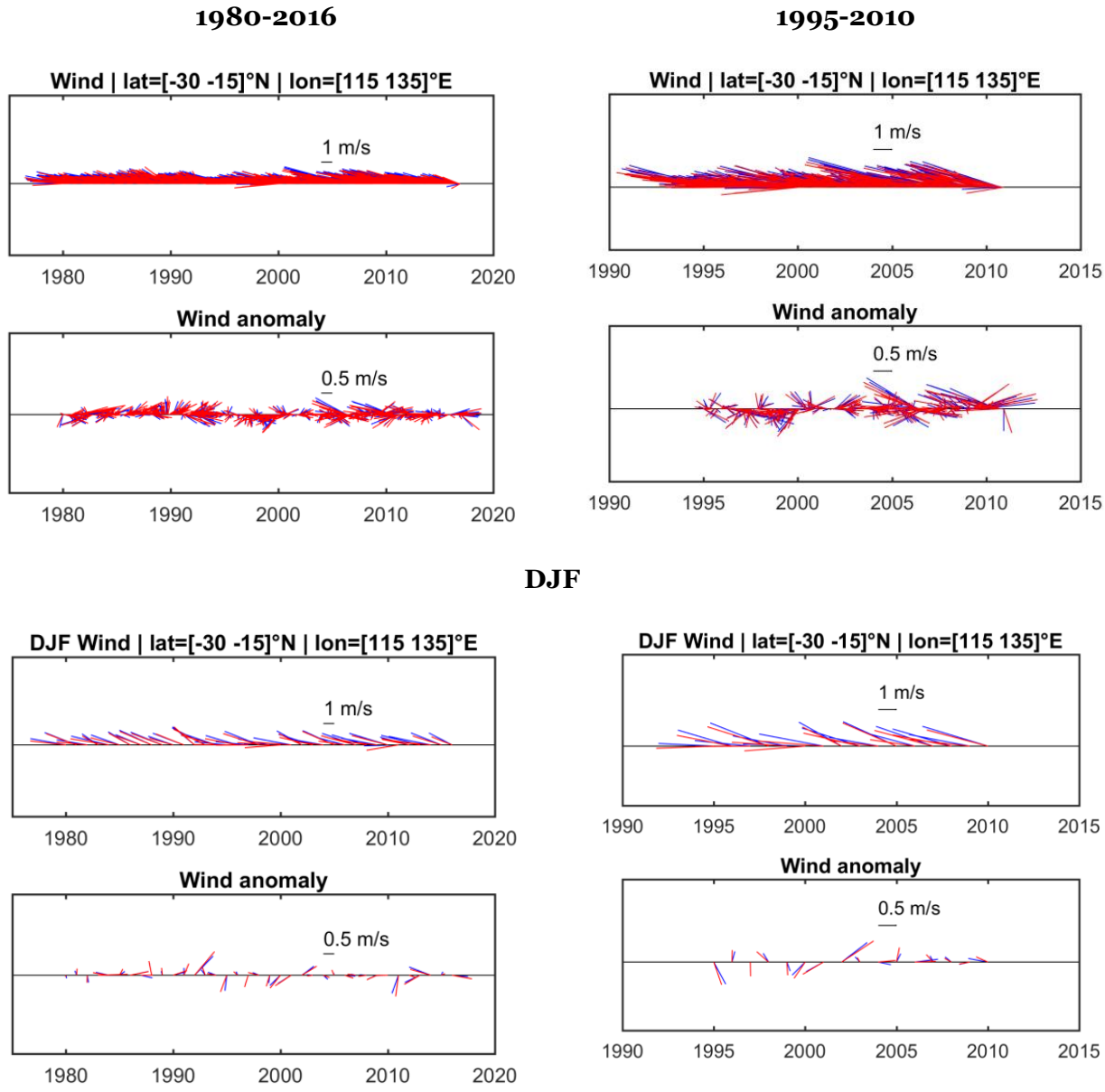

Figure 13: Wind speed and wind direction anomalies time series for a box over Western Australia, using ERA-Interim (blue) and MERRA-2 (red) data, for both the 1995-2010 and the 1980-2016 time periods (both annual and DJF analysis).

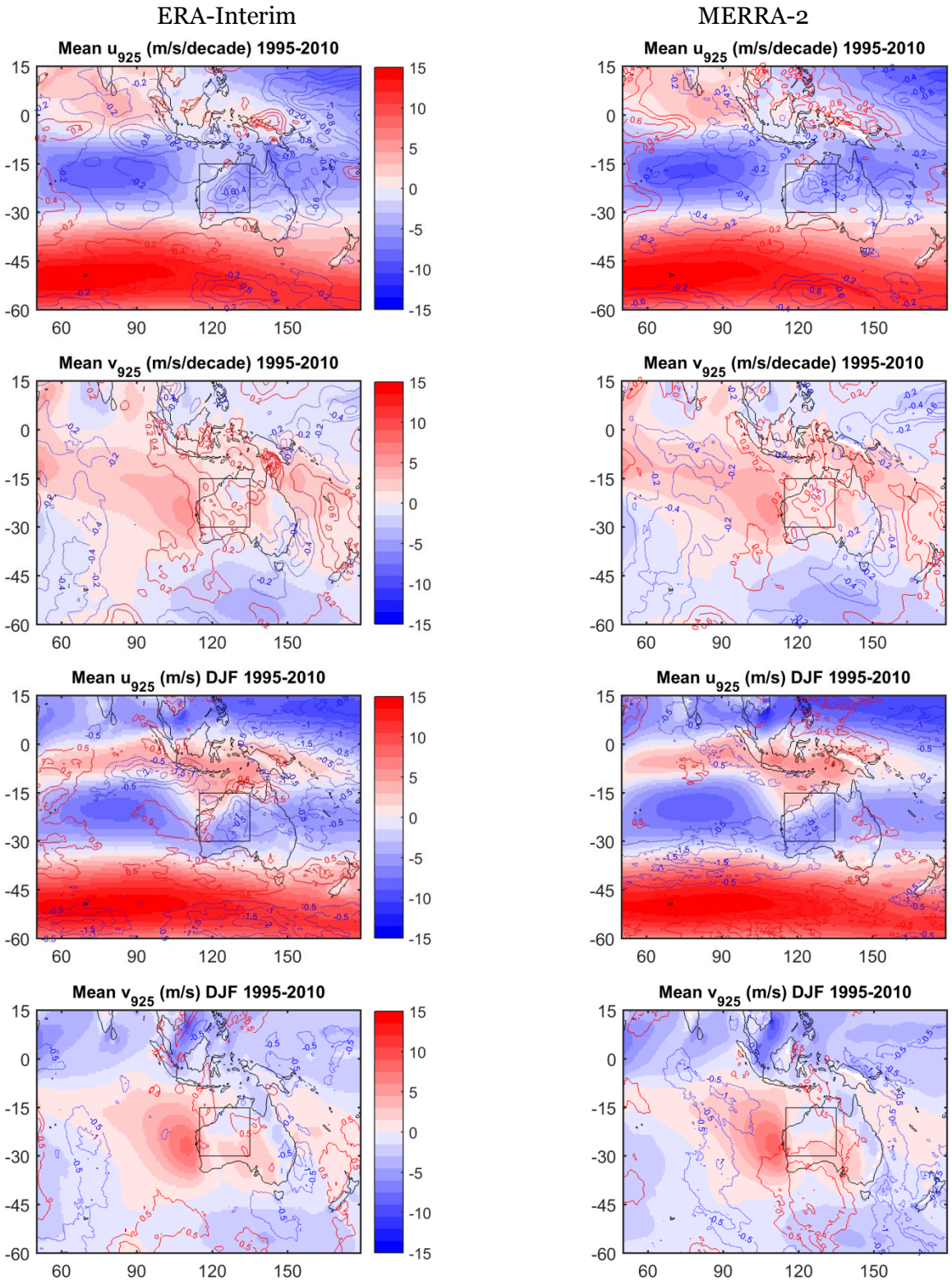

Figure 14: Zoom over Western Australia of the mean annual and DJF fields and trends of the u and v wind components at 925 hPa, and and their trends (contours). The area of focus (where IWV trends are most intense in ERA-Interim) is marked by a box.

Analysis over Western/central Africa

Over eastern Sahel, the annual trend in IWV in MERRA-2 over the long period is close to zero and not significant (Fig. 15), while that of ERA-Interim is significantly negative. IWV values over this area are higher in ERA-Interim at the beginning of the period and lower at the end of the period. From 2006, there is a clear divergence between both reanalyses with significantly warmer and drier air in ERA-Interim than in MERRA-2. However, both reanalyses present four different periods: a drying trend at the very beginning (1980-1985) followed by a moistening trend until 1995, then followed by a new drying period. From around 2008, the trend seems to stop. As a consequence, over the shorter period, both reanalyses show a significant annual drying, even though for ERA-Interim the trend is twice as intense.

1980-2016 **1995-2010**

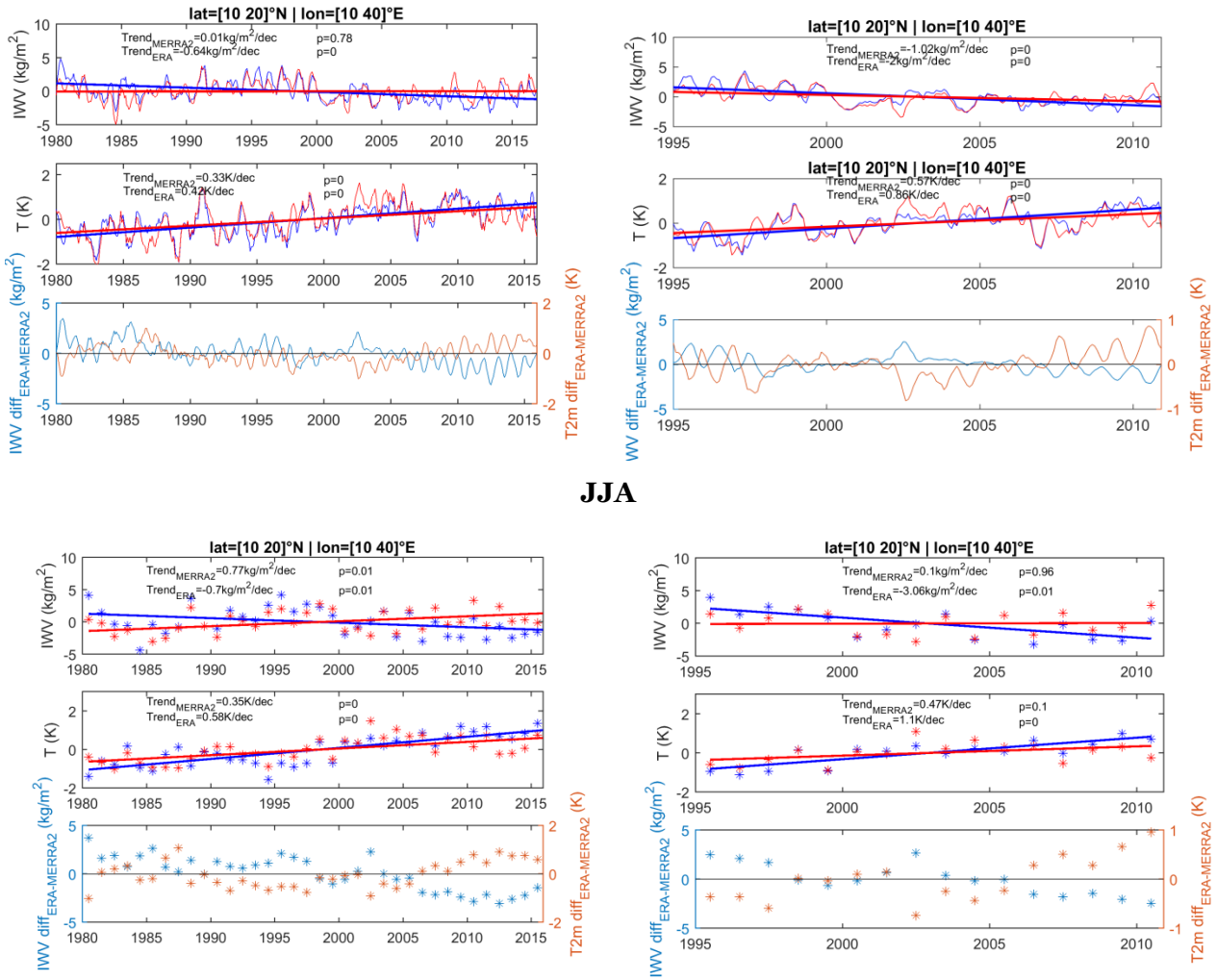

Figure 15: Temperature and IWV anomalies time series for a box over Eastern Sahel, using ERA-Interim (blue) and MERRA-2 (red) data, for both the 1995-2010 and the 1980-2016 time periods (both annual and JJA analysis).

As observed for IWV, the trend in T stops at around 2008. Before that period, the temperature is increasing significantly, despite strong variability that mostly corresponds to seasonal cycle. However, no correlation appears between IWV and T when considering annual variability. In JJA, the trend is strong and goes on after 2008. In JJA, while the interannual correlation between both reanalyses is quite good, there are strong differences in the estimate of the IWV between both. MERRA-2 presents an overall moistening trend in JJA over the long period, while ERA-Interim shows a drying. Over the short period, the trend in JJA in MERRA-2 is close to zero while it is strongly negative in ERA-Interim.

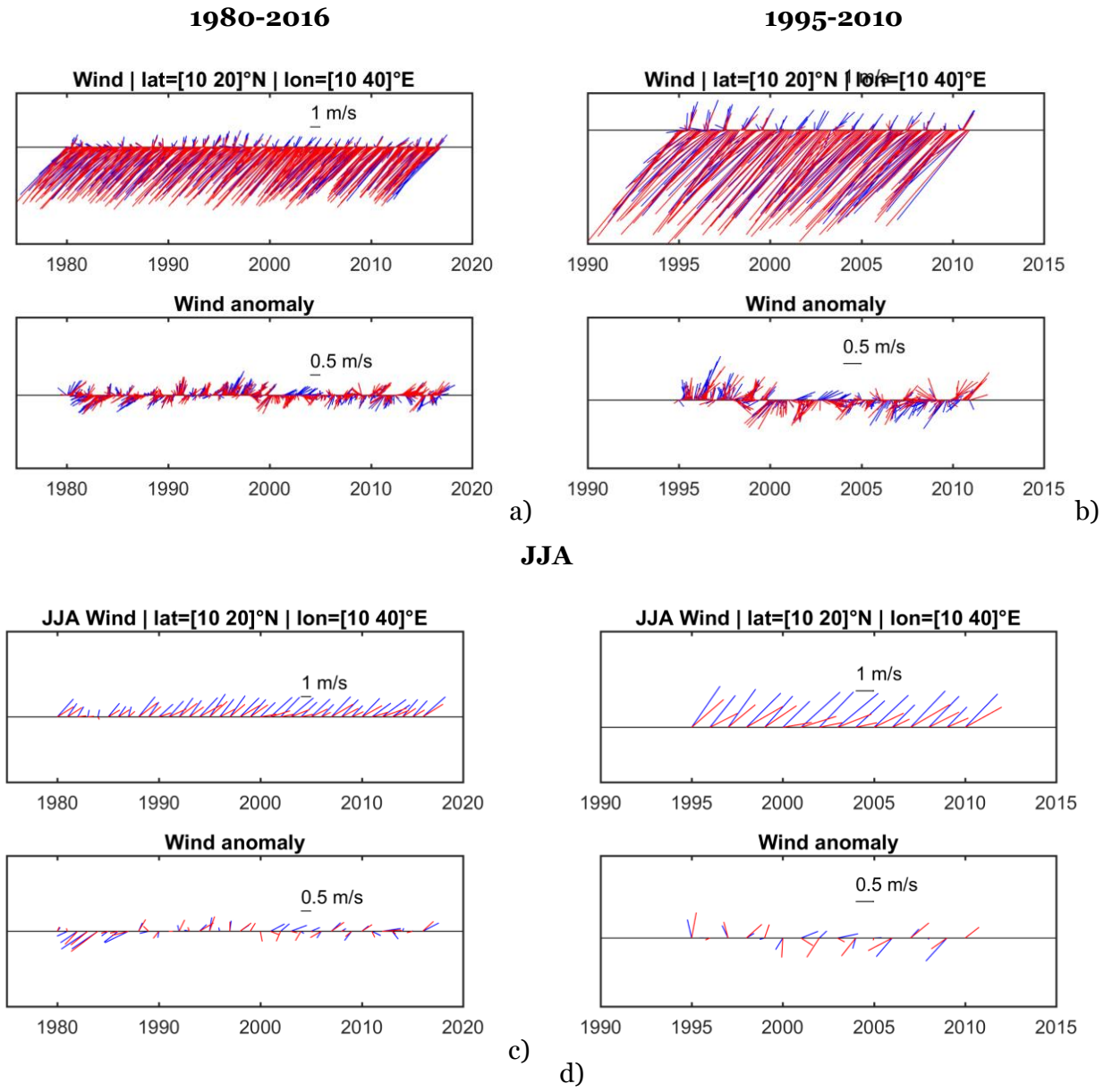

Figure 16: Wind speed and wind direction anomalies time series for a box over Northern Africa, using ERA-Interim (blue) and MERRA-2 (red) data, for both the 1995-2010 and the 1980-2016 time periods (annual and JJA analysis).

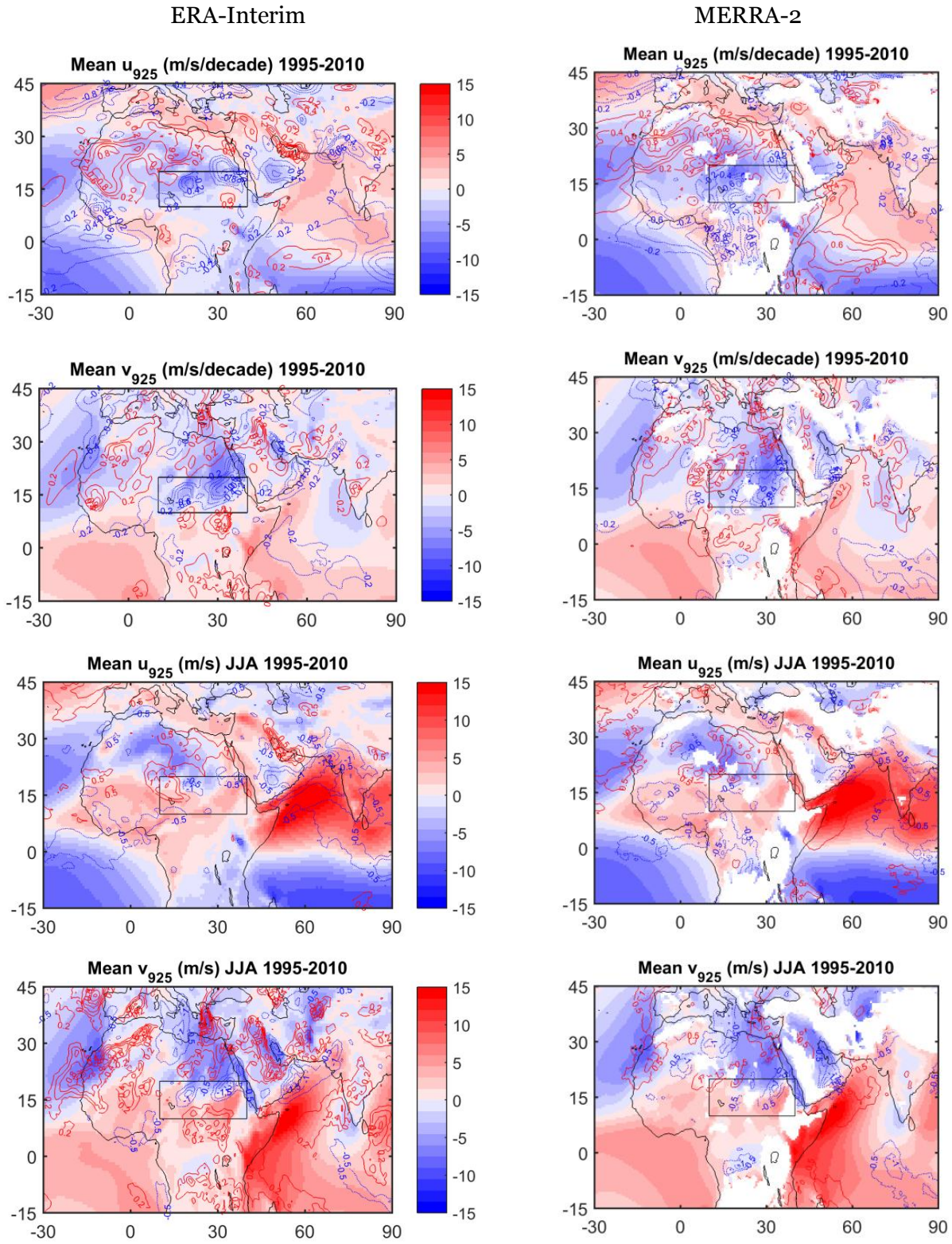

Figure 17: Zoom over North Africa of the mean annual and JJA fields and trends of the u and v wind components at 925 hPa, and and their trends (contours). The area of focus (where IWV trends are most intense in ERA-Interim) is marked by a box.

The annual time series of the wind (in Figs. 16 a) and b)) clearly indicate the periods when the monsoon flow reaches the box. This flow appears stronger in ERA-Interim than in MERRA most of the time. The period 1990-2000 shows more intense southerly flow in both reanalyses. And when looking at the wind anomaly, it appears that the southerly component is stronger in summer but the northerly wind is also weaker for the other months, suggesting a large-scale anomaly of circulation during this period generating a low-level wind convergence northwards than before and after. Since most of humidity is advected in summer by the monsoon flow, we looked at JJA in more detail (Figs. 16 c) and d)). The time series of wind in JJA in MERRA clearly indicates the same four periods than for IWV with a weakening of the south-westerly wind between 1980 and 1985, followed by an intensification of the monsoon flow arriving in this box between 1985 and 1995, and a wind decreasing and turning to the west until 2005 or 2006 and then becoming more stable in average. In ERA-Interim, we only observe two main periods: a weaker south/south-westerly wind at the beginning of the period and an intensification around 1990. The wind intensity is maximum between 1995 and 2000 but stays quite intense and with a south/south-westerly direction until the end of the period, being stronger and more southerly than in MERRA after 2000. The different dynamics of the two reanalyses observed in this box partly explains the increasing deviation between both reanalyses at the end of the period. Since these time series are an average over the box, we plotted the spatial map of the zonal and meridional wind components at 925hPa over the short period (Fig. 17). The mean states are plotted in colors over which the contours of the trends are superposed. The mean states in u925 and v925 are similar in both reanalyses, with a southwesterly wind in JJA that covers most of the area. This wind is a bit stronger in ERA-Interim than in MERRA. For both reanalyses, the trends in the zonal component are weak. For the meridional component, a southerly acceleration in the south part of the box is seen in ERA-Interim and not in MERRA, likely reducing the marine origin of the air arriving in this region and explaining partly the drying trend. At annual scale, there is also an intensification of the northeasterly flow into the box in both reanalyses, with more intensity in ERA-Interim, enhancing the difference in IWV annual trend between both reanalyses.

Summary

In this paper we used IWV data from GPS observations and reanalyses (ERA-Interim and MERRA-2) to study water vapour trends and variability for the 1995-2010 period. We found that the means and variability are well represented in ERA-Interim, even in regions of high IWV gradients. Some differences were pointed out between GPS and ERA-Interim at certain stations. These sites are mostly located in coastal regions and regions of complex topography.

Representativeness errors are the suspected cause, due to the large variations in the altitude in the surrounding grid points to the GPS station, or the large height different between the model surface and the GPS antenna.

Next, the ERA-Interim and GPS data were used to study the trends in IWV over the period 1995-2010. Strong annual trends were found in ERA-Interim. Over the oceans, significant moistening trends were observed over most of the tropical oceans and over the Arctic, while significant drying was observed in south-tropical eastern Pacific region, west of the United States and generally south of 60°S. Over land, significant positive trends were observed in northern South America, Central Africa, and Indonesia, over northern North America, Greenland, most of Europe and Siberia. Significant negative trends over land were observed over North Africa, Australia, Antarctica, central Asia, and most of the USA. These trends were compared with GPS and were found to be in general good agreement, but with opposite sign trend at some sites. Discrepancies at most of these sites were found to be due to gaps in the GPS time series (when time-matched series are compared, the agreement is improved) and discontinuities (some of which explained by reported GPS equipment changes), but drifts in the reanalysis are also plausible.

To better understand the trends, we separated them by seasons (DJF or JJA), which presented stronger absolute and relative trends. In some regions, trends can have opposite signs in winter and summer, which emphasizes the role of atmospheric circulation in IWV trends. The comparison of ERA-Interim and GPS seasonal trends is consistent with the annual trends. However, the differences are generally of larger magnitudes and a few more sites show trends with opposite signs. This is mainly due to the enhanced impact of time gaps for the short seasonal time series.

To complete the study and determine whether these differences are due to errors in ERA-Interim or in the GPS data, a second reanalysis, MERRA-2, was also analyzed. The results for MERRA-2 appear to be different from ERA-Interim over several parts of the globe, in particular over Indonesia and Indian Ocean, central Africa, Western (coastal) and Northern Africa, Central Asia and Antarctica (where there appears to be some uncertainty in all datasets). The trends for 1995-2010 were also compared with longer-term trends, for the 1980-2016 period. For both long and short term periods, important differences were found between ERA-Interim and MERRA2 over Africa and Antarctica. These areas correspond to areas with very few observations available for data assimilation, which suggest that the physical processes might not be well represented. A more detailed investigation of the dynamics over Africa and Australia was presented. We

considered the wind at 925 hPa to assess the role of dynamics in these trend and variability. Anomalies in the wind speed and direction were associated with differences in IWV anomalies, and differences in the winds for both reanalyses were found to enhance the differences in IWV trends.

References

Barnston, A. G., & Livezey, R. E. (1987). Classification, seasonality and persistence of low-frequency atmospheric circulation patterns. Monthly weather review, 115(6), 1083-1126.

Bastin S., Bock O., Chiriaco M., Drobinski P., R. Roehrig, Ahrens B., Gallardo C., M. Dominguez-Alonso, L. Li: Evaluating the impact of humidity bias on light precipitation estimates in Med-CORDEX/Hymex simulations using long term GPS network and ground-based datasets. *Sub. to ACP special issue*

Bengtsson, L., Hagemann, S., & Hodges, K. I. (2004). Can climate trends be calculated from reanalysis data?. *Journal of Geophysical Research: Atmospheres*, *109*(D11).

Bock, O., Bouin, M. N., Walpersdorf, A., Lafore, J. P., Janicot, S., & Guichard, F. (2007). Comparison of GPS precipitable water vapour to independent observations and Numerical Weather Prediction model reanalyses over Africa. QJR Meteorol. Soc.

Bock, O., Willis, P., Wang, J., & Mears, C. (2014). A high-quality, homogenized, global, long-term (1993–2008) DORIS precipitable water data set for climate monitoring and model verification. *Journal of Geophysical Research: Atmospheres*, *119*(12), 7209-7230.

Bock, O., Bosser, P., Pacione, R., Nuret, M., Fourrié, N., & Parracho, A. (2016). A high-quality reprocessed ground-based GPS dataset for atmospheric process studies, radiosonde and model evaluation, and reanalysis of HyMeX Special Observing Period. *Quarterly Journal of the Royal Meteorological Society*, *142*(S1), 56-71.

Brown, J. R., Moise, A. F., Colman, R., & Zhang, H. (2016). Will a Warmer World Mean a Wetter or Drier Australian Monsoon?. Journal of Climate, 29(12), 4577-4596.

Byun, S.H., and Y. E. Bar-Server (2009), A new type of troposphere zenith path delay product of the international GNSS service, J. Geod, 83(3-4), 367-373, DOI: 10.1007/s00190-008-0288-8.
Collins M. and co-authors, 2010: the impact of global warming on the tropical Pacific Ocean and El Nino. Nat. Geos., 3, 391-397.

Collins, M., An, S. I., Cai, W., Ganachaud, A., Guilyardi, E., Jin, F. F., ... & Vecchi, G. (2010). The impact of global warming on the tropical Pacific Ocean and El Niño. Nature Geoscience, 3(6), 391-397.

Dee, D. P., Uppala, S. M., Simmons, A. J., Berrisford, P., Poli, P., Kobayashi, S., ... & Bechtold, P. (2011). The ERA-Interim reanalysis: Configuration and performance of the data assimilation system. *Quarterly Journal of the royal meteorological society*, *137*(656), 553-597.

Dessler, A. E., & Davis, S. M. (2010). Trends in tropospheric humidity from reanalysis systems. *Journal of Geophysical Research: Atmospheres*, *115*(D19).

Hamed, K. H., & Rao, A. R. (1998), "A modified Mann-Kendall trend test for autocorrelated data", Journal of Hydrology, 204(1-4), 182-196.

Held, I. M., & Soden, B. J. (2006). Robust responses of the hydrological cycle to global warming. *Journal of Climate*, *19*(21), 5686-5699.

Hendon, Harry H.; Thompson, David W. J.; Wheeler, Matthew C. : Australian Rainfall and Surface Temperature Variations Associated with the Southern Hemisphere Annular Mode. Journal of Climate. June 2007, Vol. 20 Issue 11, p2452-2467. 16p. 4 Charts, 11 Maps.

Holloway, C. E., & Neelin, J. D. (2009). Moisture vertical structure, column water vapor, and tropical deep convection. *Journal of the Atmospheric Sciences*, *66*(6), 1665-1683.

IGSMAIL-6298, Reprocessed IGS Trop Product now available with Gradients, by Yoaz Bar-Sever, 11 Nov 2012, http://igscb.jpl.nasa.gov/pipermail/igsmail/2010/007488.html.

King, Andrew; Donat, Markus; Alexander, Lisa; Karoly, David The ENSO-Australian rainfall teleconnection in reanalysis and CMIP5..Climate Dynamics. May2015, Vol. 44 Issue 9/10, p2623-2635. 13p. DOI: 10.1007/s00382-014-2159-8

Kondratev, K. Y. (1972). Radiation Processes in the Atmosphere (Geneva: World Meteorological Organization).

Lorenz, D. J., & DeWeaver, E. T. (2007). Tropopause height and zonal wind response to global warming in the IPCC scenario integrations. *Journal of Geophysical Research: Atmospheres*, *112*(D10).

Lorenc, A. C. (1986), Analysis methods for numerical weather prediction. Q.J.R. Meteorol. Soc., 112: 1177–1194. doi:10.1002/qj.49711247414

Mieruch, S., Schröder, M., Noël, S., & Schulz, J. (2014). Comparison of decadal global water vapor changes derived from independent satellite time series. *Journal of Geophysical Research: Atmospheres*, *119*(22).

Molod, A., Takacs, L., Suarez, M., & Bacmeister, J. (2015). Development of the GEOS-5 atmospheric general circulation model: evolution from MERRA to MERRA2. *Geoscientific Model Development*, *8*(5), 1339-1356.

Neelin, J. D., Peters, O., & Hales, K. (2009). The transition to strong convection. Journal of the Atmospheric Sciences, 66(8), 2367-2384.

Ning, T., Wickert, J., Deng, Z., Heise, S., Dick, G., Vey, S., & Schöne, T. (2016). Homogenized time series of the atmospheric water vapor content obtained from the GNSS reprocessed data. *Journal of Climate*, *29*(7), 2443-2456.

Power, S., F. Tseitkin, S. Torok, B. Lavery, and B. McAvaney, 1998: Australian temperature, Australian rainfall, and the Southern Oscillation, 1910–1996: Coherent variability and recent changes. Aust. Meteor. Mag., 47, 85–101.

Ross, R. J., & Elliott, W. P. (1996). Tropospheric water vapor climatology and trends over North America: 1973–93. *Journal of Climate*, *9*(12), 3561-3574.

Ross, R. J., & Elliott, W. P. (2001). Radiosonde-based Northern Hemisphere tropospheric water vapor trends. *Journal of Climate*, *14*(7), 1602-1612.

Rousseeuw, Peter J.; Leroy, Annick M. (2003), ”Robust Regression and Outlier Detection”, Wiley Series in Probability and Mathematical Statistics, 516, Wiley, p. 67, ISBN 978-0-471-48855-2.

Ruti, P. M., Somot, S., Giorgi, F., Dubois, C., Flaounas, E., Obermann, A., ... & Ahrens, B. (2016). MED-CORDEX initiative for Mediterranean climate studies. *Bulletin of the American Meteorological Society*, *97*(7), 1187-1208.

Sahany, S., Neelin, J. D., Hales, K., & Neale, R. B. (2012). Temperature–moisture dependence of the deep convective transition as a constraint on entrainment in climate models. *Journal of the Atmospheric Sciences*, *69*(4), 1340-1358.

Schröder, M., Lockhoff, M., Forsythe, J. M., Cronk, H. Q., Vonder Haar, T. H., & Bennartz, R. (2016). The GEWEX Water Vapor Assessment: Results from Intercomparison, Trend, and Homogeneity Analysis of Total Column Water Vapor. *Journal of Applied Meteorology and Climatology*, *55*(7), 1633-1649.

Semenov, V., & Bengtsson, L. (2002). Secular trends in daily precipitation characteristics: greenhouse gas simulation with a coupled AOGCM. *Climate Dynamics*, *19*(2), 123-140.

Sen, P. K. (1968), "Estimates of the regression coefficient based on Kendall's tau", Journal of the American Statistical Association, 63 (324): 1379–1389, JSTOR 2285891, MR 0258201, doi:10.2307/2285891.

Theil, H. (1950), "A rank-invariant method of linear and polynomial regression analysis. I, II, III", Nederl. Akad. Wetensch., Proc., 53: 386–392, 521–525, 1397–1412, MR 0036489.

Trenberth, K. E., Fasullo, J., & Smith, L. (2005). Trends and variability in column-integrated atmospheric water vapor. *Climate dynamics*, *24*(7-8), 741-758.

Trenberth, K. E., Smith, L., Qian, T., Dai, A., & Fasullo, J. (2007). Estimates of the global water budget and its annual cycle using observational and model data. *Journal of Hydrometeorology*, *8*(4), 758-769.

Vey, S., Dietrich, R., Fritsche, M., Rülke, A., Steigenberger, P., & Rothacher, M. (2009). On the homogeneity and interpretation of precipitable water time series derived from global GPS observations. *Journal of Geophysical Research: Atmospheres*, *114*(D10).

Wagner, T., Beirle, S., Grzegorski, M., & Platt, U. (2006). Global trends (1996–2003) of total column precipitable water observed by Global Ozone Monitoring Experiment (GOME) on ERS-2 and their relation to near-surface temperature. *Journal of Geophysical Research: Atmospheres*, *111*(D12).

Wang, J., L. Zhang, and A. Dai (2005), Global estimates of water-vapor-weighted mean temperature of the atmosphere for GPS applications, J. Geophys. Res., 110, D21101, doi:10.1029/2005JD006215

Wang, J., Dai, A., & Mears, C. (2016). Global Water Vapor Trend from 1988 to 2011 and Its Diurnal Asymmetry Based on GPS, Radiosonde, and Microwave Satellite Measurements. *Journal of Climate*, *29*(14), 5205-5222.

Wardle, R., and I. Smith, 2004: Modeled response of the Australian monsoon to changes in land surface temperatures. Geophys. Res. Lett., 31, L16205, doi:10.1029/2004GL020157.

Wolter, K., & Timlin, M. S. (1993, March). Monitoring ENSO in COADS with a seasonally adjusted principal component index. In *Proc. of the 17th Climate Diagnostics Workshop* (Vol. 5257).

Wolter, K., & Timlin, M. S. (1998). Measuring the strength of ENSO events: How does 1997/98 rank?. *Weather*, *53*(9), 315-324.

3.3 Supplement to the paper: Intercomparison between ERA-Interim and MERRA-2, and ERA-20C and NOAA-20CR V2

In this section, ERA-Interim is compared in more detail with MERRA-2, and both reanalyses are compared with two twentieth century reanalyses, ERA-20C and NOAA's 20th Century Reanalysis Version 2 (20CR). ERA-Interim and MERRA-2 assimilate conventional and satellite observations, while:

- ERA-20C assimilates surface pressures from the International Surface Pressure Databank v3.2.6 and ICOADS v 2.5.1, and surface winds over the oceans from ICOADS v2.5.1, using a 4D VAR data assimilation scheme as described by Poli et al. (2016);
- 20CR assimilates observations of surface pressure and sea level pressure from the International Surface Pressure Databank station component version 2, ICOADS, and the International Best Track Archive for Climatic Stewardship every six hours, using a 56-member Ensemble Filter as described in Compo et al. (2011).

The objectives for this analysis were twofold. On the one hand, to assess the 20th century reanalyses, as these reanalyses cover a more extensive period and could, for instance, be used to validate/nudge climate models over extended periods (e.g. 1950-present). On the other hand, the comparison between the two types of reanalyses can be used to analyse the impact of observations on IWV.

3.3.1 Mean IWV

Figure 3.16 shows the means in IWV for ERA-Interim, for DJF and JJA. Similar mean patterns are observed in all four reanalyses for both seasons, although maximum values over the ITCZ have different intensities. In order to better gauge the differences, mean difference fields between the reanalyses and ERA-Interim are shown in Fig. 3.17. It is observed that ERA-Interim is drier than MERRA-2 in the tropics, but moister than ERA-20C (almost) globally, and 20CR around the Equator. As expected, the agreement between ERA-Interim and MERRA-2 is better (under 5 $kg.m^{-2}$ vs. up to 10 $kg.m^{-2}$ for the other reanalyses), and both 20th century reanalysis are drier around the Equator. For ERA-20C, the differences are more intense over land, while for 20CR, the differences over the ocean are high, and mostly positive (20CR is moister).

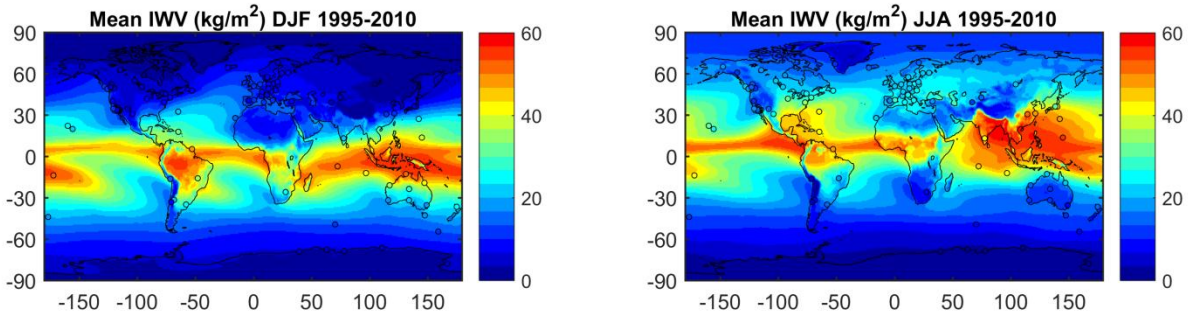

Figure 3.16: Mean IWV in ERA-Interim for DJF and JJA.

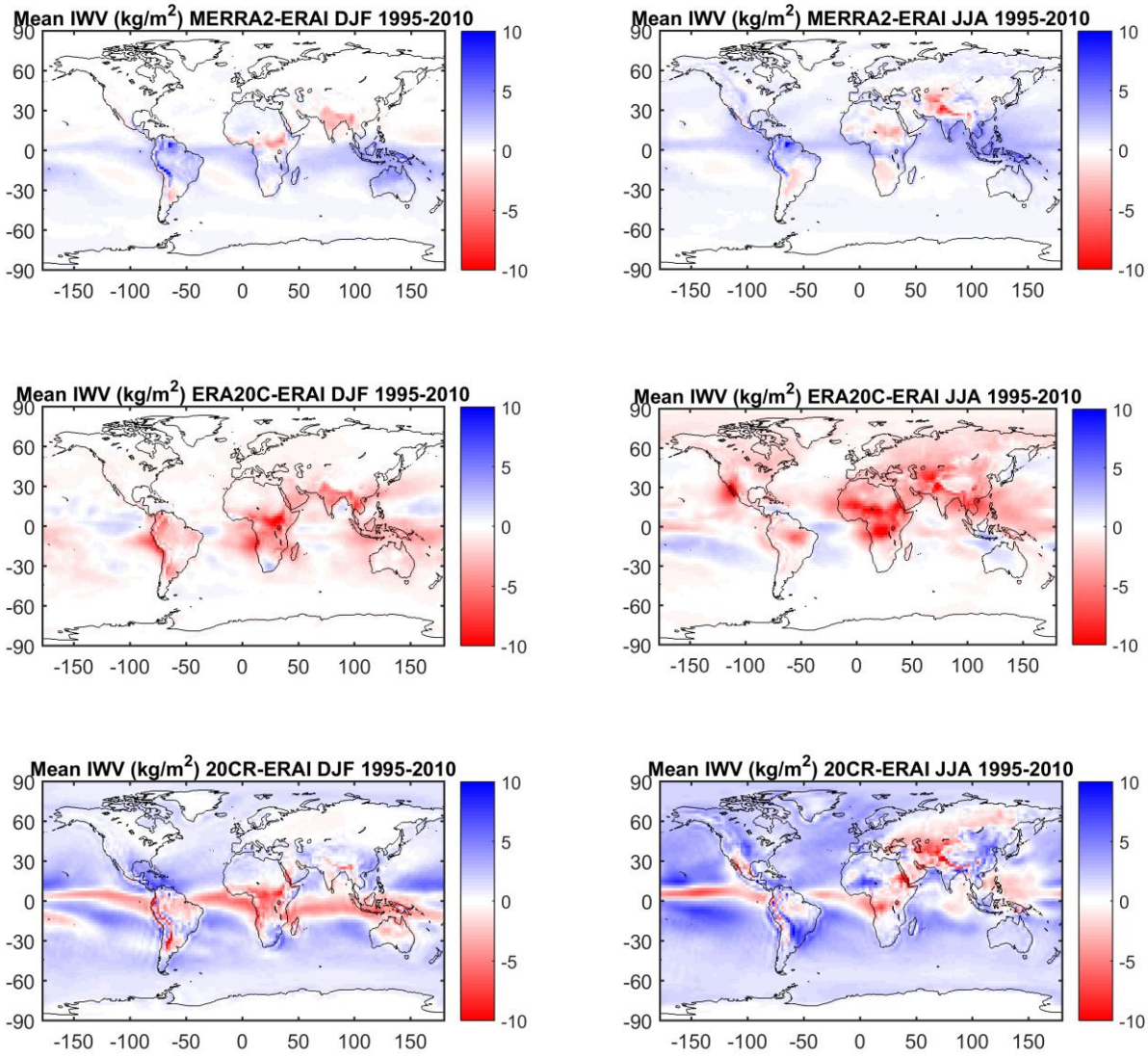

Figure 3.17: Difference in mean IWV between the MERRA-2, REA20C, and NOAA-20CR V2 reanalyses and ERA-Interim.

The twentieth century reanalyses appear to underestimate IWV over the ITCZ, and the maximum values are lower than for ERA-I, which in turn is drier than MERRA-2 over this region. In addition, ERA-20C in particular appears to have difficulty with the advection of IWV into the continents at the tropical latitudes (e.g. into West Africa in JJA). On the other hand, in 20CR the band of higher IWV is not as well defined as in the other reanalyses (e.g. over the Pacific and the Indo-Pacific regions in DJF). This large difference over the Tropics may be due to the fact that surface winds are not assimilated in 20CR (in contrast with the other reanalyses). The lower resolution of this reanalysis (presented in Chapter 1, in Table 1.2) may also be a factor.

3.3.2 Interannual variability of IWV

Figure 3.18 shows the interannual variability in IWV for DJF for the four reanalyses. ERA-Interim and ERA-20C have similar patterns, but variability is more intense in ERA-20C for the regions of high variability (i.e. Arctic, Siberia, Greenland, West Africa, Australia, Tropical Pacific and Antarctica). The differences shown in Fig.3.20 show a mostly positive difference between ERA-Interim and ERA-20C in these regions. There are similar maxima of variability in MERRA-2, over the Arctic, Tropical Pacific, and Siberia and West Africa (to a lesser extent). Over Australia and Antarctica, the variability is lower in MERRA-2 than in the previous two reanalyses, while over Canada the variability is higher. Figure 3.20 highlights these differences. For 20CR, the variability is generally higher over Antarctica, and lower over the Arctic and tropical Pacific. Figure 3.20 confirms this and highlights a difficulty in this reanalysis to represent the IWV variability especially over sea. The high variability in Australia, Siberia, Alaska, India is also observed in the GPS data. And in general, there is better agreement between GPS and ERA-Interim than MERRA-2, especially at higher latitudes. However, some of the areas of interest are not covered by the long-term GPS observations.

GPS IWV interannual variability for JJA (Fig.3.19) also showed good agreement with ERA-Interim, except over Antarctica. The intense variability in Australia and the Andes were also observed in GPS. These are also observed in MERRA-2, but are not as intense, especially in Australia (where GPS is in better agreement with ERA-Interim). On the other hand, the very strong variability found in Antarctica for MERRA-2 is in better agreement with GPS data. NOAA-20CR shows higher variability over central Asia and Antarctica, over land, and ERA-20C shows slightly higher variability over North Africa than the rest of the reanalyses. In spite of the differences in intensity (which can be relatively high, at up to 10 $kg.m^{-2}$) and extension, the rough pattern of maximum IWV variability is consistent across reanalyses.

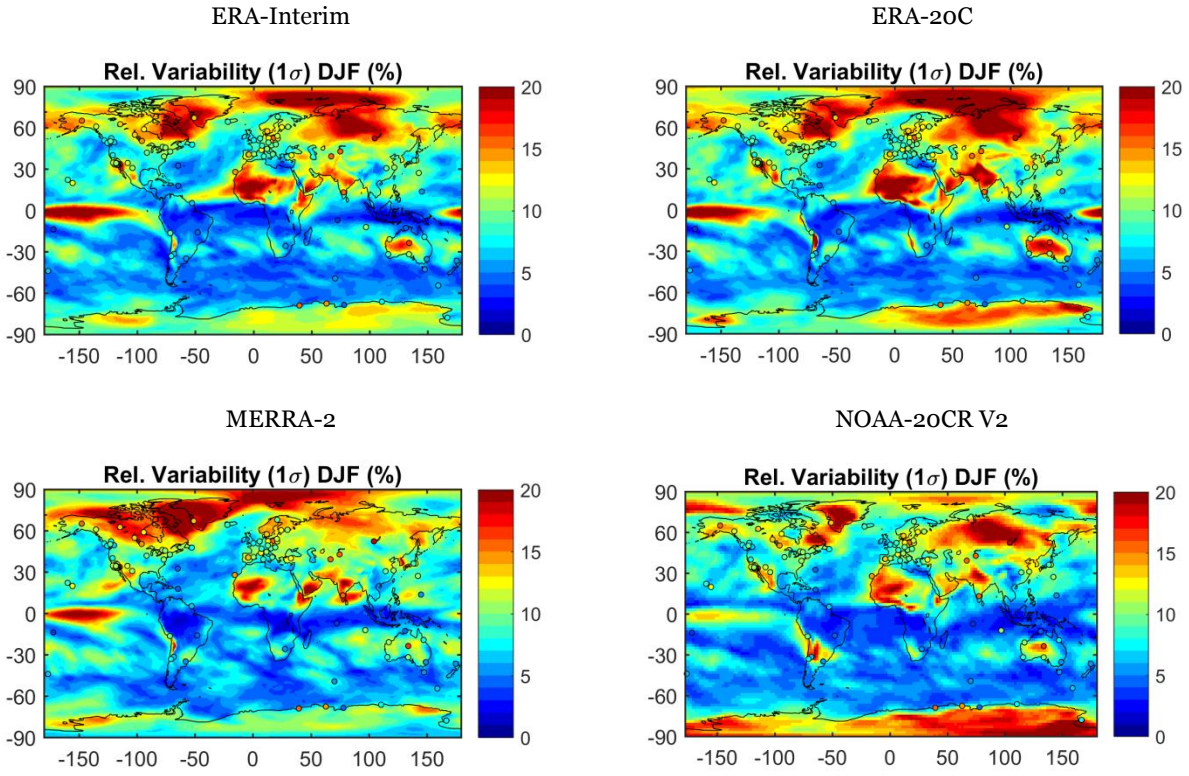

Figure 3.18: Interannual variability in IWV for the four reanalyses for DJF.

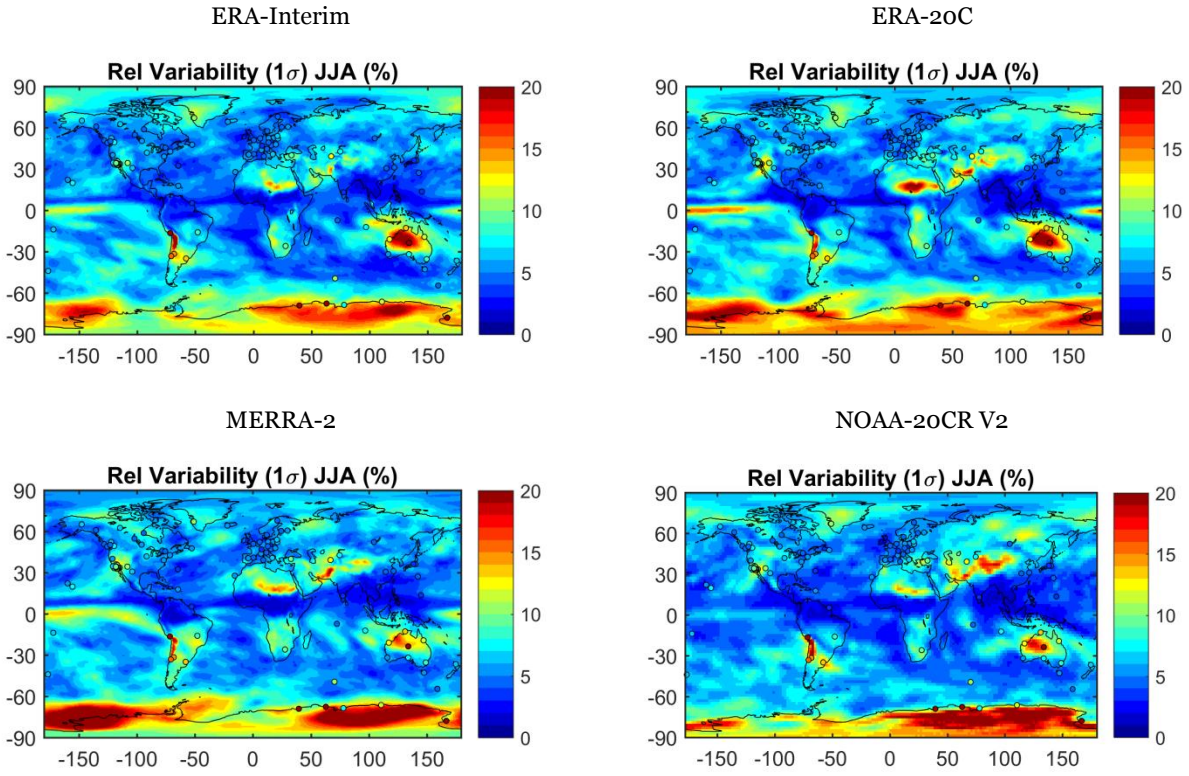

Figure 3.19: Same as Figure 3.18 but for JJA.

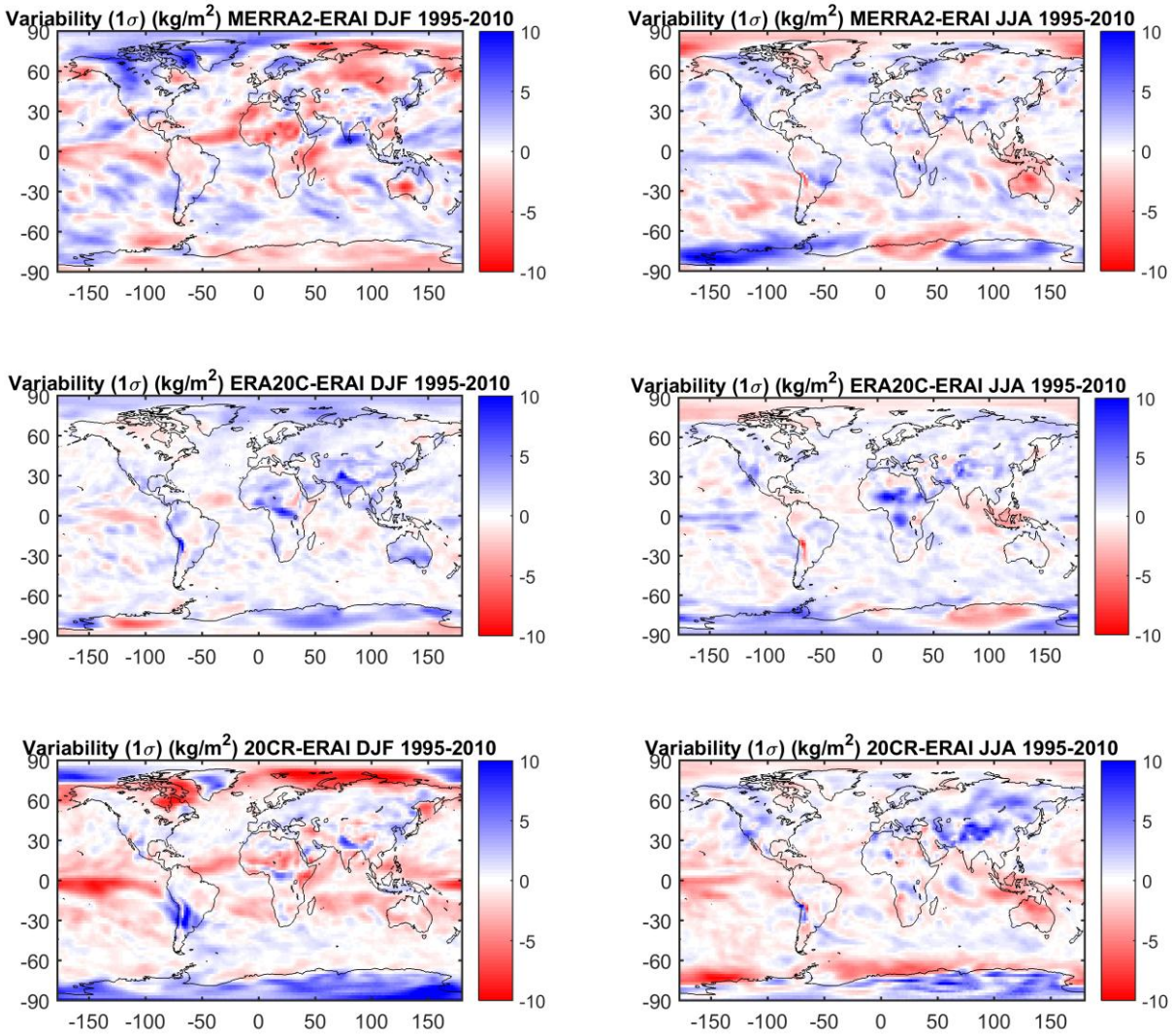

Figure 3.20: Difference in interannual variability in IWV between the MERRA-2, REA20C, and NOAA-20CR V2 reanalyses and ERA-Interim.

In general, 20CR underestimates the variability over the Arctic and tropical Pacific, while overestimating the variability over Antarctica. MERRA-2 underestimates the variability in Australia, and struggles at the latitudes above 60°N, in comparison with GPS. ERA-20C also tends to overestimate the maxima in variability, but on the whole the results for this reanalyses are quite consistent with ERA-Interim and GPS.

3.3.3 Linear trends in IWV

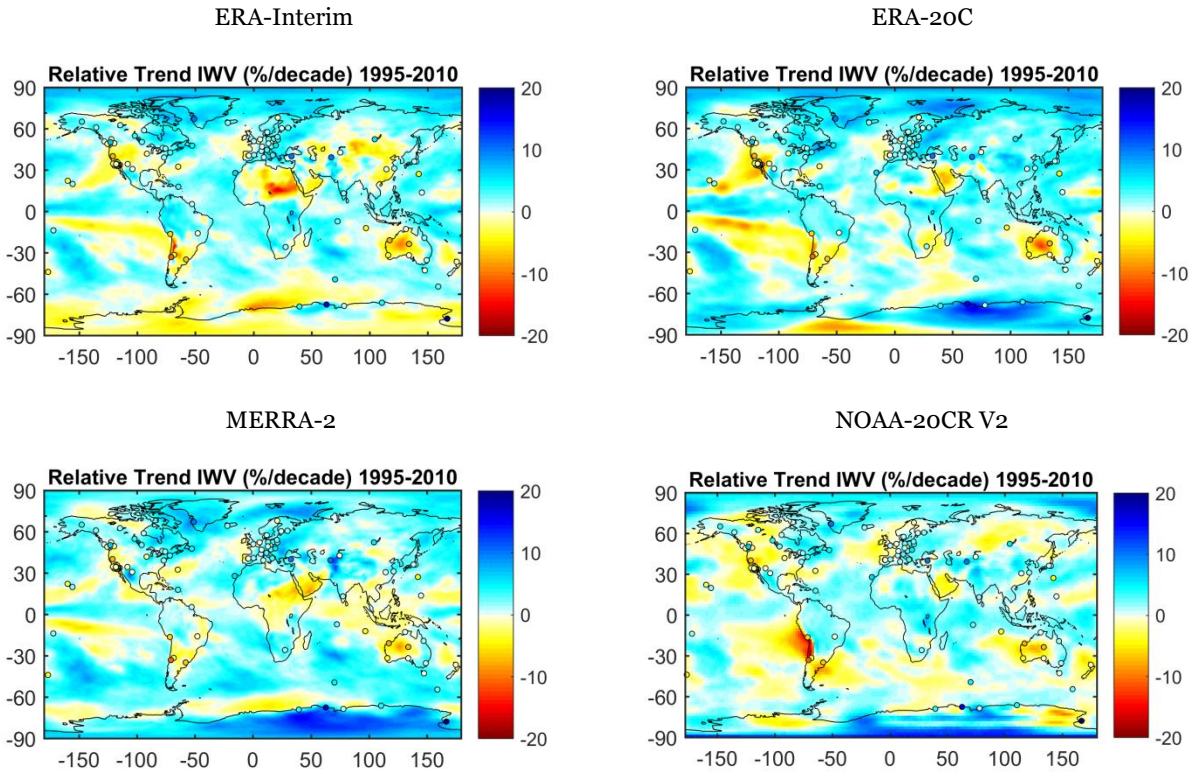

Figure 3.21: Linear trends in IWV for the four reanalyses.

Figure 3.21 shows the IWV trends in the four reanalyses. Some of the main IWV trend patterns (described previously) are present in all four reanalyses, although the intensities may vary. The most striking differences occur over Antarctica, where ERA-Interim shows different sign trends from the rest of the reanalyses. The trends over Asia also display some differences: more drying is observed in ERA-Interim and moistening in ERA-20C. ERA-20C is in better agreement with the GPS data that also shows moistening (although the coverage is sparse). The drying trend that was previously highlighted for North Africa in ERA-Interim is not as intense or extensive for ERA-20C and MERRA-2. For these reanalyses some drying is still observed, whereas there is a general moistening observed for 20CR.

ERA-Interim

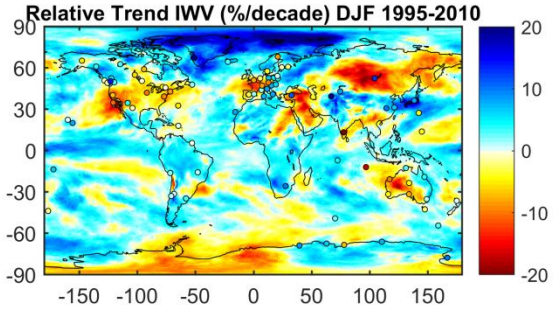

ERA-20C

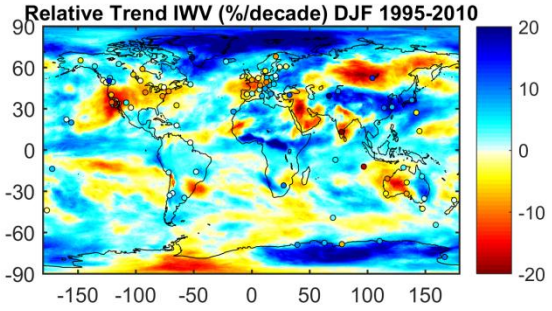

MERRA-2

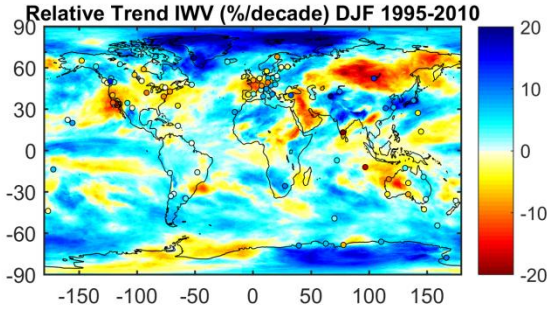

NOAA-20CR V2

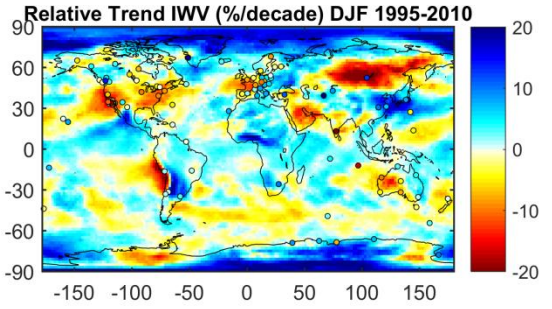

Figure 3.22: Same as Figure 3.21 but for DJF.

ERA-Interim

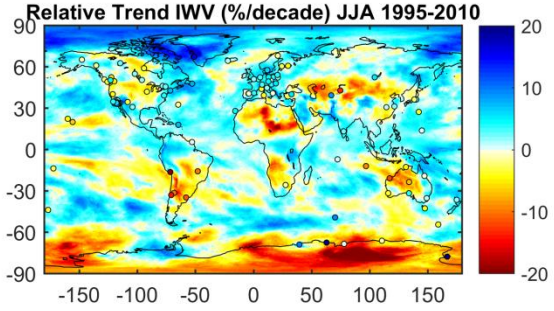

ERA-20C

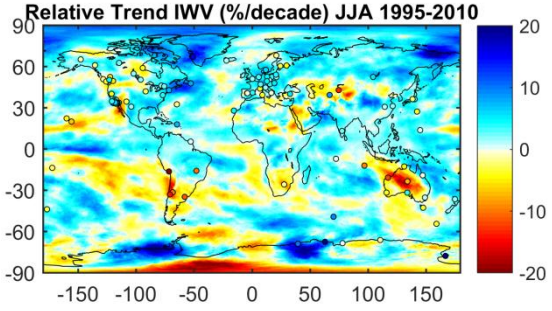

MERRA-2

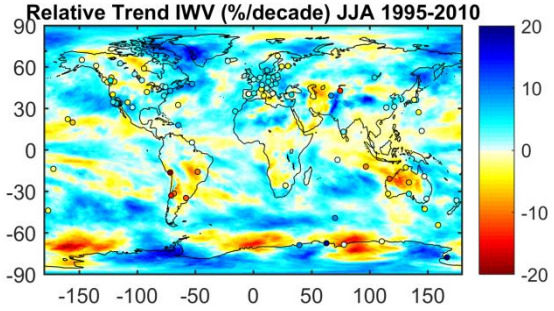

NOAA-20CR V2

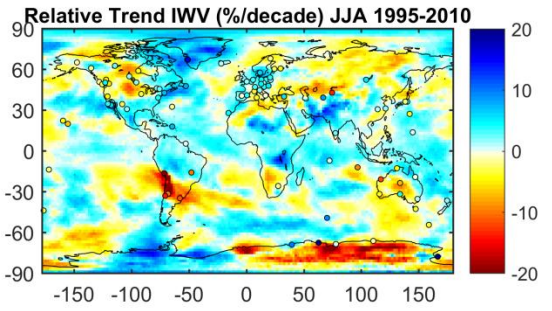

Figure 3.23: Same as Figure 3.21 but for JJA.

Figure 3.22 shows similar patterns of negative/ positive trends in DJF are observed for all reanalyses. In the southern part of the Atlantic and Indian oceans, the ERA-Interim/-20C simulations and 20CR show more drying trends than MERRA-2. Over Antarctica, the moistening trends are more extensive and intense in all reanalyses except ERA-Interim. The trends over Africa are similar in ERA-Interim and MERRA-2, but different from the other two reanalyses. For ERA-20 and NOAA-20CR the trends over Africa are similar and show a more intense moistening, especially over central Africa, along the Equator.

For JJA (Fig. 3.23), the strong drying observed for ERA-Interim over North Africa is not observed in the other reanalyses. For NOAA-20CR there is a moistening, while for ERA-20 there is a less extensive and less intense drying trend. For Australia, the drying in the Western part of the country is stronger in ERA-20C, but less intense and to the centre of the country in 20CR. Over Antarctica, all four reanalyses show different trend patterns. However, there appears to be a consistent moistening in the portion located south of South America. In ERA-Interim and NOAA-20CR, there is a strong drying in the Eastern half of the continent, which is not observed in MERRA-2 and ERA-20C (where there are alternated positive and negative trends).

These results suggest there might be an issue with the strong drying trends observed in ERA-Interim for North Africa and Antarctica in JJA, as all three other reanalyses show a large positive difference. These intense trends might result from discontinuities in the data.

3.3.4 Conclusions

The twentieth century reanalyses are able to represent the structures of the means, variability and trends relatively well, with similar patterns of maximum means and variability and of positive and negative trends. However, the differences in intensity can be quite high between reanalyses, and results are different for certain regions (e.g. trends and variability over Antarctica and trends over North Africa).

Due to their lower resolution and limited assimilated data, the twentieth century reanalyses should only be used when longer time periods are necessary. When considering the 1980-present time period, the more comprehensive reanalyses (such as ERA-Interim and MERRA-2) should be used. When twentieth century reanalyses are used, their shortcomings (e.g. too low IWV means in the tropics) should be kept in mind when analyzing the results.

Chapter 4: Assessment of simulations from global climate models using GPS data and atmospheric reanalyses

Water vapor is responsible for the most important positive feedback in climate change. Although this water vapor feedback is a robust feature across all climate models (Soden et al., 2005), simulated water vapor variabilities have been found to differ from observations (Pierce et al., 2006). Uncertainties in convective and turbulent parameterizations, cloud microphysics, land surface/atmosphere interactions in climate models lead to uncertainties in the accuracy of simulated water vapour and, ultimately, to uncertainties in climate predictions. Hence, an effort has been made to improve model representation of clouds and water vapour, guided by different types of observation (e.g. Jiang et al., 2012).

In the previous chapter, ERA-Interim integrated water vapor was compared with IWV converted from GPS measurements, in order to intervalidate both data sets. It was concluded that while ERA-Interim had some uncertainties in some regions, such as Antarctica and North Africa, some GPS stations also had representativeness and discontinuity problems. Because both GPS and ERA-Interim data have advantages and drawbacks, both data sets are used in this section to assess four configurations of the IPSL atmospheric general circulation model, LMDZ.

4.1 The LMDZ model

The model configurations used in this section consisted of two versions of LMDZ5: LMDZ5A (Hourdin et al.,2013a), used within the IPSL-CM5A model; and LMDZ5B (Hourdin et al.,2013b), used within the IPSL-CM5B model. LMDZ5A uses similar physical parametrizations to LMDZ4, a previous version of the model used in the Coupled Model Intercomparison Project (CMIP3), described in Hourdin et al. (2006), while LMDZ5B uses different parameterizations of turbulence, convection and clouds. Both versions of the model were used in CMIP5 and will be referred in this chapter as CM5A (standard physics) and CM5B ("new" physics), respectively.

For each physics, two runs were performed: one free run and one run that is nudged towards ERA-Interim wind fields every 6 hours, so that the dynamics of this run is very close to those of ERA-Interim. The results of the analysis for the period between 1995 and 2009 (the longest common period with the GPS data), at a 1.9°x3.75° resolution (low resolution, LR) are presented in terms of means, interannual variability and trends in IWV.

The analysis and comparison with GPS and ERA-Interim will be focused on several points. 1) How well are the different configurations of the model able to represent the IWV means, variability and trends? 2) How are the model simulations of IWV impacted by the nudging, and

consequently, how is IWV impacted by large-scale dynamics? 3) What is the impact of the different parameterizations on IWV (i.e. do we see an improvement in the "new" physics)?

4.2 Model assessment: comparison with GPS and ERA-Interim (1995-2009)

Although the GPS stations used in this chapter were the same as those used in the previous chapter (104 globally-distributed stations with over 15 years of data), in order to solve the problem of breaks in the GPS data, the time series were homogenized using ERA-Interim as a reference. In this case, GPS IWV means were aligned to ERA-Interim over the time periods delimited by reported equipment changes. The GPS data was also corrected to height of the model, using ERA-Interim pressure level data, as described in the previous chapter. The ERA-Interim data was originally obtained at a 0.75° resolution. In order to compare it with the models, the ERA-Interim fields were filtered (using a 2-D finite impulse response (FIR) filter) and interpolated to the model grid.

4.2.1 Mean IWV

4.2.1.1 DJF

The mean pattern of IWV for DJF shown in Figure 4.1 is consistent in the four configurations of the model, with higher mean values at the Equator, which roughly decrease with latitude. The model fields are also consistent with the GPS mean values, which are superposed as circles. In order to better identify differences between the models and GPS, the differences at the GPS site are plotted as circles in Fig. 4.2. The differences are mostly between -2 and 2 kg.m^{-2}, with some notable exceptions: station KOKB in Hawaii (moist biases that are more intense in the free models), stations KARR, DARW, and TOW2 in Northern Australia and KOUR in French Guiana (dry biases in the models). These differences are more intense in the free configurations.

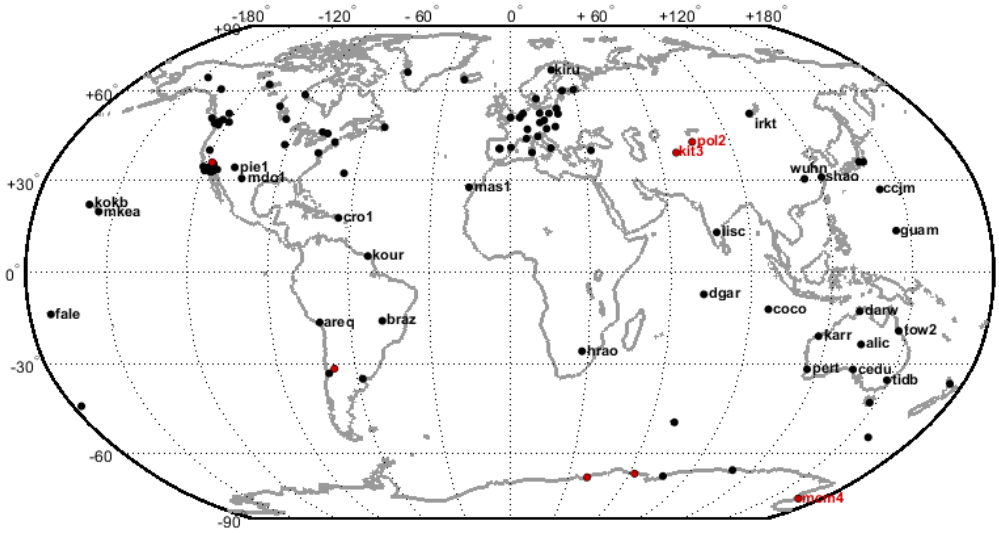

Figure 4.1 Distribution of the GPS stations used in this chapter. Stations mentioned in the text are labeled on the map.

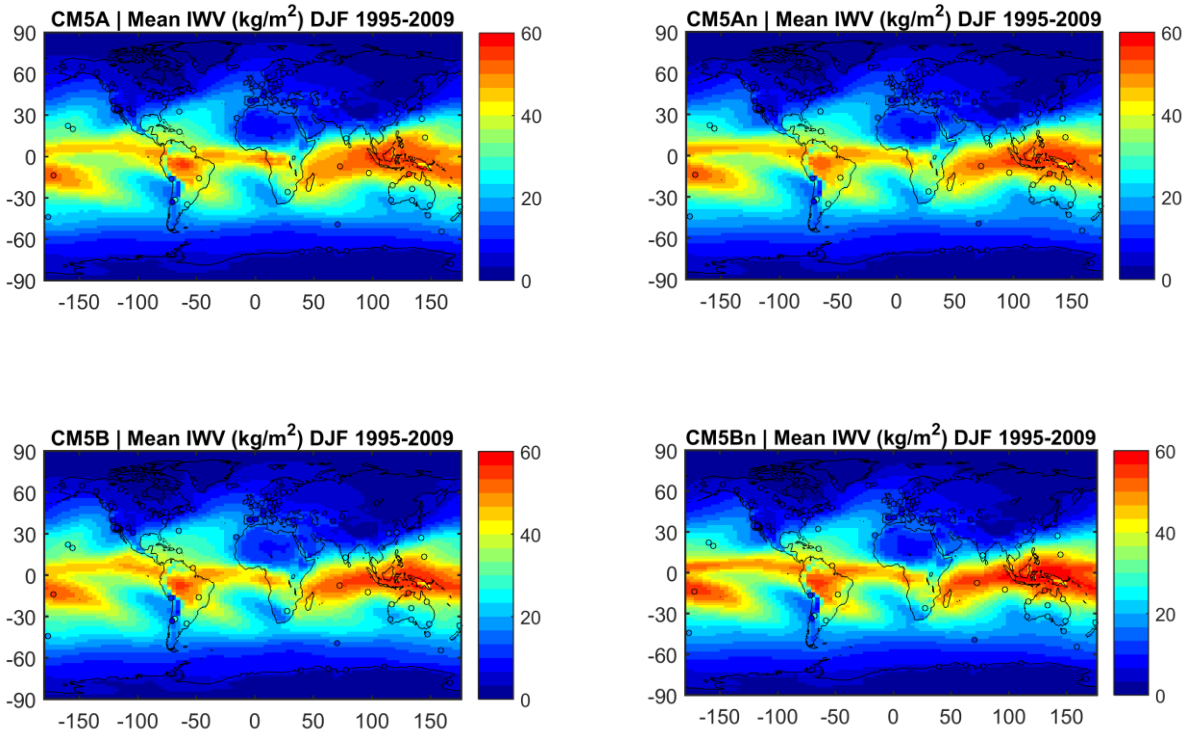

Figure 4.1 Mean IWV fields in model with GPS means as points for DJF

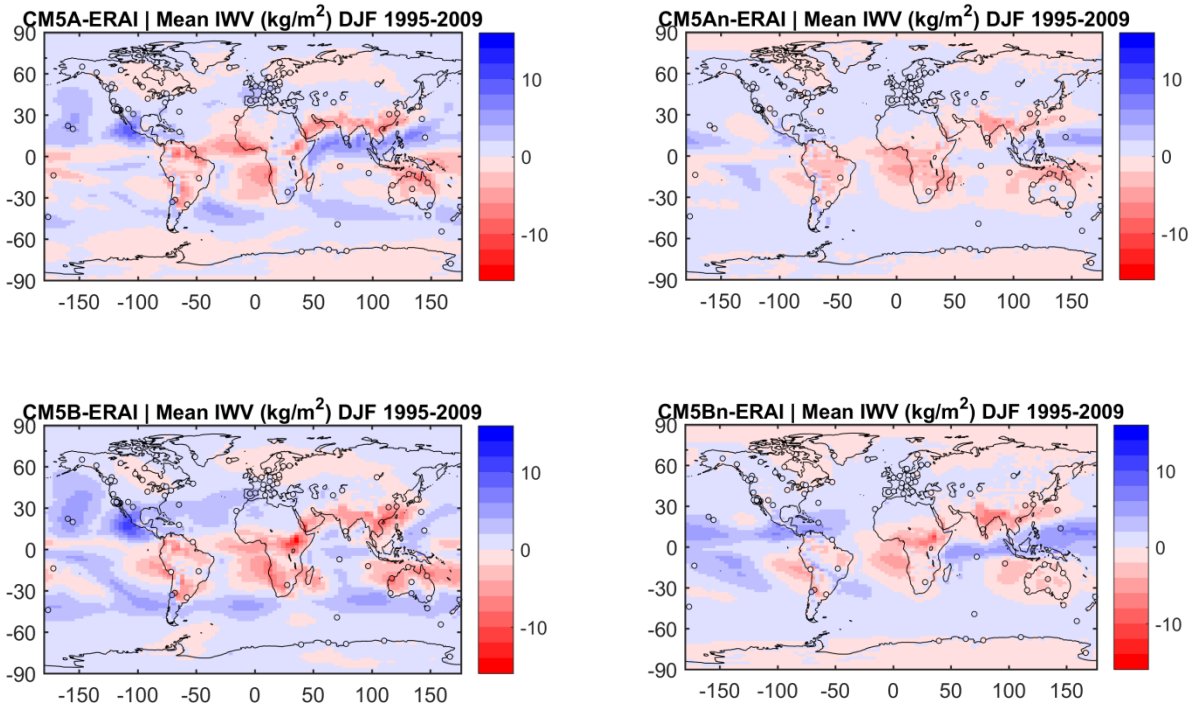

Figure 4.2 Difference fields between model and ERA-I means for DJF.

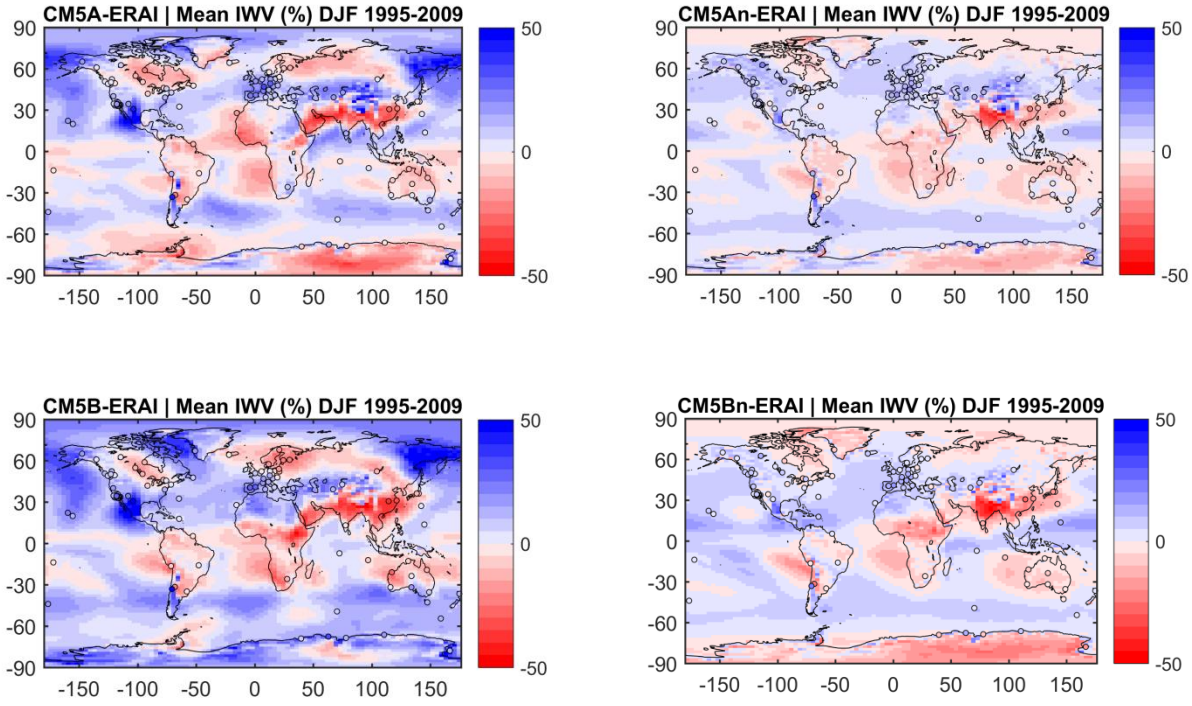

Figure 4.3 Relative difference fields between model and ERA-I (and GPS data, superposed as circles) means for DJF.

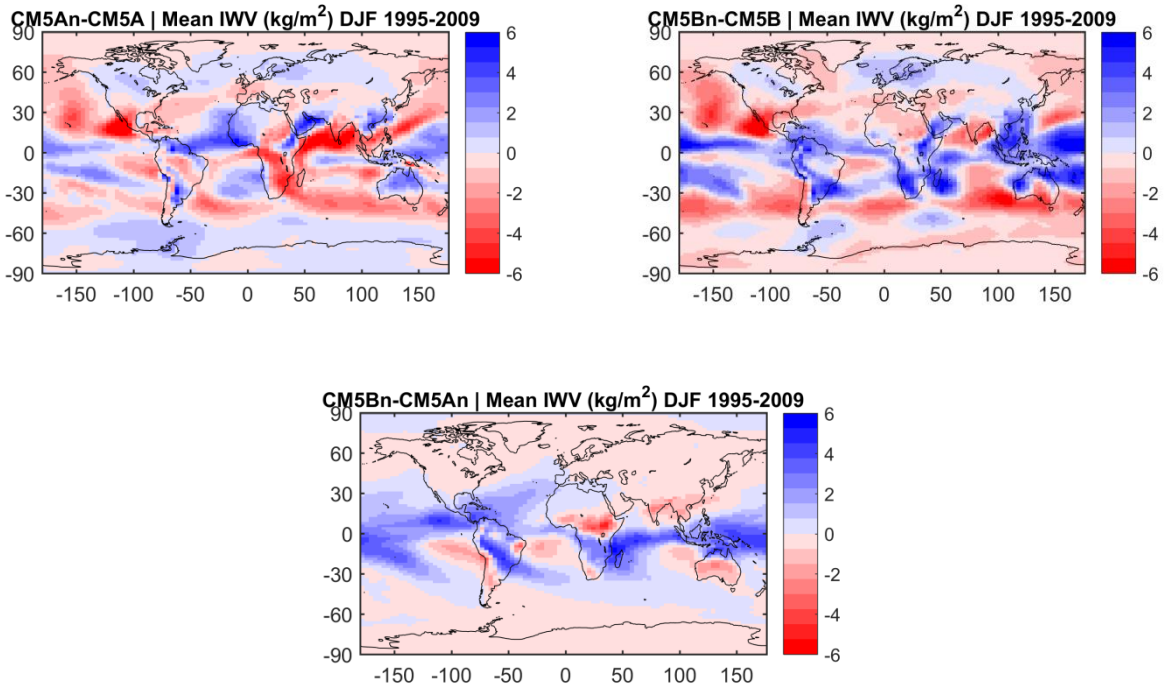

Figure 4.4 Difference fields between different configurations of the climate model.

The mean IWV pattern in the model simulations is also compared with ERA-Interim for the same period. Although the general pattern of IWV means is consistent with that observed for ERA-Interim, in order to observe the differences in more detail, mean difference fields between each model configuration and ERA-Interim were mapped and shown in Fig. 4.2. In spite of the general good agreement, there are regions where the differences between model and ERA-Interim are considerable, such as off the coast of Mexico in the free simulations and the Indo-Pacific region (moist biases) and in the Atlantic between 30°S and 0°, Eastern Africa, the Arabian Peninsula, India, Southern China, and Northern Australia (dry bias). The differences appear to be more intense for the free simulations, while for the nudged simulations the dry biases appear to be more intense for CM5A and the moist biases for CM5B, especially in the tropical latitudes. For the latitudes between 30°S and 30°N, the mean bias for CM5An is -0.5 $kg.m^{-2}$, whereas for CM5Bn it is 0.5 $kg.m^{-2}$ (Table 4.1). In general, the differences with GPS are consistent with the differences with ERA-Interim, which is expected as GPS is homogenized using ERA-Interim.

The relative mean difference (Fig. 4.3) highlights differences at higher latitudes for the free simulations, and is similar for both physics except over Antarctica where CM5A has a drier bias, and CM5B has a moister bias (mostly in DJF). In the nudged simulations a dry bias is highlighted over India in DJF and Central Asia in JJA, which is observed for both physics.

In order to better determine the differences between the configurations, the difference fields were plotted and presented in Fig. 4.4. The impact of the nudging in both physics has similarities, such as a drying over Canada, Northern Europe, around the Equator in the Pacific and Atlantic oceans, and Northern Australia; and a moistening in the Northern Pacific, in the Southern United States, Mexico, Southern Europe, and in the ocean around 30°S. For CM5B, there is a strong moistening over the tropics with the nudging, that is not as intense for CM5A.

In terms of the impact of physics, it is more intense over the tropics, between 30°S and 30°N, and it is of the same order of magnitude as the differences between nudged and free simulations. At higher latitudes the differences in the means are below 1 $kg.m^{-2}$. The new physics is, in general, moister over the tropics, with the exception of most of Australia, Central Africa, south of South America and off its coast (both in the Pacific and part of the Atlantic oceans). In order to quantify which configuration is closer to GPS observations, biases at the GPS stations between the aforementioned latitudes were assessed (Table 4.2). The results show that for DJF, and for the stations located between 30°S and 30°N, there is better agreement with GPS for the CM5A nudged configuration (hereafter named CM5An), with an overall mean absolute bias of 1.6 $kg.m^{-}$

$^{-2}$, as opposed to 1.9 kg.m^{-2} for CM5B nudged (CM5Bn). However, CM5Bn has lower biases for six of the stations (FALE (Pacific), AREQ and BRAZ (South America), HRAO (South Africa), and DARW and TOW2 (Northern Australia)), and a lower overall dry bias of 0.2 kg.m^{-2}, while CM5An has a relatively larger dry bias of 1 kg.m^{-2}.

When compared with ERA-Interim, for the same latitude band, these results are reinforced as CM5An presents a dry bias of 0.5 kg.m^{-2} and CM5Bn a moist bias. This moist bias in CM5B in DJF is also seen globally, with a mean difference of 0.3 kg.m^{-2}, while for CM5A the overall bias is null. In terms of mean absolute bias, CM5An has one of 0.8 kg.m^{-2}, and CM5B of 1 kg.m^{-2}.

4.2.1.2 JJA

As with the mean IWV fields for DJF, the general pattern of mean IWV for JJA is consistent in all four simulations, and is higher for the tropical regions and lower at high latitudes (Fig. 4.5). In comparison with DJF, there is a shift northward of the maximum mean IWV band, with the lowest values occurring southward of 60°S. The most obvious differences between simulations occur in the Indo-Pacific region, where the maximum values are more intense with CM5B and CM5Bn, and less intense for the free configuration of CM5A.

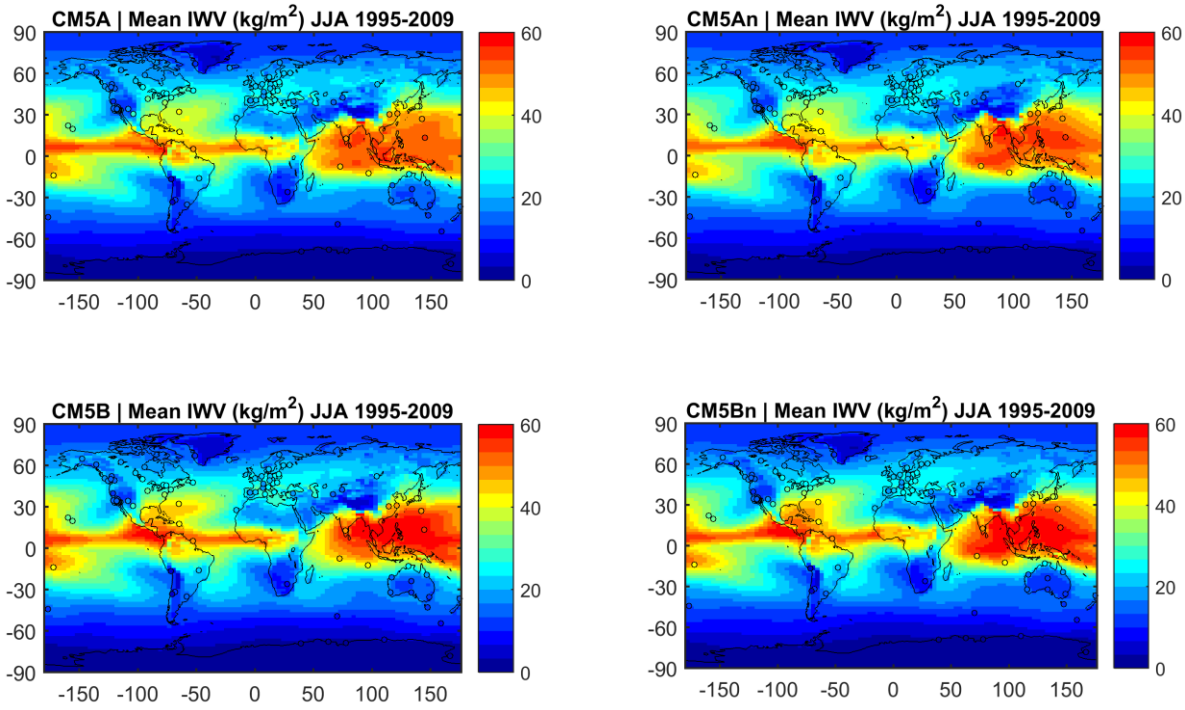

Figure 4.5 Mean IWV fields in model with GPS means as points for JJA

Over Australia, there is a difference between the nudged and free simulations, where the nudged simulations show lower values of mean IWV. When comparing with GPS, differences are higher in the Pacific (GUAM and CCJM stations in the new physics, and FALE in the four configurations) and Indian (DGAR in all configurations except CM5B) oceans (moist biases in the simulations), and over the Southern United States (PIE1 and MDO1) and Eastern China (WUHN) in the free configurations (dry biases in the simulations). Station KIT3 (Uzbekistan) also has a relatively high dry bias in all four simulations.

The pattern of differences between models and ERA-Interim (Fig. 4.6 and Fig. 4.7) has similarities for both free configurations and for both nudged simulations, with more intense dry biases over the Southern United States, South America, Africa and India; and moist biases over Canada and Alaska, Australia, Western Europe, and most of the Pacific. On the other hand, the difference pattern also depends on the model physics: there are dry biases in CM5A and CM5An in the Gulf of Mexico, off the East Coast of the United States, and in the South China Sea that is a moist bias in CM5B and CM5Bn. In general, the biases appear to be more positive in the CM5B model. In fact, according to the values presented in Table 2, CM5A(n) has lower mean differences with ERA-Interim, and CM5B(n) has higher positive differences. The moist bias in CM5B is also more intense over the tropics.

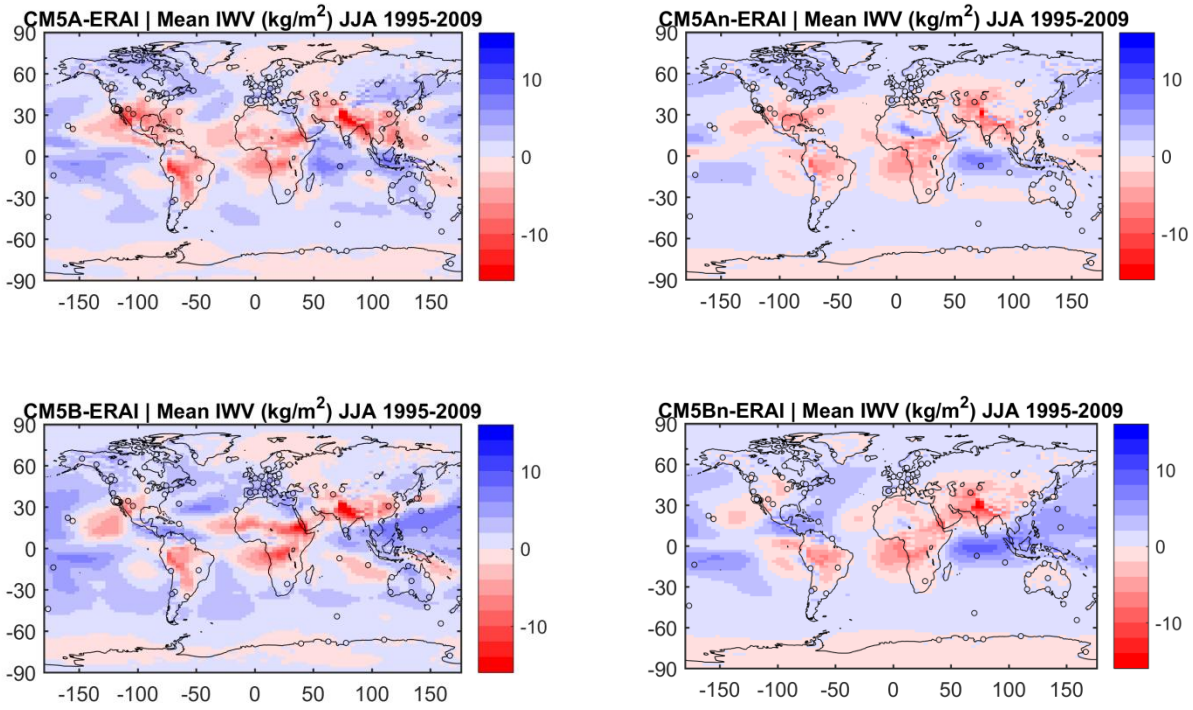

Figure 4.6 Difference fields between models and ERA-I (and GPS, circles) means for JJA.

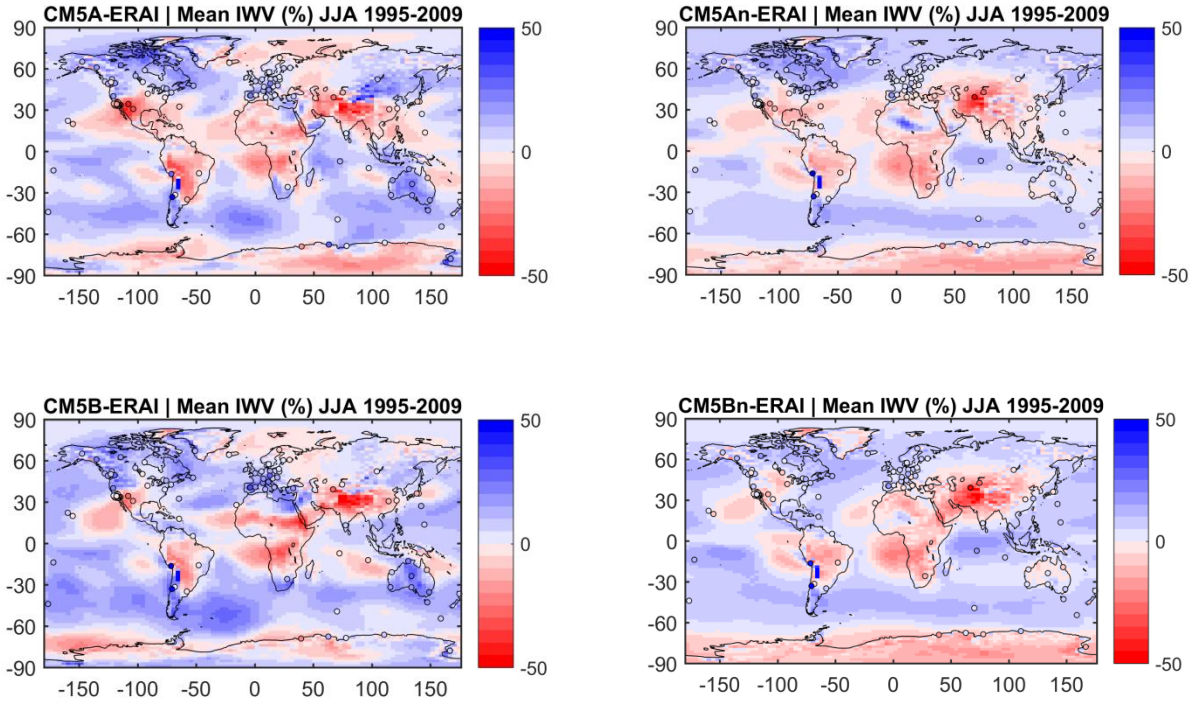

Figure 4.7 Relative difference fields between models and ERA-I (and GPS, circles) means for JJA.

As observed for DJF, the patterns of differences between nudged and free configurations (Fig. 4.8) are roughly similar for both physics, which suggests the importance of large-scale dynamics in IWV mean distribution. In JJA in particular there is a dipole structure over West Africa that results from the improved representation of the monsoon flow, in the nudged simulations. The nudging improves the water advection, and allows the monsoon to penetrate further north.

On the other hand, for the Indo-Pacific region, the impact of nudging is different for the two physics. The difference between both nudged simulations, which highlights the impact of model physics on IWV, shows a strong moist bias for CM5Bn in the tropics, with the exception of North Africa, the Arabian Peninsula and Northern India. In general, for both seasons, it appears that the nudging in CM5B does not improve the model results around the ITCZ, but rather reinforces the biases. There are a few (7) GPS stations over the regions of strongest difference between CM5An and CM5Bn: FALE, CRO1, KOUR, DGAR, COCO, CCJM and GUAM. For all stations, the mean differences between model and GPS are smaller for CM5An, with CM5Bn presenting persistent moist biases, which are particularly high for stations FALE (4.6 $kg.m^{-2}$ as opposed to 2 $kg.m^{-2}$ in CM5An) and DGAR (6.8 $kg.m^{-2}$ as opposed to 6.1 $kg.m^{-2}$ in CM5An) over the Pacific and Indian oceans, respectively. The largest differences in biases are found for CCJM (4.1 $kg.m^{-2}$ in CM5Bn and 0.5 $kg.m^{-2}$ in CM5An) and GUAM (3.5 $kg.m^{-2}$ in CM5Bn and 0.5 $kg.m^{-2}$ in

CM5An). The mean (absolute) bias over these seven stations is 1.6 (2) kg.m^{-2} for CM5An and 3.6 (3.6) kg.m^{-2} CM5Bn.

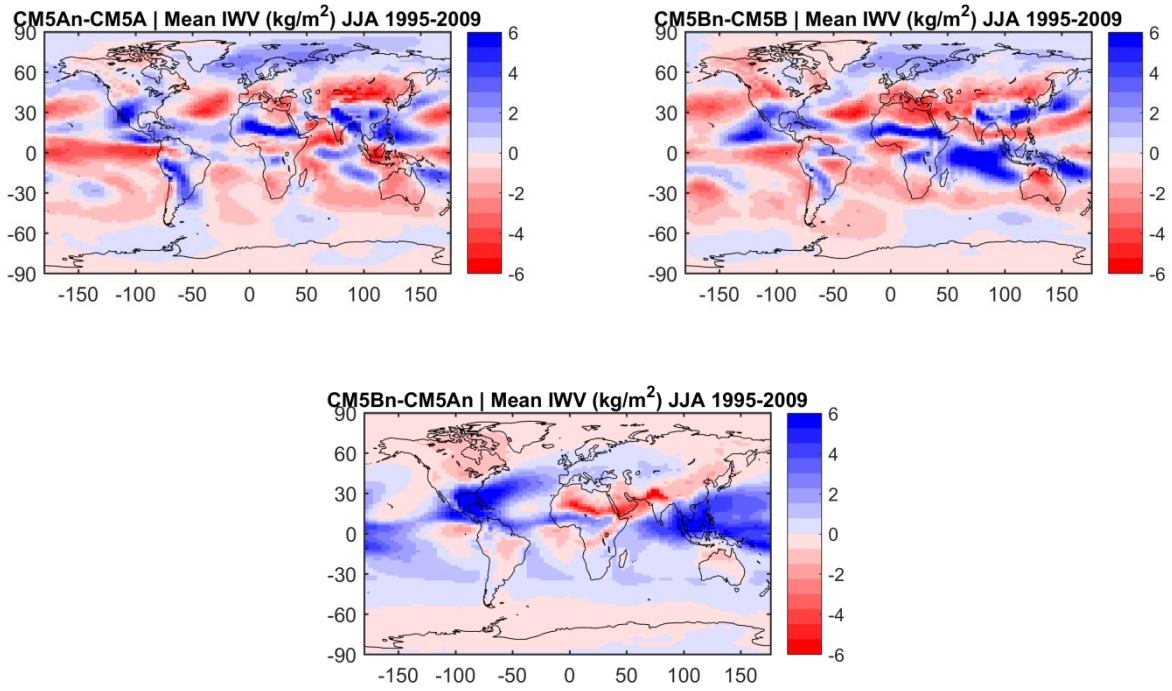

Figure 4.8 Difference fields between different configurations of the climate model.

Table 4.1: Mean differences between model and ERA-Interim (kg.m^{-2}).

Area		CM5A		CM5B		CM5An		CM5Bn	
		DJF	JJA	DJF	JJA	DJF	JJA	DJF	JJA
Global	Bias	0,2	0,4	0,5	0,8	0,0	0,3	0,3	0,7
	Abs bias	1,2	1,5	1,5	1,7	0,7	1,2	1,0	1,4
[-30°S:30°N]	Bias	-0,2	-0,2	-0,3	0,7	-0,5	-0,3	0,5	0,9
	Abs bias	2,2	2,5	2,5	2,9	1,5	1,7	2,2	2,6

Table 4.2: Mean differences between model and GPS for the stations pictured above (kg.m^{-2}).

Station	CM5A		CM5B		CM5An		CM5Bn	
	DJF	JJA	DJF	JJA	DJF	JJA	DJF	JJA
'ALIC'	-2,5	2,1	-0,1	2,6	-0,2	0,2	-2,3	-0,1
'AREQ'	1,5	1,2	-1,1	2,1	1,2	2	-0,1	1,8
'BRAZ'	-0,4	-0,9	0,1	0	-1,4	-1,3	0,4	-1,4
'CCJM'	0,2	1,2	0	5,3	-2,4	0,5	-2,7	4,1
'COCO'	0,1	0	-2,2	-2,7	-2,3	1,7	-3,7	2,2
'CRO1'	1,3	-2,5	0,7	-0,1	0,2	-0,3	2,6	2,3
'DARW'	-6,1	3,8	-4,1	4,7	-4,9	2,6	-0,9	1,3
'DGAR'	-1,5	6,5	1,7	-0,6	-0,3	6,1	2,7	6,8
'FALE'	-2,6	2	-1,6	3,9	-1,8	2	1,3	4,6
'GUAM'	1,6	-2,2	0,5	4,2	2,5	0,5	4,1	3,5
'HRAO'	1,7	0,3	-3,5	1	-1,8	-1,2	-1,2	-1,1
'IISC'	2,7	2	-0,7	2,9	-2,9	-1,3	-3,4	0,7
'KARR'	-2,6	2,7	-9,2	1,3	-1,8	0,8	-3,4	0,4
'KOKB'	4,4	0,6	5,6	2,5	1	1,5	2,1	1,3
'KOUR'	-4,9	-1,9	-1,3	0,5	-0,6	-1,3	1,1	1,9
'MAS1'	-2,5	-1,1	0,4	0	-0,2	-1,1	0,5	-1
'MKEA'	2,9	-2,6	3,7	-1,4	-0,3	-1,4	0,8	-1,8
'TOW2'	-5	-1,7	-5,2	-1,2	-2,3	-1,3	-1,6	-1,5
Mean Bias	**-0,7**	**0,5**	**-0,9**	**1,4**	**-1**	**0,5**	**-0,2**	**1,3**
Mean Absolute Bias	**2,5**	**2,0**	**2,3**	**2,1**	**1,6**	**1,5**	**1,9**	**2,1**

4.2.2 Interannual variability of IWV

The interannual variability of IWV was computed by dividing the standard deviation of DJF and JJA means by the mean seasonal value over the 15 years at study. The results are presented below for each season.

4.2.2.1 DJF

For DJF, the interannual variability of IWV is noticeably different in the free and nudged simulations (Figure 4.10). The nudged simulations have well-defined regions of higher variability over the Arctic and Siberia, West Africa, India, Australia and the tropical Pacific Ocean around the Equator, whereas the free configurations have maximum values over Canada and Alaska. In comparison with GPS, it is clear that the nudged simulations are better at representing the IWV interannual variability for DJF. Although there are no GPS stations over the Arctic and Siberia, the stations over Canada and Alaska have lower variability than the free simulations (around 10%, as opposed to over 20% in CM5A and CM5B). They are in better agreement with nudged simulations, but some stations still indicate an overestimation of interannual variability in CM5An and CM5Bn (e.g Alaska, Greenland).

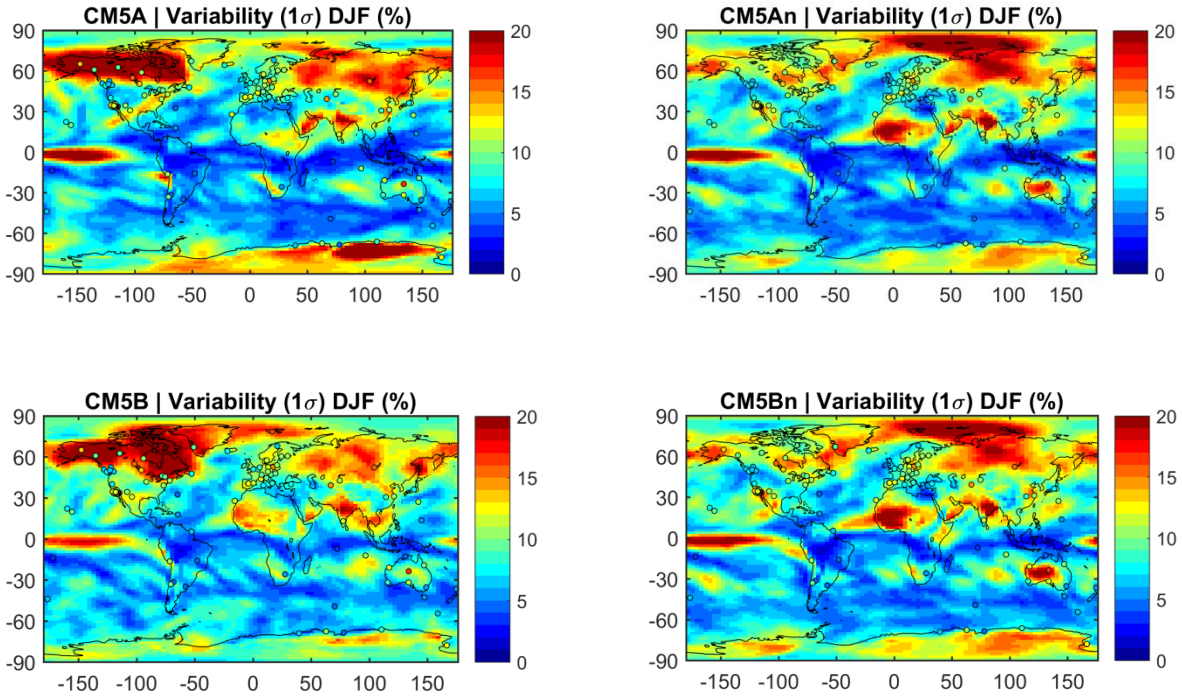

Figure 4.10 Variability in IWV fields in model with GPS variability as points for DJF

On the other hand, over Australia, GPS station ALIC presents higher variability, which is once again better captured by the nudged simulations than by the free ones. This can be observed in more detail in the time-series at the ALIC station for CM5A and CM5An (in Fig. 4.11). From the time series for CM5A it is observed that higher (lower) IWV events for DJF in 2000 (2005) are not well captured by the model.

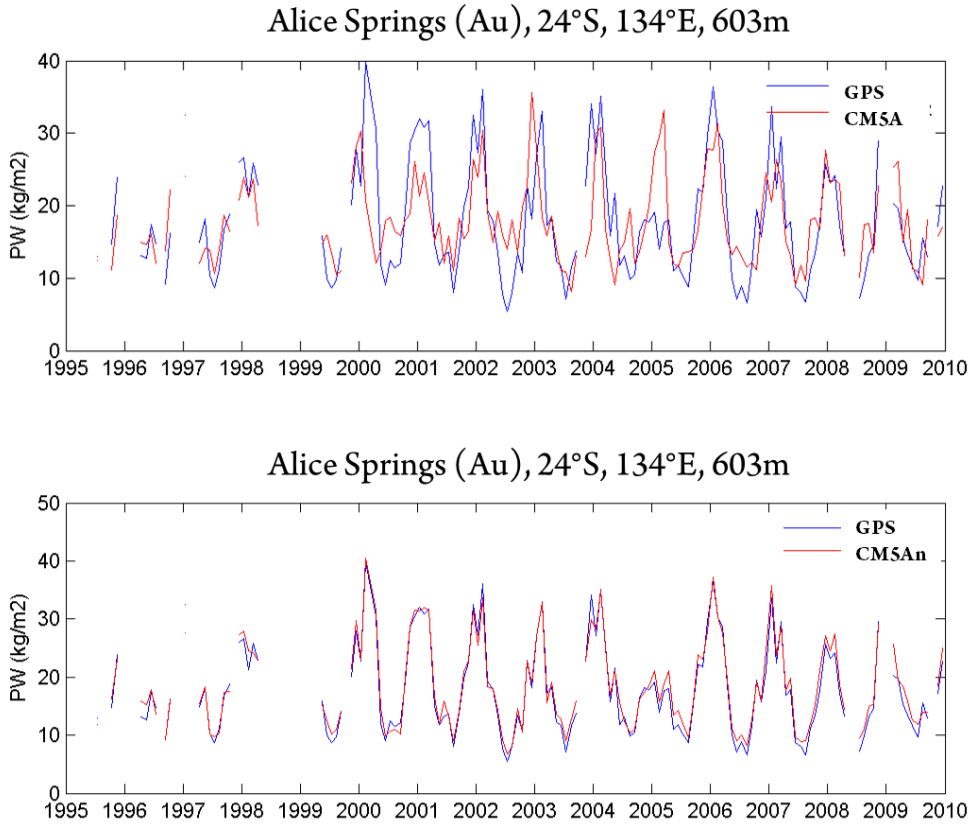

Figure 4.11 Time series of GPS IWV at the ALIC (Alice Springs in Australia) site and IWV for CM5A and CM5An at the GPS site.

The nudged simulations are also in better agreement with ERA-Interim (Figure 4.12), with differences of between -5% and 5%, in contrast with differences of up to 15% in the free simulations for Canada and Alaska (in CM5A and CM5B) and Antarctica (in CM5A) and -15% over the Arctic (CM5A and CM5B) and West Africa (CM5A). The differences are also more intense in CM5A than CM5B, especially over West Africa where CM5B is able to capture some of the higher variability. Over Antarctica, one physics (CM5A) indicates higher variability than ERA-interim while the other (CM5B) indicates lower variability in the free simulations. In section 3, we have shown that reanalyses over this area present divergent results and GPS

stations that are located around the coastline do not allow to conclude on what happens over the continental area, due to strong contrast with the surrounding ocean.

The comparison between nudged and free simulations (Figure 4.13) shows patterns consistent between both physics (with the notable exception of the Antarctica region). This confirms the importance of large-scale dynamics in controlling IWV variability. In fact, the differences in variability between model physics are of lower magnitude compared to differences between nudged and free simulations (notice that the scale is different) but they do exist. Over Australia, higher variability is seen in CM5B, whereas in the equatorial Pacific, higher variability is observed in CM5A. There are a few (7) GPS stations over Australia, and their variabilities were compared with the models' variabilities. All stations except for TOW2 show lower differences for CM5Bn (Table 4.3).

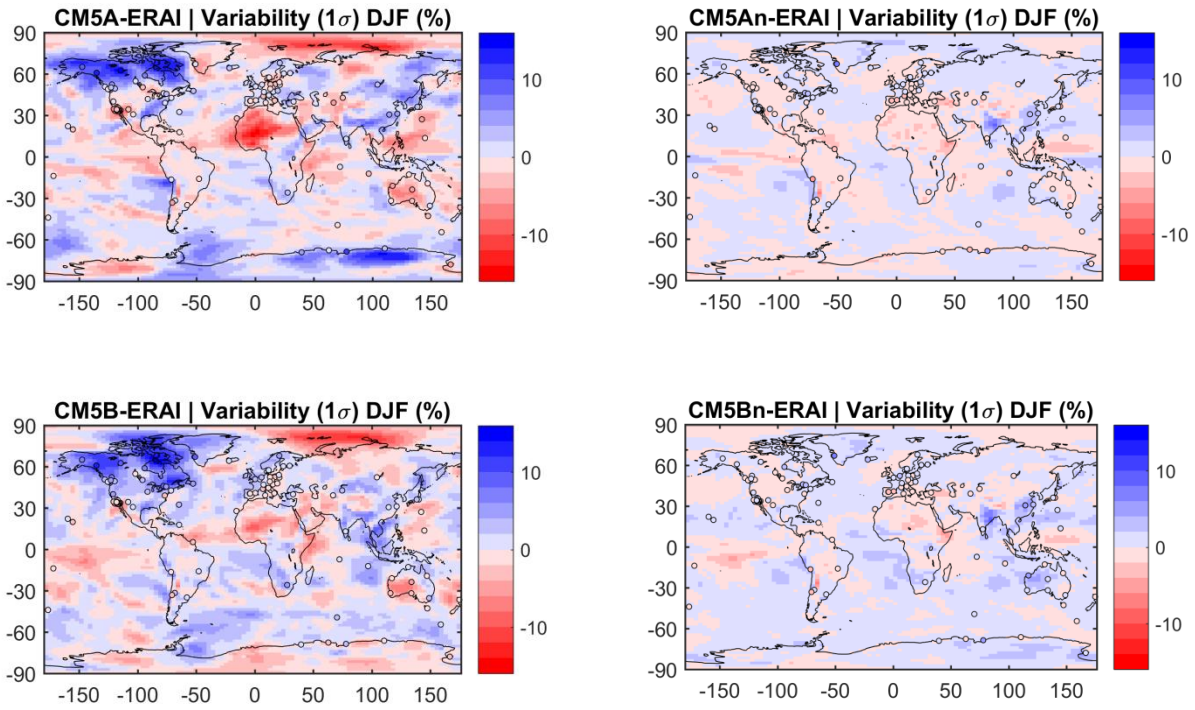

Figure 4.12 Difference fields between model and ERA-I (and GPS, in circles) IWV interannual variability for DJF.

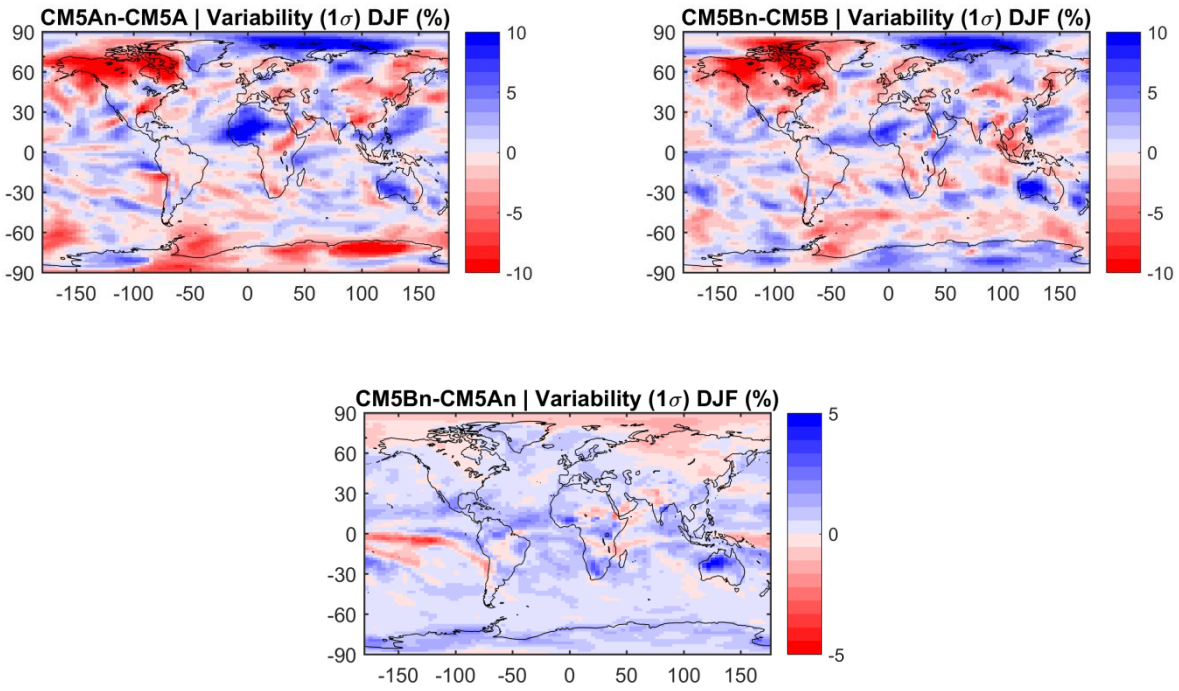

Figure 4.13 Difference in IWV interannual variability for DJF between different configurations of the climate model.

Table 6: Difference in variability (%) between Model and GPS for stations over Australia

Model-GPS | Variability DJF (%) over Australia				
	CM5A	CM5B	CM5An	CM5Bn
'ALIC'	-5,7	-1,7	-4,8	0,4
'CEDU'	3,5	-2,1	-1,5	-1,3
'DARW'	-4,6	0,4	-2,7	0,4
'KARR'	-2,4	0	-0,7	0
'PERT'	-0,1	-0,9	0,9	-0,8
'TIDB'	0,1	1,6	4,1	1,8
'TOW2'	2,2	1,9	1,6	2,5

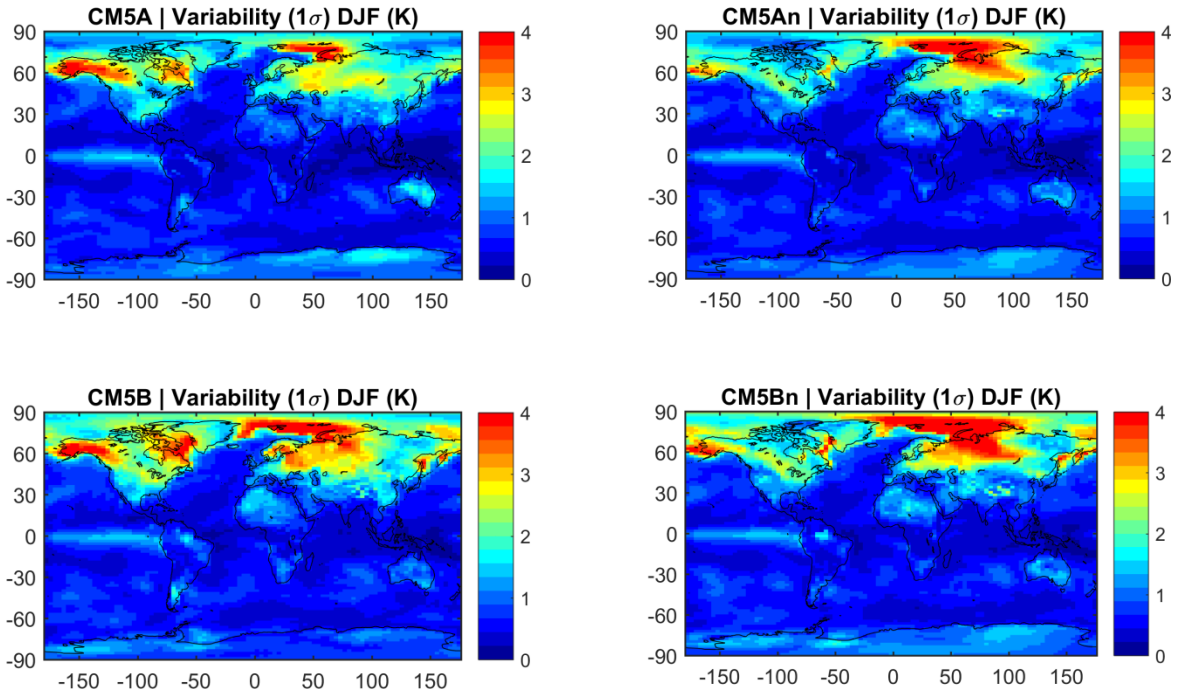

Figure 4.14 Interannual variability in T_{2m} fields in the model for DJF

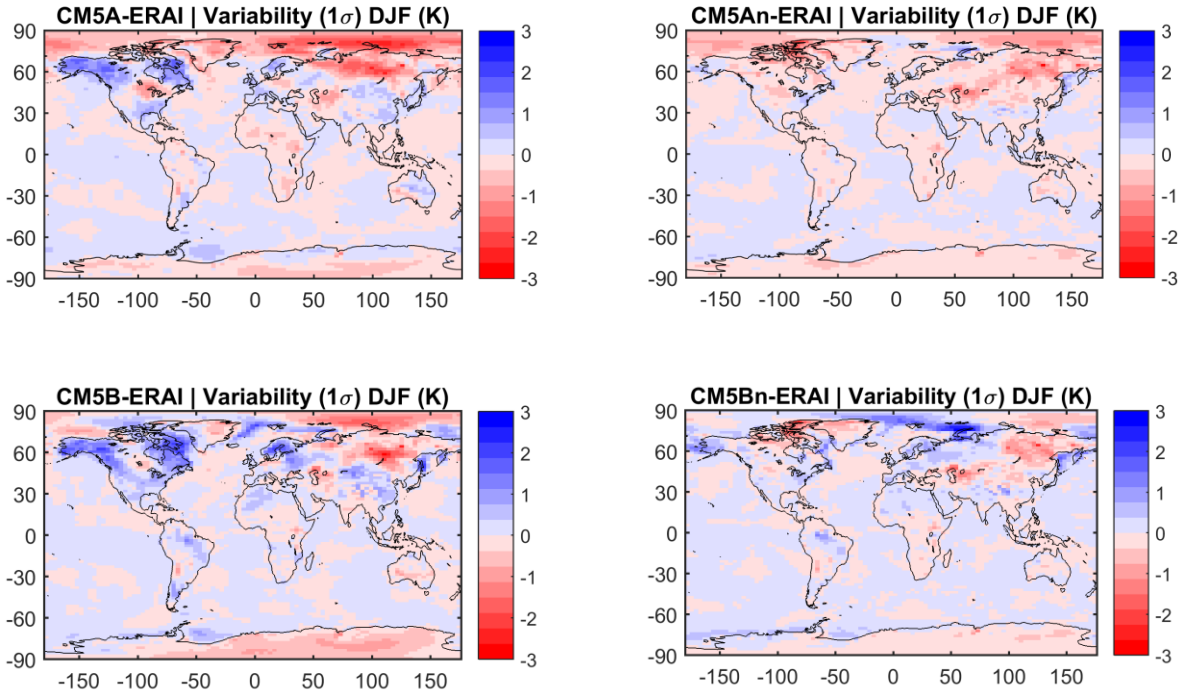

Figure 4.15 Difference fields between model and ERA-I T_{2m} interannual variability for DJF.

Figure 4.14 shows the interannual variability of the 2-metre temperature (T_{2m}) in each configuration of the model, for DJF. At the high latitudes in the northern hemisphere (over 60°N), the differences in the patterns are consistent with the differences found in IWV. While the free runs have a relatively high variability over Canada and Alaska, the nudged simulations have higher variabilities over the Arctic and Siberia. The same pattern of differences is also observed when comparing the models with ERA-Interim (Fig. 4.15). At the aforementioned latitude band, regions where the free runs overestimate (underestimate) the temperature variation roughly correspond to the areas of overestimation (underestimation) of IWV variability. It is thought this problem in the temperature and IWV variability north of 60°N might be due to problems in the sub-grid scale orography parameterizations. In order to check this, model results using different orography parameterizations should be analyzed.

4.2.2.2 JJA

For JJA, the interannual variability in IWV shows more similar patterns across the four configurations than in DJF (Fig. 4.16). There is a maximum of variability over Antarctica, which appears to be overestimated in the model in comparison with GPS, especially for CM5A and with the exception of MCM4 (the easternmost station). There is also strong variability over Australia, which is slightly underestimated in all models, in comparison with the GPS station ALIC (in the center of Australia).

The comparison with ERA-Interim highlights the difference for CM5A over Antarctica (especially the western part) that is not as intense for CM5B (in Fig. 4.17). For the rest of the globe, CM5B (CM5A) appears to have more of an overestimation (underestimation) of variability. For the nudged simulations, the differences in variability with ERA-Interim are relatively small (mostly within 2%) and similar between the two physics, which highlights the importance of the large-scale dynamics in the IWV interannual variability (in addition to the near-surface temperature, seen previously for DJF). This impact is reinforced by Figure 4.18 where the differences with the nudging reach up to 10%, and are predictably more intense for CM5An and CM5A over Antarctica. Figure 4.18 also shows that the difference between CM5Bn and CM5An is mostly positive, with the exception of regions around the tropics such as Australia, the Indo-Pacific region and off the coast of South America. The higher variability found for CM5Bn is particularly noteworthy over Northwest Africa, which is also in better agreement with ERA-Interim.

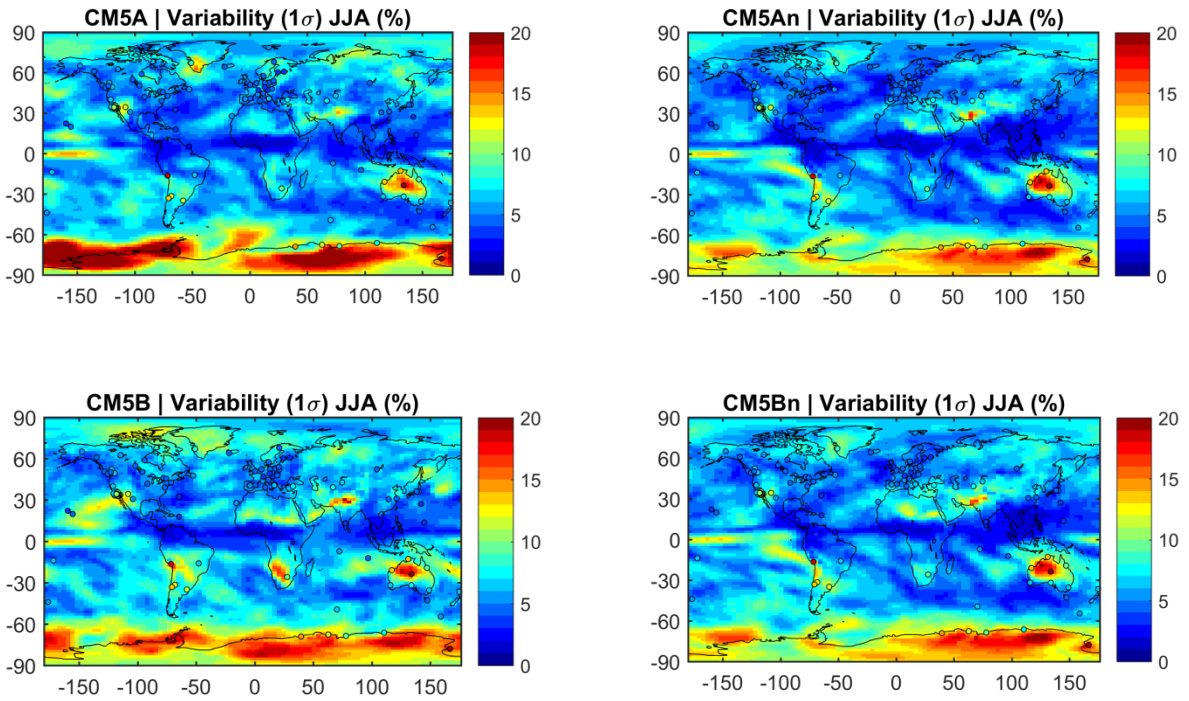

Figure 4.16 Variability in IWV fields in model with GPS variability as points for JJA

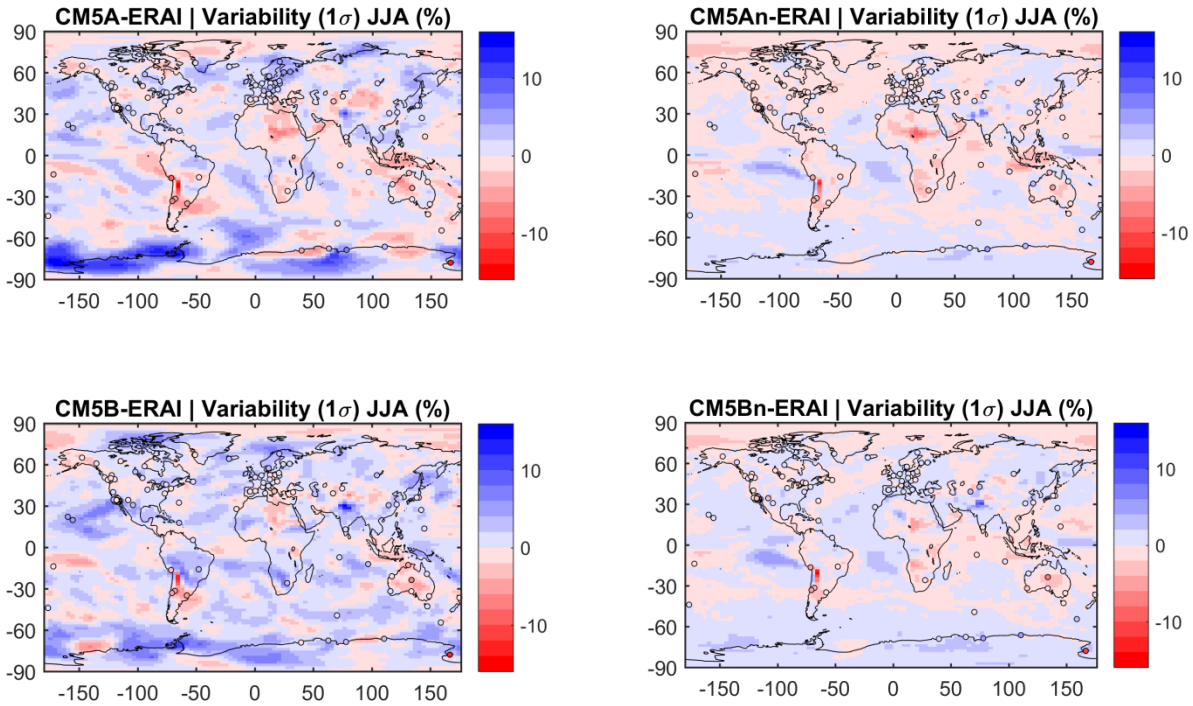

Figure 4.17 Difference fields between models and ERA-I variability (and GPS, circles) for JJA

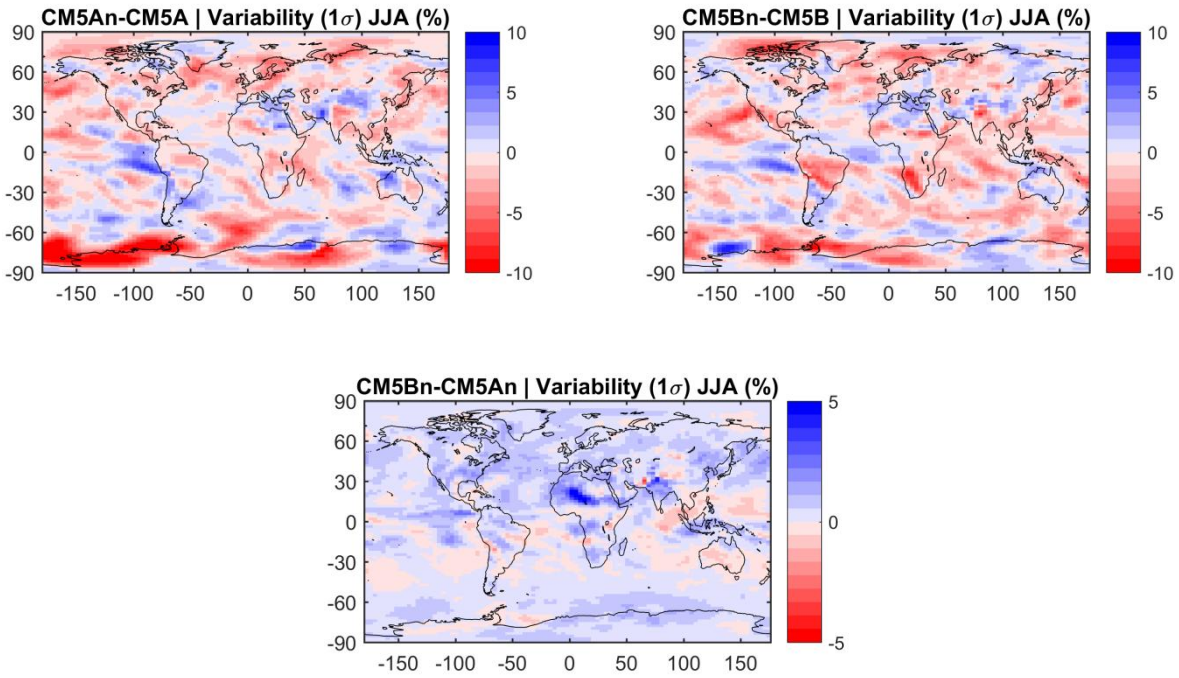

Figure 4.18 Difference in interannual variability for JJA between different configurations of the climate model.

4.2.3 Linear trends in IWV

The linear trends in IWV were computed using the full time series of monthly means for the 1995-2010 period and the seasonal means for DJF and JJA. The annual, DJF and JJA results are presented below.

4.2.3.1 Annual

Figure 4.19 shows the annual trends in IWV for the four model configurations with superposed GPS IWV trends. The stippling denotes the significant trends in the model. Although there are differences in the computed trends, especially when it comes to the free and nudged simulations, there are trend structures that are consistent in all four configurations. These include a moistening over Northern Europe and Siberia, western coast of North America, the Western Pacific, and over part of the Indian Ocean; and a drying over the Western United States and off the coast into the Pacific. On the other hand, the drying over Western Australia and the moistening over southern Africa are observed for CM5An, CM5B and CM5Bn (but not CM5A) and are consistent with the trends computed at the GPS stations over these regions. Furthermore, CM5B is also able to reproduce the dipole structure in IWV trends in the tropical Pacific, which had been observed for ERA-Interim in the previous chapter, and which is a result of the strong 1997/98 El Niño event. This structure is not as significant in CM5A. On the other hand, there are significant trends which are only present in the nudged simulations, such as the

moistening over Eastern Antarctica, which is in agreement in sign with the GPS stations, and most of South America; and the drying in Eastern Sahel, analyzed in chapter 3, which is more significant in CM5Bn.

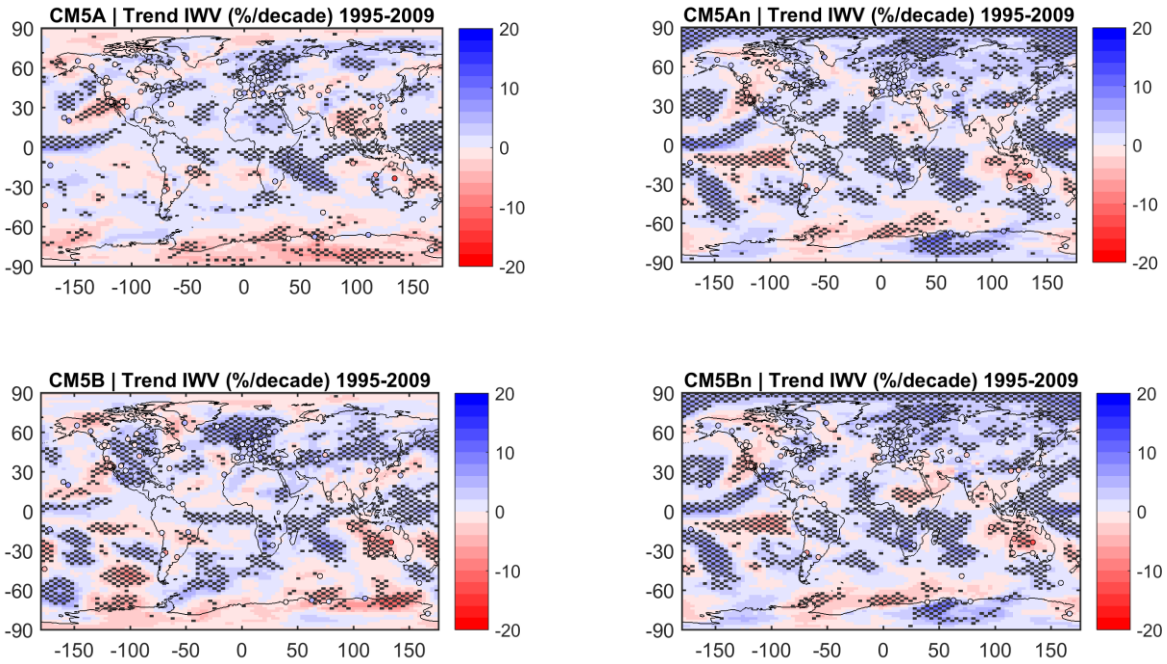

Figure 4.19 Trends in IWV fields in model with GPS trends as points

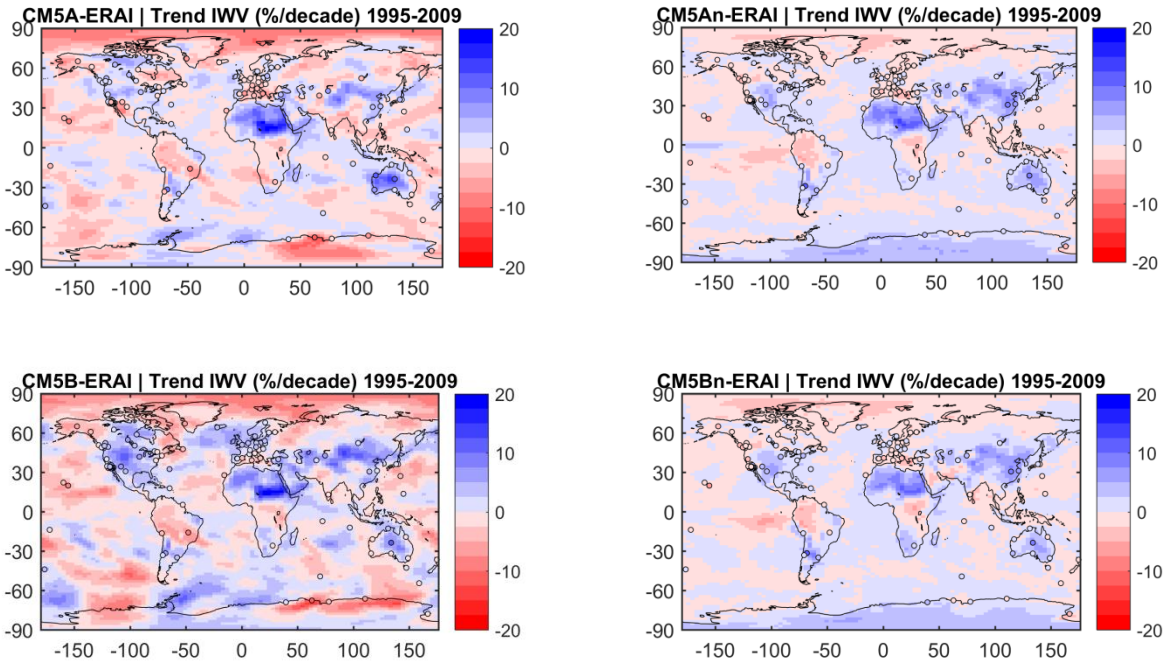

Figure 4.20 Difference fields between model and ERA-I trends (and GPS, circles).

The difference between IWV trends in the models and ERA-Interim is shown in Figure 4.20, with the difference with GPS superposed as circles. The differences with GPS are consistent with the differences with ERA-Interim, and they are more intense for the free simulations, with values of the same order of magnitude as the trends themselves. This highlights the uncertainty associated with the IWV trends for certain regions, and for such a limited time period. The regions of highest differences are Northern Africa, especially in CM5A, CM5An and CM5B, and Australia in CM5A, where ERA-Interim has more intense drying trends than the simulations. Antarctica in CM5A and CM5B, and the Artic in all configurations have a negative difference between model and ERA-Interim, which means the moistening is stronger in ERA-Interim. Overall, for the annual IWV trends, the more intense differences between models and observations/ reanalysis are roughly consistent in sign across the four configurations.

4.2.3.2 Seasonal

For the seasonal trends in both seasons, there is poorer agreement between the trend patterns observed for the free and nudged simulations, although the nudged simulations show similar trend patterns. This, again, confirms the importance of dynamics over the trends in IWV. For DJF in particular (Figure 4.21), the nudged simulations show strong moistening over the Arctic and Northern Europe, Antarctica, China and South America; and strong drying over the West and East coasts of North America, the Arabian Peninsula, and Eastern Siberia. Some of these strong trends are confirmed by the GPS observations (e.g. some stations over Antarctica, and North America), but there are notable exceptions, such as the two stations over China (WUHN and SHAO) and KIRU over Sweden, which register a drying (instead of moistening). However, overall, the trends observed at the GPS sites are in better agreement with the nudged simulations. This is also clearly observed for the comparisons with ERA-Interim, presented in Figure 4.22, where the differences in IWV trends for CM5A and CM5B are of the same order of magnitude as the trends themselves (and reach over 20%/decade). The differences between nudged simulations and ERA-Interim are less intense, although differences are still intense (around 10%/decade) over Sahel and Australia. The differences over Australia are also consistent with the differences with the GPS observations. Furthermore, the patterns of the differences show similarities between both physics (e.g. over most of North and South America, over Russia and Siberia, Australia and the Arabian Peninsula). This suggests that the impact of the difference in physical parametrizations is much lighter, which is confirmed by Figure 4.23, where the

impact of nudging is much more intense (in the 20% range) than the impact of the physics (in the 5% range, with the exception of Sahel and Western Australia, as seen previously).

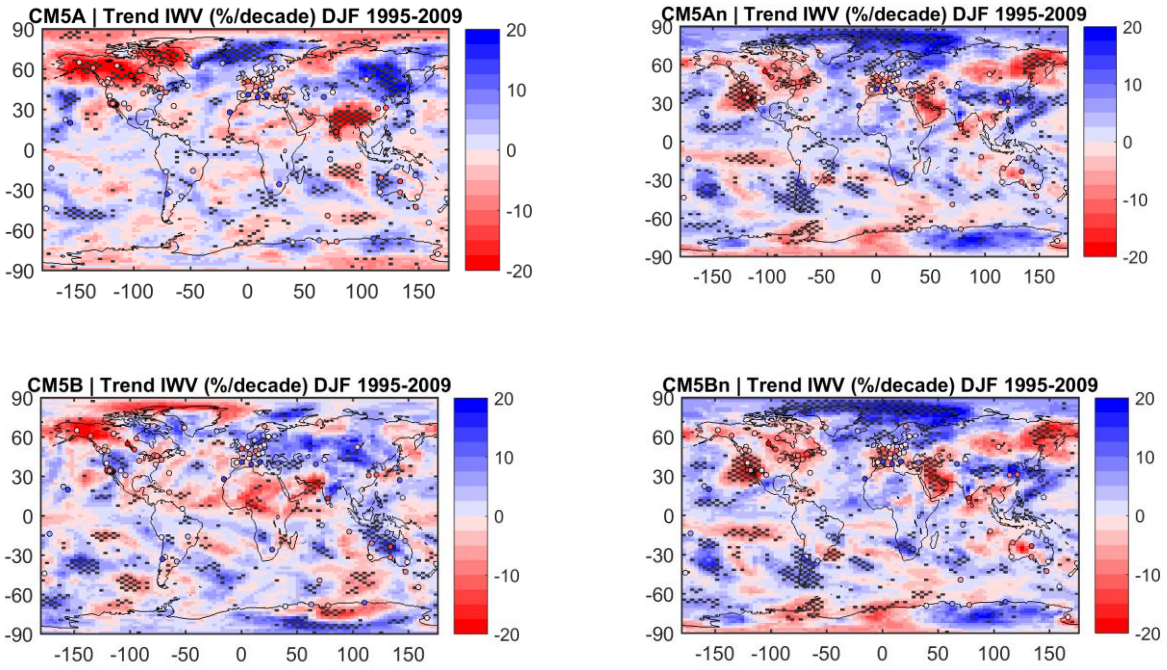

Figure 4.21 Trends in IWV fields in model with GPS trends as points for DJF

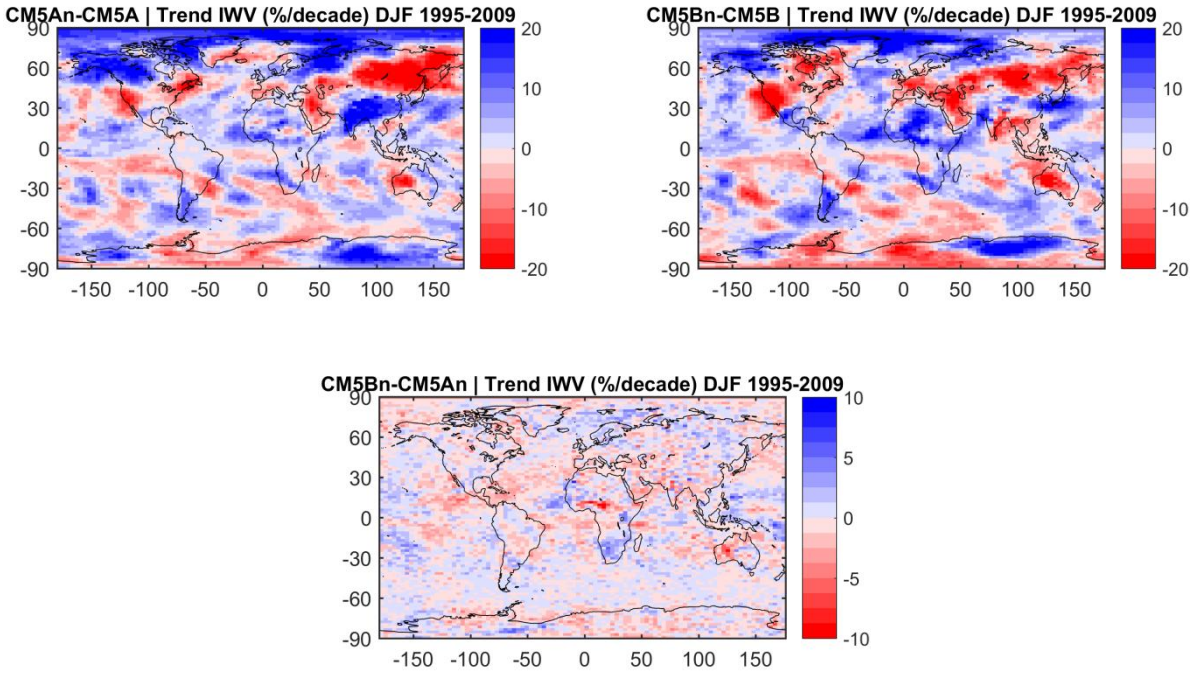

Figure 4.22 Difference in IWV trends for DJF between different configurations of the climate model.

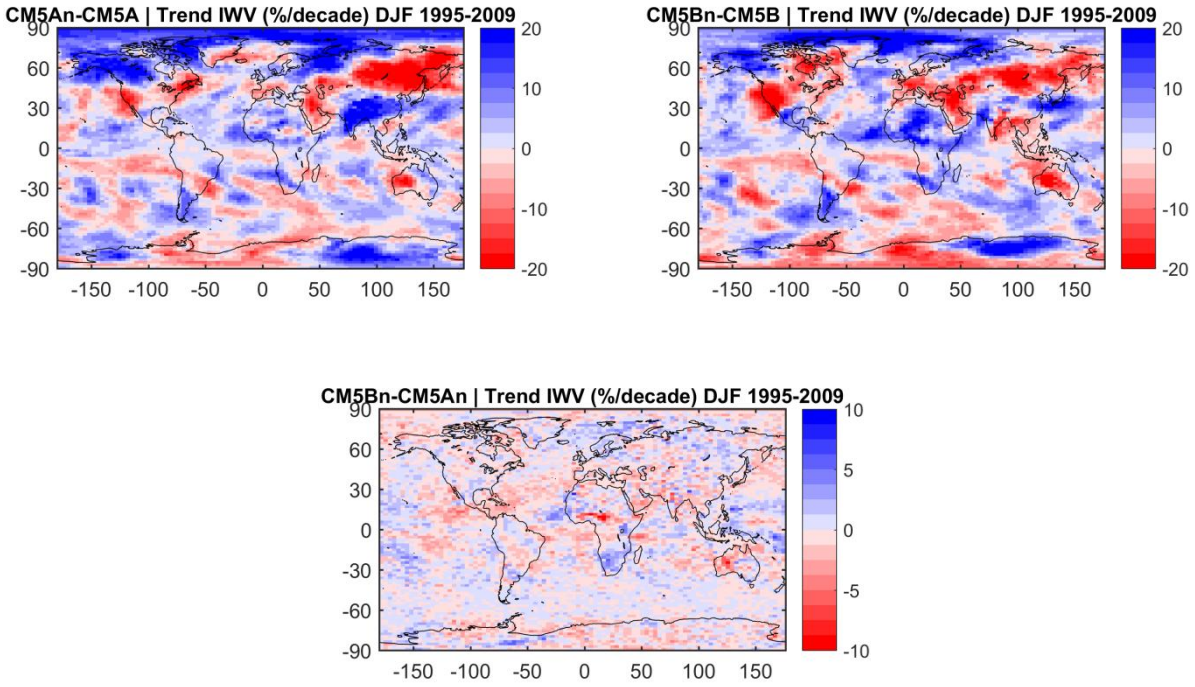

Figure 4.23 Difference in IWV trends for DJF between different configurations of the climate model.

Most of the conclusions found for DJF are also seen for the JJA season, although for this season, there are trend structures that are observed in all four simulations. In Figure 4.24, a few same sign significant trends are observed for Australia (drying), Western Europe (moistening), and the Indian Ocean (mostly positive, but partly negative in the eastern part, which is confirmed by the two GPS stations, DGAR and COCO).

The difference between model simulations and ERA-Interim is shown in Figure 4.25. As in DJF, the most intense differences are seen for the free simulations, although for JJA in particular, even the nudged simulations show an intense difference over North Africa. This suggests that the drying trends in ERA-I are likely overestimated and not realistic. Small differences are observed between physics also for JJA in Figure 4.26.

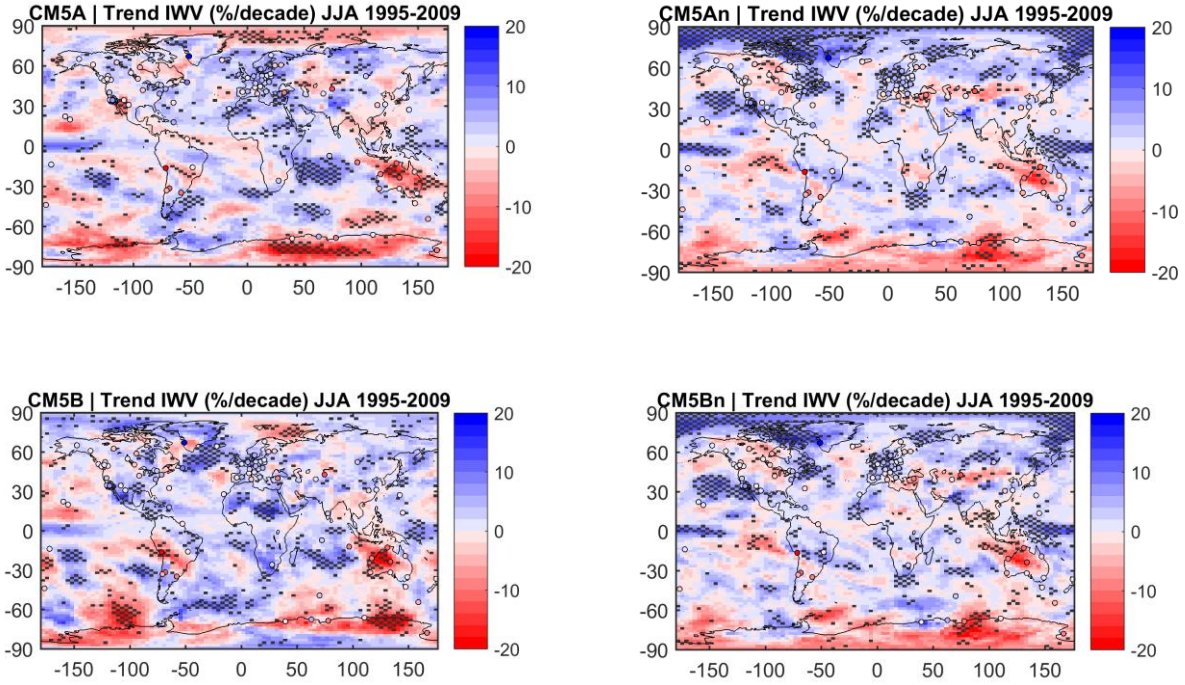

Figure 4.24 Trends in IWV fields in model with GPS trends as points for JJA

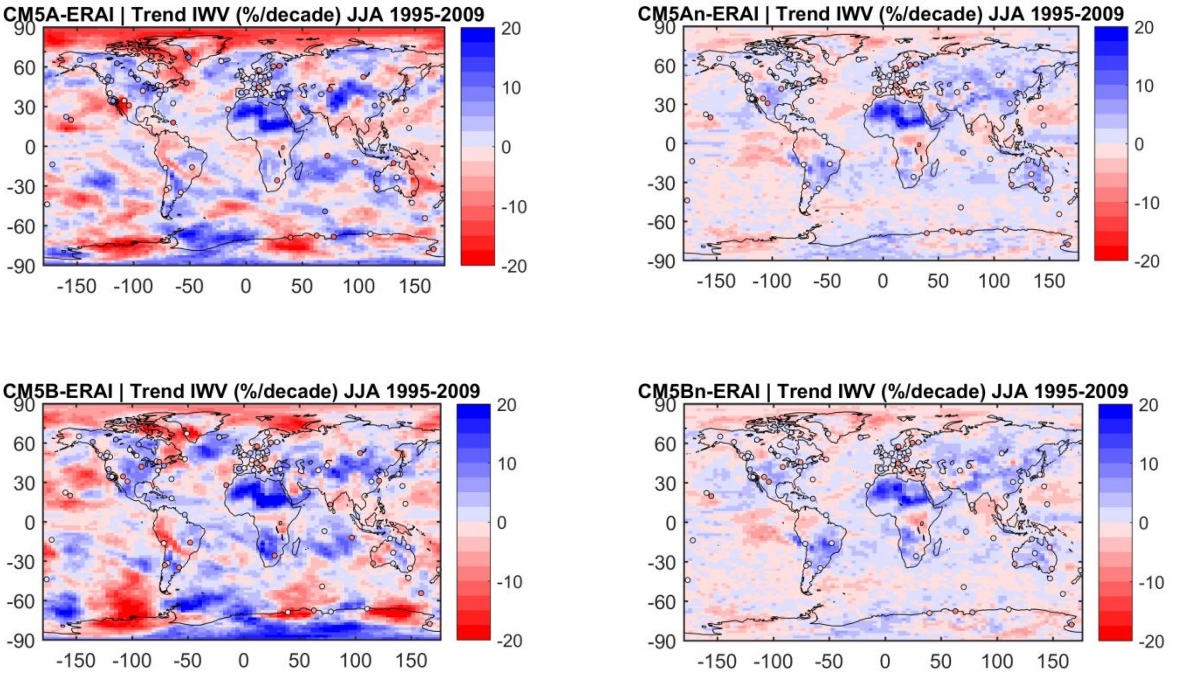

Figure 4.25 Difference fields between model and ERA-I trends (and GPS, circles) for JJA

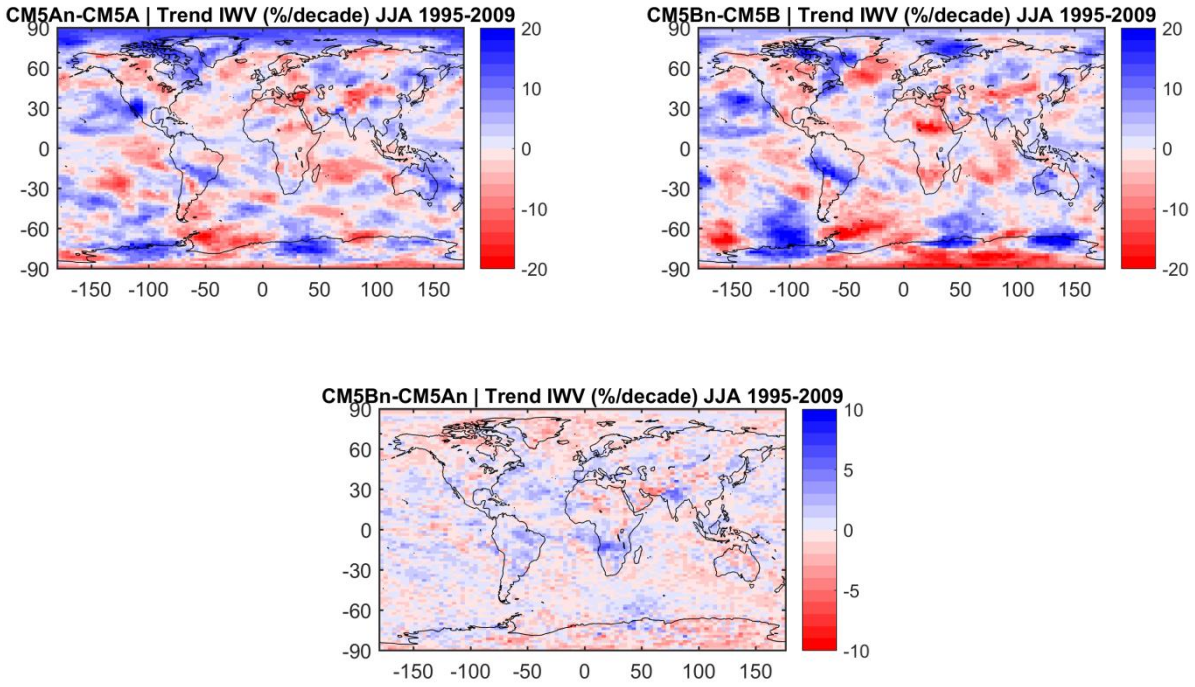

Figure 4.26 Difference in IWV trends for JJA between different configurations of the climate model.

In order to synthesize and quantify the differences in trends at the GPS site, scatter plots are presented in Figure 4.27, with corresponding values of correlation coefficient and root mean square error. The results confirm the difficulty that the free simulations have in modeling the seasonal IWV trends, with low (and even negative) correlation coefficients and large root mean square errors in the trends. CM5Bn shows better results for annual trends and DJF, while CM5An has betters results for JJA.

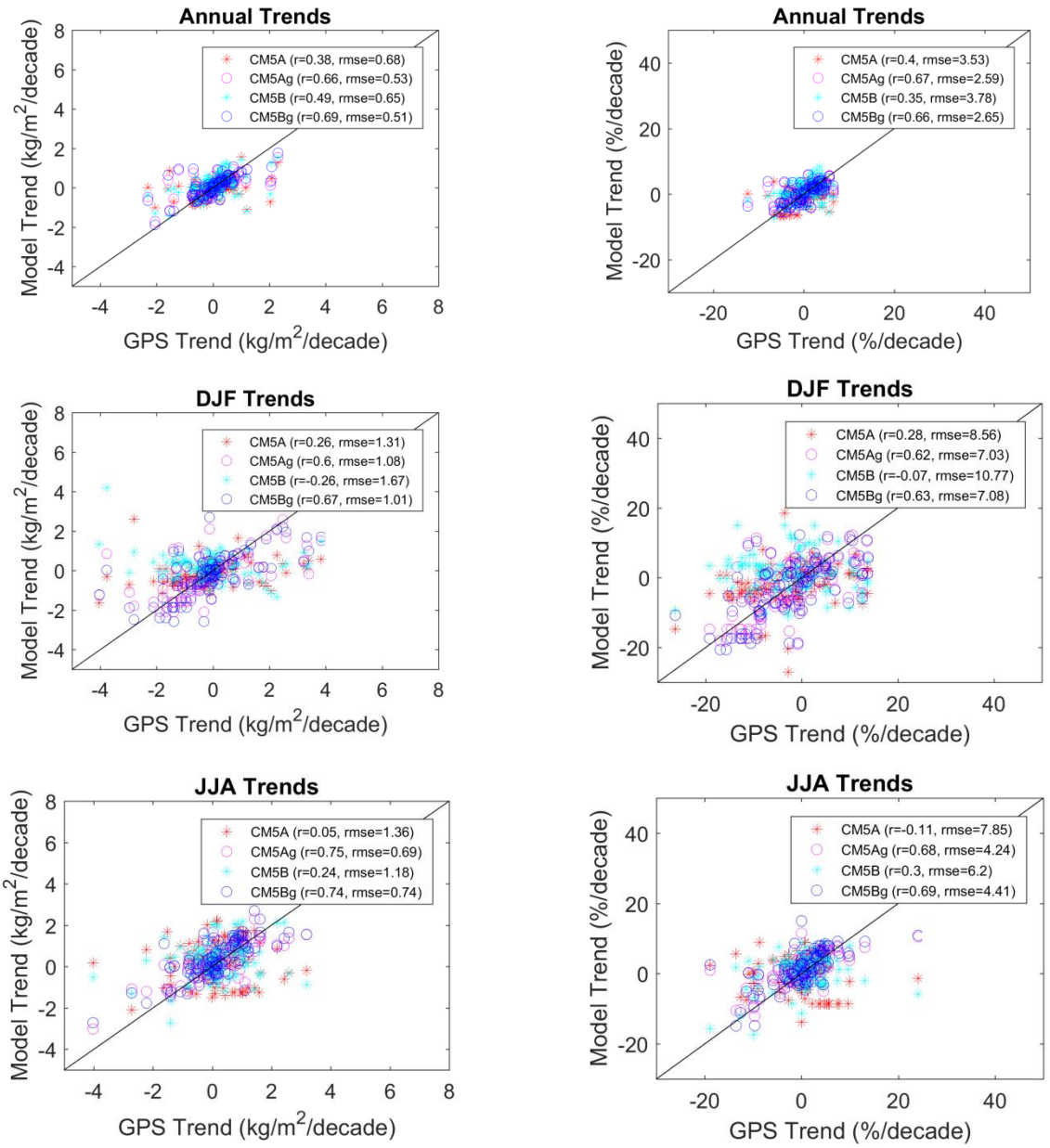

Figure 4.27 Scatter plots of the IWV trends in GPS and each model configuration.

4.3 Conclusions

The comparison between free and nudged configurations of two different physics of the LMDZ model and GPS observations and reanalyses data yielded the following results.

The free and nudged simulations show a consistent mean IWV distributions with small biases compared to homogenized GPS data. Although the pattern of higher IWV values is consistent between models and ERA-Interim, when differences are computed, there are regions of relatively high biases. Furthermore, while nudging has an important impact on the means, the differences between physics are of the same order of magnitude, and denote a moist bias for the "new" physics over the tropical oceans.

The free runs have difficulty in representing variability in IWV, mainly in the winter hemisphere. For the variability, the impact of nudging outweighs the impact of the difference in physics. In fact, when the simulations are nudged, the variability follows that observed for ERA-Interim more closely, and the agreement with GPS is improved.

The same is observed for the IWV trends to some extent, although some regions still show relatively high differences between the model and ERA-Interim. These regions include North Africa, Australia and Antarctica that had been singled out in Chapter 3 for their intense trends in ERA-Interim that were not always in agreement with the MERRA-2 reanalysis. Here, the drying trends in ERA-Interim are more intense than even the nudged simulations (by about 10%/decade). This suggests that the trends in ERA-Interim are not realistic, and are overestimated.

Finally, the fact that nudging significantly improves the results, demonstrates that dynamics (moisture transport) controls IWV variability and trends at both global and regional scales.

Chapter 5: Conclusions and perspectives

5.1 Summary of conclusions

Water vapour has an important role in the climate system. It is part of the most important climate feedback, the water vapour-lapse rate feedback, is linked with temperature and precipitation, and might affect extreme weather events in a warming climate. Even though, the water vapour-lapse rate feedback is robustly represented in climate models, there is still high uncertainty on water vapour trends, especially at a regional level. Therefore, climate models could benefit from being assessed by long term WV data.

There are several different sources of water vapour data observations (e.g.: radiosondes, GPS, satellite data). Each dataset presents advantages and short comings for long term analysis. They have been used in different studies of long-term IWV trends, and although the results pertain to different time periods, and different spatial coverage, a general positive trend in IWV was found in the data, overall.

There are uncertainties associated with IWV observations (up to 2 $kg.m^{-2}$ in the case of GPS). In order to get a more consistent product in time and space, atmospheric reanalyses are often used. Reanalysis data provide a multivariate, spatially complete, and coherent record of the global atmospheric circulation, which means that the analysed parameters are consistent with observations in regions where observations exist while they are based on model physics in data-spare regions (e.g. Africa). Different reanalyses are produced at different institutes, and their quality has been improved over successive generations, thanks to improvements of the model physics and of the assimilation systems (e.g. 4D-var, variationnal bias correction, assimilation of rain-related radiances).

Because the data assimilated by reanalyses is ever-changing, the question of homogenization has also been posed. And although in theory reanalysis should be homogeneous, this has been called into question by different studies, and my own results. Observations, reanalyses and climate models were therefore used in tandem.

First, the goal was to obtain a high quality long term-term IWV GPS data set. In order to do so the auxiliary data (i.e.: surface pressure and weighted mean temperature) that goes into the ZTD to IWV conversion formula was assessed. Different surface pressure (SYNOP, ERA-I) and mean temperature (TUV, ERA-I) data sets and computation methods (extrapolation from surface fields or integration/interpolation from pressure level data) were compared. In the end it was

concluded that it was better to compute these two variables from ERA-Interim pressure level data, as this decreases the extrapolation of data. The results were used to compute the GPS data set used throughout the rest of the thesis.

A global comparison between GPS and ERA-Interim highlighted problems in both data sets. In the GPS data, representativeness issues were found in coastal areas and regions of complex topography (mountain ranges, islands), in addition to gaps and inhomogeneities in the GPS IWV time series, which affect variability and trend estimation. For ERA-Interim, too strong trends were found in certain regions (e.g.: North Africa, Northern South America, Australia), and uncertainty in other regions (Antarctica).

Comparison with a second reanalysis (MERRA-2) was analyzed and the period of study was extended to the 1980-2016 period. Differences were found in the trends for the two reanalyses at both time periods (e.g.: Africa, Antarctica where uncertainty is high, and Australia). A focused study on Africa and Australia highlighted the connection between anomalies in IWV and anomalies in the wind intensity and direction in these regions. This suggests that differences in the wind fields may be one of the reasons for the differences in IWV in both reanalyses. Temperature anomalies for these regions were found to be anti-correlated with IWV anomalies. ERA-Interim and MERRA-2 were also compared with two twentieth century reanalyses, and differences were found, although some of the main means, variability and trend structures were observed.

The GPS and ERA-Interim data were then compared with four different configurations of the LMDZ model (two different physics, both nudged and free runs) in terms of means, interannual variability and trends in IWV. Since problems with the homogeneity of GPS data were found when comparing it with ERA-Interim, for the model assessment a rough homogenization was performed by aligning the means of GPS on ERA-Interim when equipment changes were reported in the GPS data.

An impact of the model physics on the mean IWV was shown. The “new” physics was found to be overall moister at tropical latitudes, when compared to the standard physics. At these latitudes, a moist bias in the “new” physics was also observed in relation to the GPS and ERA-Interim data. On variability and trends in IWV, the nudging has a relatively higher impact, with both physics showing consistent results. It was shown that the model has difficulty in reproducing the trends and variability observed for ERA-Interim and GPS in the free runs. This shows that the large-scale dynamics is important for trends and variability.

5.2 Perspectives

In future work on this topic, we hope to improve the homogenization of GPS IWV data, as well as expand the comparison to other reanalysis. This would include both new global reanalyses (e.g.: ERA5), and regional reanalyses (e.g. UERRA over Europe). ERA5 is the fifth generation of ECMWF atmospheric reanalyses of the global climate and will replace ERA-interim. It will span the modern observing period from 1979 at a much higher resolution (hourly analysis fields at a horizontal resolution of 31 km on 139 levels) and will include new or reprocessed observations for data assimilation. UERRA is a European FP7 reanalysis project of meteorological observations over Europe. It includes recovery of historical (last century) data, estimating uncertainties in the reanalyses and user friendly data services. The UERRA reanalyses will be made at quite high resolution, from 40 km of ensembles and 20 or 11 km and 5 km for the various model based reanalyses. The dense GPS network of GPS over Europe that has not been fully maximised in this study will be an interesting tool to evaluate such high resolution datasets.

A focus on a more detailed study of regions where uncertainty in IWV trends is high (i.e.: Africa, Antarctica, Australia) should be done, with the use of complementary data. For this, shorter-term GPS time series are available, for instance, over Africa from the African Monsoon Multidisciplinary Analysis (AMMA) project. Satellite IWV data over land (e.g. MODIS since 1999, AIRS since 2002, IASI since 2006) could also be used.

In addition, the study of other variables from reanalysis data (e.g.: moisture fluxes) should be done in order to better understand the origin of the trends and variability found in this work. This would also benefit from a more in depth study of the interaction between IWV and other variables in the climate model, such as temperature and precipitation.

In regards to the climate model assessment, the results shown here could be compared with results obtained with newer LMDZ simulations (LMDZ6), and with other climate models from the CMIP simulations.

Bibliography

Alexandrov, M. D., Schmid, B., Turner, D. D., Cairns, B., Oinas, V., Lacis, A. A., ... & Eilers, J. (2009). Columnar water vapor retrievals from multifilter rotating shadowband radiometer data. *Journal of Geophysical Research: Atmospheres*, *114*(D2).

Allen, M. R., Ingram, W. J., & Stainforth, D. A. (2002). Constraints on future changes in climate and the hydrologic cycle. *Nature*, *419*(6903), 224.

Bengtsson, L., Hagemann, S., & Hodges, K. I. (2004). Can climate trends be calculated from reanalysis data?. *Journal of Geophysical Research: Atmospheres*, *109*(D11).

Bengtsson, L. (2010). The global atmospheric water cycle. *Environmental Research Letters*, *5*(2), 025202.

Berg, H. (1948). Allgemeine Meteorologie. Dümmler's Verlag, Bonn.

Betts, A. K. (1998). Climate–convection feedbacks: Some further issues. *Climatic Change, 39*, 35–38.

Bevis, M., Businger, S., Herring, T. A., Rocken, C., Anthes, R. A., & Ware, R. H. (1992). GPS meteorology: Remote sensing of atmospheric water vapor using the Global Positioning System. Journal of Geophysical Research: Atmospheres, 97(D14), 15787-15801.

Bock, O., E. Doerflinger, F. Masson, A. Walpersdorf, J. Van-Baelen, J. Tarniewicz, M. Troller, A. Somieski, A. Geiger, B. Bürki, " GPS Water Vapor Project associated to the ESCOMPTE Programme: Description and first results of the field experiment," Phys. Chem. Earth, 29, 149-157, 2004

Bock, O., Bouin, M. N., Walpersdorf, A., Lafore, J. P., Janicot, S., & Guichard, F. (2007). Comparison of GPS precipitable water vapour to independent observations and Numerical Weather Prediction model reanalyses over Africa. *QJR Meteorol. Soc.*

Bock, O., Bosser, P., Bourcy, T., David, L., Goutail, F., Hoareau, C., Keckhut, P., Legain, D., Pazmino, A., Pelon, J., Pipis, K., Poujol, G., Sarkissian, A., Thom, C., Tournois, G., and Tzanos, D. (2013) Accuracy assessment of water vapour measurements from in-situ and remote sensing techniques during the DEMEVAP 2011 campaign at OHP, Atmos. Meas. Tech., 6, 2777-2802, 2013, doi:10.5194/amt-6-2777-2013

Bock, O., Willis, P., Wang, J., & Mears, C. (2014). A high- quality, homogenized, global, long-term (1993–2008) DORIS precipitable water data set for climate monitoring and model verification. *Journal of Geophysical Research: Atmospheres*, *119*(12), 7209-7230.

Boer, G. J. (1993). Climate change and the regulation of the surface moisture and energy budgets. *Climate Dynamics*, *8*(5), 225-239.

Bosilovich, M. G., Schubert, S. D., & Walker, G. K. (2005). Global changes of the water cycle intensity. *Journal of Climate*, *18*(10), 1591-1608.

Bosser, P., Bock, O., Pelon, J., & Thom, C. (2007). An improved mean-gravity model for GPS hydrostatic delay calibration. IEEE Geoscience and Remote Sensing Letters, 4(1), 3-7.

Boudouris, G. (1963). On the index of refraction of air, the absorption and dispersion of centimeter waves by gases. J. Res. Natl. Bur. Stand, 67, 631-684.

Brown, J. R., Moise, A. F., Colman, R., & Zhang, H. (2016). Will a Warmer World Mean a Wetter or Drier Australian Monsoon?. Journal of Climate, 29(12), 4577-4596.

Buehler, S. A., et al. "A multi-instrument comparison of integrated water vapour measurements at a high latitude site." *Atmospheric Chemistry and Physics* 12.22 (2012): 10925-10943.

Byun, S.H., and Bar-Server Y.E. (2009). A new type of troposphere zenith path delay product of the international GNSS service, J. Geod, 83(3-4), 367-373, DOI: 10.1007/s00190-008-0288-8.

Chadwick, R., Boutle, I., & Martin, G. (2013). Spatial patterns of precipitation change in CMIP5: Why the rich do not get richer in the tropics. *Journal of Climate*, *26*(11), 3803-3822.

Chelliah, M., Ebisuzaki, W., Weaver, S., & Kumar, A. (2011). Evaluating the tropospheric variability in National Centers for Environmental Prediction's climate forecast system reanalysis. *Journal of Geophysical Research: Atmospheres*, *116*(D17).

Colman, R. (2003). A comparison of climate feedbacks in general circulation models. Climate Dynamics, 20(7-8), 865-873.

Compo, G. P., Whitaker, J. S., Sardeshmukh, P. D., Matsui, N., Allan, R. J., Yin, X., ... & Brönnimann, S. (2011). The twentieth century reanalysis project. Quarterly Journal of the Royal Meteorological Society, 137(654), 1-28.

Cortemiglia, G. C. (1988). Variazoni termometriche con la quota nel bacino della Scrivia (Piemonte meridionale). In Proc. CIMA'88: 20th Congresso Int. di Meteorologia Alpina (pp. 329-340).

Cortemiglia, G. C., Rossetti, R., Ghezzi, A., & Tortelli, M. (1989). Variations thermiques avec l'altitude dans les Alpes occidentales italiennes, Actes du colloque de Pavia, Italie, 1–3 Juin 1989. Publ Assoc Int Climatol, 2, 19-26.

Dai, A., Wang, J., Thorne, P. W., Parker, D. E., Haimberger, L., & Wang, X. L. (2011). A new approach to homogenize daily radiosonde humidity data. *Journal of Climate*, *24*(4), 965-991.

Davis, J. L., Herring, T. A., Shapiro, I. I., Rogers, A. E. E., & Elgered, G. (1985). Geodesy by radio interferometry: Effects of atmospheric modeling errors on estimates of baseline length. Radio science, 20(6), 1593-1607.

Deblonde, G., Macpherson, S., Mireault, Y., & Héroux, P. (2005). Evaluation of GPS precipitable water over Canada and the IGS network. *Journal of Applied Meteorology*, *44*(1), 153-166.

Dee, D. P., Uppala, S. M., Simmons, A. J., Berrisford, P., Poli, P., Kobayashi, S., ... & Bechtold, P. (2011). The ERA- Interim reanalysis: Configuration and performance of the data assimilation system. *Quarterly Journal of the royal meteorological society*, *137*(656), 553-597.

Dessler, A. E., & Davis, S. M. (2010). Trends in tropospheric humidity from reanalysis systems. *Journal of Geophysical Research: Atmospheres*, *115*(D19).

Durre, I., Williams, C. N., Yin, X., & Vose, R. S. (2009). Radiosonde- based trends in precipitable water over the Northern Hemisphere: An update. *Journal of Geophysical Research: Atmospheres*, *114*(D5).

Ebita, A., Kobayashi, S., Ota, Y., Moriya, M., Kumabe, R., Onogi, K., ... & Kamahori, H. (2011). The Japanese 55-year reanalysis "JRA-55": an interim report. Sola, 7, 149-152.

Emori, S., & Brown, S. J. (2005). Dynamic and thermodynamic changes in mean and extreme precipitation under changed climate. Geophysical Research Letters, 32(17).

Gelaro, R., McCarty, W., Suárez, M. J., Todling, R., Molod, A., Takacs, L., ... & Wargan, K. (2017). The modern-era retrospective analysis for research and applications, version 2 (MERRA-2). Journal of Climate, 30(14), 5419-5454.

Hagemann, S., Bengtsson, L., & Gendt, G. (2003). On the determination of atmospheric water vapor from GPS measurements. *Journal of Geophysical Research: Atmospheres*, *108*(D21).

Hall, A., & Manabe, S. (1999). The role of water vapor feedback in unperturbed climate variability and global warming. *Journal of climate*, *12*(8), 2327-2346.

Hasegawa, S., & Stokesberry, D. P. (1975). Automatic digital microwave hygrometer. Review of Scientific Instruments, 46(7), 867-873.

Healy, S. B. (2011). Refractivity coefficients used in the assimilation of GPS radio occultation measurements. Journal of Geophysical Research: Atmospheres, 116(D1).

Heise, S., Dick, G., Gendt, G., Schmidt, T., & Wickert, J. (2009). Integrated water vapor from IGS ground-based GPS observations: initial results from a global 5-min data set. Ann. Geophys, 27(7), 2851-2859.

Held, I. M., & Soden, B. J. (2006). Robust responses of the hydrological cycle to global warming. *Journal of Climate*, *19*(21), 5686-5699.

Hofmann-Wellenhof, B.; Lichtenegger, H.; Collins, J. (2008) GNSS-global navigation satellite systems, Springer, Wien (Austria), 2008, 516 p., ISBN: 978-3-211-73012-6.

Holloway, C. E., & Neelin, J. D. (2009). Moisture vertical structure, column water vapor, and tropical deep convection. *Journal of the Atmospheric Sciences*, *66*(6), 1665-1683.

Hourdin, F., Musat, I., Bony, S., Braconnot, P., Codron, F., Dufresne, J. L., ... & Krinner, G. (2006). The LMDZ4 general circulation model: climate performance and sensitivity to parametrized physics with emphasis on tropical convection. Climate Dynamics, 27(7-8), 787-813.

Hourdin, F., Foujols, M. A., Codron, F., Guemas, V., Dufresne, J. L., Bony, S., ... & Braconnot, P. (2013a). Impact of the LMDZ atmospheric grid configuration on the climate and sensitivity of the IPSL-CM5A coupled model. Climate Dynamics, 40(9-10), 2167-2192.

Hourdin, F., Grandpeix, J. Y., Rio, C., Bony, S., Jam, A., Cheruy, F., ... & Dufresne, J. L. (2013b). LMDZ5B: the atmospheric component of the IPSL climate model with revisited parameterizations for clouds and convection. Climate Dynamics, 40(9-10), 2193-2222.

ICAO (1993): Aerodrome Design Manual, Part 3, Pavements, Doc 9157-AN/901, 1991, Corrigendum N 1, 1993, International Civil Aviation Organisation, Montreal

IPCC, 2014: Climate Change 2014: Synthesis Report. Contribution of Working Groups I, II and III to the Fifth Assessment Report of the Intergovernmental Panel on Climate Change [Core Writing Team, R.K. Pachauri and L.A. Meyer (eds.)]. IPCC, Geneva, Switzerland, 151 pp.

Ingleby, B. (2014). Global assimilation of air temperature, humidity, wind and pressure from surface stations. Q. J. R. Meteorol. Soc. DOI:10.1002/qj.2372.

Ingleby, N. B. (1995). Assimilation of station level pressure and errors in station height. Weather and Forecasting 10: 172-182.

Jiang, J. H., Su, H., Zhai, C., Perun, V. S., Del Genio, A., Nazarenko, L. S., ... & Gettelman, A. (2012). Evaluation of cloud and water vapor simulations in CMIP5 climate models using NASA "A- Train" satellite observations. Journal of Geophysical Research: Atmospheres, 117(D14).

Kämpfer, N. (2013). Monitoring atmospheric water vapour. *ISSI Scientific Report Series*, *10*, 326.

Kanamitsu, M., Ebisuzaki, W., Woollen, J., Yang, S. K., Hnilo, J. J., Fiorino, M., & Potter, G. L. (2002). Ncep–doe amip-ii reanalysis (r-2). Bulletin of the American Meteorological Society, 83(11), 1631-1643.

Kistler, R., Collins, W., Saha, S., White, G., Woollen, J., Kalnay, E., ... & van den Dool, H. (2001). The NCEP–NCAR 50–year reanalysis: Monthly means CD–ROM and documentation. Bulletin of the American Meteorological society, 82(2), 247-267.

Kondratev, K. Y. (1972). Radiation Processes in the Atmosphere (Geneva: World Meteorological Organization).

Liu, Z., Wong, M. S., Nichol, J., & Chan, P. W. (2013). A multi- sensor study of water vapour from radiosonde, MODIS and AERONET: a case study of Hong Kong. *International Journal of Climatology*, *33*(1), 109-120.

McCarthy, M. P., Thorne, P. W., & Titchner, H. A. (2009). An analysis of tropospheric humidity trends from radiosondes. *Journal of Climate*, *22*(22), 5820-5838.

Mears, C. A., Santer, B. D., Wentz, F. J., Taylor, K. E., & Wehner, M. F. (2007). Relationship between temperature and precipitable water changes over tropical oceans. *Geophysical Research Letters*, *34*(24).

Mieruch, S., Noël, S., Bovensmann, H., & Burrows, J. P. (2008). Analysis of global water vapour trends from satellite measurements in the visible spectral range. *Atmospheric Chemistry and Physics*, *8*(3), 491-504.

Miloshevich, L. M., Vömel, H., Whiteman, D. N., & Leblanc, T. (2009). Accuracy assessment and correction of Vaisala RS92 radiosonde water vapor measurements. *Journal of Geophysical Research: Atmospheres*, *114*(D11).

Minder, J. R., Mote, P. W., & Lundquist, J. D. (2010). Surface temperature lapse rates over complex terrain: Lessons from the Cascade Mountains. Journal of Geophysical Research: Atmospheres, 115(D14).

Morland, J., Liniger, M. A., Kunz, H., Balin, I., Nyeki, S., Mätzler, C., & Kämpfer, N. (2006). Comparison of GPS and ERA40 IWV in the Alpine region, including correction of GPS observations at Jungfraujoch (3584 m). *Journal of Geophysical Research: Atmospheres*, *111*(D4).

Morland, J., Collaud Coen, M., Hocke, K., Jeannet, P., & Mätzler, C. (2009). Tropospheric water vapour above Switzerland over the last 12 years. *Atmospheric chemistry and physics*, *9*(16), 5975-5988.

Neelin, J. D., Peters, O., & Hales, K. (2009). The transition to strong convection. Journal of the Atmospheric Sciences, 66(8), 2367-2384.

Niell, A. E., Coster, A. J., Solheim, F. S., Mendes, V. B., Toor, P. C., Langley, R. B., & Upham, C. A. (2001). Comparison of measurements of atmospheric wet delay by radiosonde, water vapor radiometer, GPS, and VLBI. *Journal of Atmospheric and Oceanic Technology*, *18*(6), 830-850.

Ning, T., Haas, R., Elgered, G., & Willén, U. (2012). Multi-technique comparisons of 10 years of wet delay estimates on the west coast of Sweden. *Journal of Geodesy*, *86*(7), 565-575.

Ning, T., Wickert, J., Deng, Z., Heise, S., Dick, G., Vey, S., & Schöne, T. (2016). Homogenized time series of the atmospheric water vapor content obtained from the GNSS reprocessed data. Journal of Climate, 29(7), 2443-2456.

O'Gorman, P. A., Allan, R. P., Byrne, M. P., & Previdi, M. (2012). Energetic constraints on precipitation under climate change. *Surveys in geophysics*, *33*(3-4), 585-608.

Onogi, K., Tsutsui, J., Koide, H., Sakamoto, M., Kobayashi, S., Hatsushika, H., ... & Kadokura, S. (2007). The JRA-25 reanalysis. Journal of the Meteorological Society of Japan. Ser. II, 85(3), 369-432.

Pacione, R., & Di Tomaso, S. (2016, April). A reference GNSS tropospheric dataset over Europe. In EGU General Assembly Conference Abstracts (Vol. 18, p. 12828).

Pałm, M., Melsheimer, C., Noël, S., Heise, S., Notholt, J., Burrows, J., & Schrems, O. (2010). Integrated water vapor above Ny Ålesund, Spitsbergen: a multi-sensor intercomparison. *Atmospheric Chemistry and Physics*, *10*(3), 1215-1226.

Paltridge, G., Arking, A., & Pook, M. (2009). Trends in middle-and upper-level tropospheric humidity from NCEP reanalysis data. *Theoretical and Applied Climatology*, *98*(3-4), 351-359.

Pérez- Ramírez, D., Whiteman, D. N., Smirnov, A., Lyamani, H., Holben, B. N., Pinker, R., ... & Alados- Arboledas, L. (2014). Evaluation of AERONET precipitable water vapor versus microwave radiometry, GPS, and radiosondes at ARM sites. *Journal of Geophysical Research: Atmospheres*, *119*(15), 9596-9613.

Pierce, D. W., Barnett, T. P., AchutaRao, K. M., Gleckler, P. J., Gregory, J. M., & Washington, W. M. (2006). Anthropogenic warming of the oceans: observations and model results. Journal of Climate, 19(10), 1873-1900.

Pierrehumbert, R. T., Brogniez, H., & Roca, R. (2007). On the relative humidity of the Earth's atmosphere. *The General Circulation*.

Poli, P., Hersbach, H., Dee, D. P., Berrisford, P., Simmons, A. J., Vitart, F., ... & Trémolet, Y. (2016). ERA-20C: An atmospheric reanalysis of the twentieth century. Journal of Climate, 29(11), 4083-4097.

Randall, D. A., Wood, R. A., Bony, S., Colman, R., Fichefet, T., Fyfe, J., ... & Stouffer, R. J. (2007). Climate models and their evaluation. In *Climate change 2007: The physical science basis. Contribution of Working Group I to the Fourth Assessment Report of the IPCC (FAR)* (pp. 589-662). Cambridge University Press.

Rienecker, M. M., Suarez, M. J., Gelaro, R., Todling, R., Bacmeister, J., Liu, E., ... & Bloom, S. (2011). MERRA: NASA's modern-era retrospective analysis for research and applications. *Journal of climate*, *24*(14), 3624-3648.

Rind, D. (1998). Just add water vapor. *Science*, *281*(5380), 1152-1153.

Roads, J. O., Chen, S. C., Marshall, S. & Oglesby, R. (1998). Atmospheric moisture cycling rates. *GEWEX News, Vol. 8*, International GEWEX Project Office, 7–10.

Rolland, C. (2003). Spatial and seasonal variations of air temperature lapse rates in Alpine regions. Journal of Climate, 16(7), 1032-1046.

Ross, R. J., & Elliott, W. P. (2001). Radiosonde-based Northern Hemisphere tropospheric water vapor trends. *Journal of Climate*, *14*(7), 1602-1612.

Rüeger, J. M. (2002). Refractive indices of light, infrared and radio waves in the atmosphere. School of Surveying and Spatial Information Systems, University of New South Wales.

Saastamoinen, J. (1972). Atmospheric correction for the troposphere and stratosphere in radio ranging satellites. The use of artificial satellites for geodesy, 247-251.

Saha, S., Moorthi, S., Pan, H. L., Wu, X., Wang, J., Nadiga, S., ... & Liu, H. (2010). The NCEP climate forecast system reanalysis. *Bulletin of the American Meteorological Society*, *91*(8), 1015-1057.

Sahany, S., Neelin, J. D., Hales, K., & Neale, R. B. (2012). Temperature–moisture dependence of the deep convective transition as a constraint on entrainment in climate models. *Journal of the Atmospheric Sciences*, *69*(4), 1340-1358.

Schöne, T., Schön, N., & Thaller, D. (2009). IGS tide gauge benchmark monitoring pilot project (TIGA): scientific benefits. Journal of Geodesy, 83(3), 249-261.

Schröder, M., Lockhoff, M., Forsythe, J. M., Cronk, H. Q., Vonder Haar, T. H., & Bennartz, R. (2016). The GEWEX Water Vapor Assessment: Results from Intercomparison, Trend, and Homogeneity Analysis of Total Column Water Vapor. *Journal of Applied Meteorology and Climatology*, *55*(7), 1633-1649.

Semenov, V., & Bengtsson, L. (2002). Secular trends in daily precipitation characteristics: greenhouse gas simulation with a coupled AOGCM. *Climate Dynamics*, *19*(2), 123-140.

Shi, L., & Bates, J. J. (2011). Three decades of intersatellite- calibrated High- Resolution Infrared Radiation Sounder upper tropospheric water vapor. *Journal of Geophysical Research: Atmospheres*, *116*(D4).

Smit, H., Kivi, R., Vömel, H., & Paukkunen, A. (2013). Thin film capacitive sensors. In *Monitoring Atmospheric Water Vapour* (pp. 11-38). Springer New York.

Smith, E. K., & Weintraub, S. (1953). The constants in the equation for atmospheric refractive index at radio frequencies. Proceedings of the IRE, 41(8), 1035-1037.

Soden, B. J., Jackson, D. L., Ramaswamy, V., Schwarzkopf, M. D., & Huang, X. (2005). The radiative signature of upper tropospheric moistening. Science, 310(5749), 841-844.

Soden, B. J., & Held, I. M. (2006). An assessment of climate feedbacks in coupled ocean–atmosphere models. *Journal of Climate*, *19*(14), 3354-3360.

Spencer, R. W., & Braswell, W. D. (1997). How dry is the tropical free troposphere? Implications for global warming theory. *Bulletin of the American Meteorological Society*, *78*(6), 1097-1106.

Stocker, T. F., Willebrand, J., Böning, C. W., Visbeck, M., Timmermann, A., & Lemke, P. (2001). Physical Climate Processes and Feedbacks. In: IPCC WG1 Third Assessment Report. Cambridge University Press.

Stocker, T. (Ed.). (2014). *Climate change 2013: the physical science basis: Working Group I contribution to the Fifth assessment report of the Intergovernmental Panel on Climate Change*. Cambridge University Press.

Thayer, G. D. (1974). An improved equation for the radio refractive index of air. Radio Science, 9(10), 803-807.

Thorne, P. W., & Vose, R. S. (2010). Reanalyses suitable for characterizing long-term trends: Are they really achievable?. *Bulletin of the American Meteorological Society*, *91*(3), 353-361.

Torres, B., Cachorro, V. E., Toledano, C., Ortiz de Galisteo, J. P., Berjón, A., De Frutos, A. M., ... & Laulainen, N. (2010). Precipitable water vapor characterization in the Gulf of Cadiz region (southwestern Spain) based on Sun photometer, GPS, and radiosonde data. *Journal of Geophysical Research: Atmospheres*, *115*(D18).

Trenberth, K. E., Fasullo, J., & Smith, L. (2005). Trends and variability in column-integrated atmospheric water vapor. *Climate dynamics*, *24*(7-8), 741-758.

Uppala, S. M., Kållberg, P. W., Simmons, A. J., Andrae, U., Bechtold, V. D., Fiorino, M., and co-authors. (2005). The ERA-40 re-analysis. Quarterly Journal of the Royal Meteorological Society, 131(612), 2961-3012.

van den Besselaar, E.J.M., M.R. Haylock, G. van der Schrier and A.M.G. Klein Tank. (2011). A European Daily High-resolution Observational Gridded Data set of Sea Level Pressure. J. Geophys. Res., 116, D11110, doi:10.1029/2010JD015468

Van Malderen, R., Brenot, H., Pottiaux, E., Beirle, S., Hermans, C., De Mazière, M., ... & Bruyninx, C. (2014). A multi-site intercomparison of integrated water vapour observations for climate change analysis. *Atmospheric Measurement Techniques*, *7*(8), 2487-2512.

Vecchi, G. A., Soden, B. J., Wittenberg, A. T., Held, I. M., Leetmaa, A., & Harrison, M. J. (2006). Weakening of tropical Pacific atmospheric circulation due to anthropogenic forcing. *Nature*, *441*(7089), 73.

Vey, S., Dietrich, R., Fritsche, M., Rülke, A., Steigenberger, P., & Rothacher, M. (2009). On the homogeneity and interpretation of precipitable water time series derived from global GPS observations. *Journal of Geophysical Research: Atmospheres*, *114*(D10).

Vey, S., Dietrich, R., Rülke, A., Fritsche, M., Steigenberger, P., & Rothacher, M. (2010). Validation of precipitable water vapor within the NCEP/DOE reanalysis using global GPS observations from one decade. *Journal of Climate*, *23*(7), 1675-1695.

Visbeck, M. H., Hurrell, J. W., Polvani, L., & Cullen, H. M. (2001). The North Atlantic Oscillation: past, present, and future. Proceedings of the National Academy of Sciences, 98(23), 12876-12877.

Wagner, T., Beirle, S., Grzegorski, M., & Platt, U. (2006). Global trends (1996–2003) of total column precipitable water observed by Global Ozone Monitoring Experiment (GOME) on ERS-2 and their relation to near- surface temperature. *Journal of Geophysical Research: Atmospheres*, *111*(D12).

Wang, J., Zhang, L., & Dai, A. (2005). Global estimates of water- vapor- weighted mean temperature of the atmosphere for GPS applications. Journal of Geophysical Research: Atmospheres, 110(D21).

Wang, J., Zhang, L., Dai, A., Van Hove, T., & Van Baelen, J. (2007). A near- global, 2- hourly data set of atmospheric precipitable water from ground- based GPS measurements. *Journal of Geophysical Research: Atmospheres*, *112*(D11).

Wang, J., & Zhang, L. (2008). Systematic errors in global radiosonde precipitable water data from comparisons with ground-based GPS measurements. *Journal of Climate*, *21*(10), 2218-2238.

Wang, J., Zhang, L., Dai, A., Immler, F., Sommer, M., & Vömel, H. (2013). Radiation dry bias correction of Vaisala RS92 humidity data and its impacts on historical radiosonde data. *Journal of Atmospheric and Oceanic Technology*, *30*(2), 197-214.

Wang, J., Dai, A., & Mears, C. (2016). Global Water Vapor Trend from 1988 to 2011 and Its Diurnal Asymmetry Based on GPS, Radiosonde, and Microwave Satellite Measurements. *Journal of Climate*, *29*(14), 5205-5222.

Winton, M. (2006). Amplified Arctic climate change: What does surface albedo feedback have to do with it?. Geophysical Research Letters, 33(3).

Yang, S. K., & Smith, G. L. (1985). Further study on atmospheric lapse rate regimes. Journal of the atmospheric sciences, 42(9), 961-966.

Zhang, M., & Song, H. (2006). Evidence of deceleration of atmospheric vertical overturning circulation over the tropical Pacific. *Geophysical research letters*, *33*(12).

Zhao, T., Dai, A., & Wang, J. (2012). Trends in tropospheric humidity from 1970 to 2008 over China from a homogenized radiosonde dataset. *Journal of Climate*, *25*(13), 4549-4567.